FILE COPY
NO. 6

CLASSIFICATION CANCELLED
CHANGED TO RESTRICTED

Copy No. 166
CONFIDENTIAL RM No. L6H28d

NACA

RESEARCH MEMORANDUM

AN INVESTIGATION OF A HIGH-ASPECT-RATIO WING HAVING 0.20-CHORD PLAIN AILERONS IN THE LANGLEY 8-FOOT HIGH-SPEED TUNNEL

By

Arvo A. Luoma

Langley Memorial Aeronautical Laboratory
Langley Field, Va.

THIS DOCUMENT ON LOAN FROM THE FILES OF
NATIONAL ADVISORY COMMITTEE FOR AERONAUTICS
LANGLEY AERONAUTICAL LABORATORY
LANGLEY FIELD, HAMPTON, VIRGINIA

RETURN TO THE ABOVE ADDRESS.

REQUESTS FOR PUBLICATIONS SHOULD BE ADDRESSED AS FOLLOWS:

NATIONAL ADVISORY COMMITTEE FOR AERONAUTICS
1512 H STREET, N. W.
WASHINGTON 25, D. C.

CLASSIFIED DOCUMENT

This document contains classified information affecting the national Defense of the United States within the meaning of the Espionage Act, USC 50:31 and 32. Its transmission or the revelation of its contents in any manner to an unauthorized person is prohibited by law.

Information so classified may be imparted only to persons in the military and naval services of the United States, appropriate civilian officers and employees of the Federal Government who have a legitimate interest therein, and to United States citizens of known loyalty and discretion who of necessity must be informed thereof.

CLASSIFICATION CANCELLED

AUTHORITY H.L.DRYDEN 6 -5-53

CHANGED 1408

NATIONAL ADVISORY COMMITTEE FOR AERONAUTICS

WASHINGTON

August 20, 1946

CONFIDENTIAL

CLASSIFICATION CANCELLED
CHANGED TO RESTRICTED

CLASSIFICATION CANCELLED

NATIONAL ADVISORY COMMITTEE FOR AERONAUTICS

RESEARCH MEMORANDUM

AN INVESTIGATION OF A HIGH-ASPECT-RATIO WING HAVING 0.20-CHORD PLAIN AILERONS IN THE LANGLEY 8-FOOT HIGH-SPEED TUNNEL

By Arvo A. Luoma

SUMMARY

A three-dimensional lateral-control investigation was made at high speeds of a wing of high aspect ratio having 0.20-chord straight-sided-profile plain ailerons with a span 37.5 percent of the wing semispan. Spanwise loadings and moments and rolling-moment coefficients were obtained from pressure-distribution measurements, and hinge-moment data were obtained by an electrical strain gage for Mach numbers up to 0.925 at aileron deflections from -10° to 10° and at various angles of attack.

The wind-tunnel test data indicate no unusual rolling-moment and aileron hinge-moment characteristics for an airplane with this particular wing-aileron combination and designed to operate at level-flight Mach numbers up to 0.830. At higher Mach numbers, comparable to those obtained in dives, the rolling effectiveness was reduced but the ailerons still produced some rolling moment at zero and positive lifts up to the maximum test Mach number of 0.925. At Mach numbers between 0.880 and 0.900 there is possibility, however, of flexibility-induced aileron snatch for an airplane having an aileron control system of inadequate stiffness.

INTRODUCTION

A general research program conducted in connection with the design of a high-speed airplane with a wing of high aspect ratio has been undertaken by the National Advisory Committee for Aeronautics. Basic wing characteristics including data on normal force, span loading, pitching moment, drag, and wake widths have been presented in reference 1 for a wing of this type. This wing has an

CLASSIFICATION CANCELLED

NACA 65-210 airfoil section and an aspect ratio of 9. As an aid in the design of a horizontal tail for use with this type of wing, tests were made to determine the downwash and flow fluctuations behind the wing, and the data from these tests are presented in reference 2. The effects of a solid-front dive brake, a slotted dive brake, and a dive-recovery flap on the basic wing characteristics at high Mach numbers, together with an investigation of the average incremental downwash due to the addition of the dive-recovery flap, are presented in reference 3.

The tests presented herein were made to determine the aerodynamic characteristics of 0.20-chord plain ailerons on a wing of high aspect ratio at high speeds. Lateral-control data including hinge-moment coefficients, rolling-moment coefficients, pitching-moment coefficients, and span loadings were obtained for Mach numbers from 0.400 to 0.925 and at aileron deflections from -10° to 10° for various wing angles of attack.

SYMBOLS

The symbols used herein are defined as follows:

α	angle of attack of finite-span wing
V	velocity in undisturbed stream
p_o	static pressure in undisturbed stream
p	local static pressure at a point on airfoil section
ρ	mass density in undisturbed stream
a	speed of sound in undisturbed stream
q	dynamic pressure in undisturbed stream $\left(\frac{1}{2}\rho V^2\right)$
P	pressure coefficient $\left(\frac{p - p_o}{q}\right)$
P_{cr}	critical pressure coefficient obtained when local speed of sound is reached at some point on airfoil section
M	Mach number (V/a)

δ_a aileron deflection; positive for down deflection

b_a span of aileron; model value, 0.590 ft

c section chord of wing

c_a section aileron chord measured along airfoil chord line from hinge axis of aileron to trailing edge of airfoil

$\bar{c}_a$ root-mean-square chord of aileron; model value, 0.0534 ft $\left(\bar{c}_a = \sqrt{\frac{1}{b_a}\int_0^{b_a} c_a^2\, dy}\right)$

S area of complete wing; model value, 1.10 sq ft

c' mean aerodynamic chord of wing; model value, 0.37 ft $\left(c' = \frac{2}{S}\int_0^{b/2} c^2\, dy\right)$

H_a aileron hinge moment

C_{h_a} aileron hinge-moment coefficient $\left(H_a/qb_a\bar{c}_a^2\right)$

ΔP resultant pressure coefficient across aileron seal (ΔP = (Value of P below seal) - (Value of P above seal))

x distance along chord from leading edge of airfoil section

y distance along semispan from wing center line

b span of wing; model value, 3.15 ft

c_n section normal-force coefficient of wing from pressure-distribution data

$$c_n = \frac{1}{c}\int_0^c \left(P_L - P_U\right) dx$$

CLASSIFICATION CANCELLED

Δc_n change in section normal-force coefficient of airfoil due to aileron deflection

$$\Delta c_n = \frac{1}{c} \int_0^c \left[\left(P_L - P_U \right) - \left(P_L - P_U \right)_{\delta_a = 0^\circ} \right] dx$$

c_m section pitching-moment coefficient of airfoil about quarter-chord point from pressure-distribution data; pitching moment due to chord forces not included

$$c_m = \frac{1}{c^2} \int_0^c \left(P_U - P_L \right) \left(x - \frac{c}{4} \right) dx$$

Δc_m change in section pitching-moment coefficient of airfoil about quarter-chord point due to aileron deflection

$$\Delta c_m = \frac{1}{c^2} \int_0^c \left[\left(P_U - P_L \right) - \left(P_U - P_L \right)_{\delta_a = 0^\circ} \right] \left[\left(x - \frac{c}{4} \right) \right] dx$$

C_N normal-force coefficient of semispan wing

$$C_N = \frac{2}{S} \int_0^{b/2} c_n c \, dy$$

ΔC_N change in normal-force coefficient of semispan wing due to aileron deflection

$$\Delta C_N = \frac{2}{S} \int_0^{b/2} \Delta c_n \, c \, dy$$

C_m pitching-moment coefficient of semispan wing about quarter-chord line of wing

$$C_m = \frac{2}{Sc'} \int_0^{b/2} c_m c^2 \, dy$$

ΔC_m change in pitching-moment coefficient of semispan wing about quarter-chord line of wing due to aileron deflection

$$\Delta C_m = \frac{2}{Sc'} \int_0^{b/2} \Delta c_m \, c^2 \, dy$$

C_l rolling-moment coefficient, due to aileron deflection, about axis collinear with chord line in plane of symmetry

$$C_l = -\frac{1}{Sb} \int_0^{b/2} \Delta c_n \, cy \, dy$$

C_{l_p} damping-moment coefficient about axis collinear with chord line in plane of symmetry, computed simply by the equation

$$C_{l_p} = \frac{57.3}{S} \left(\frac{2}{b}\right)^2 \int_0^{b/2} \frac{dc_n}{d\alpha} \, cy^2 \, dy$$

where $dc_n/d\alpha$ is the experimentally determined rate of change of section normal-force coefficient with angle of attack of finite-span wing

Subscripts:

U upper surface

L lower surface

APPARATUS AND TESTS

The tests were made in the Langley 8-foot high-speed tunnel, which is a single-return closed-throat tunnel with an air-stream turbulence that is small but slightly higher than free air. For these tests the airspeed was continuously controllable to a choking Mach number of 0.950 (uncorrected).

The wing with plain aileron used for the lateral-control investigation is the same wing that was used for the tests of reference 1. The wing as tested is shown in figure 1. The wing has an NACA 65-210 airfoil section, an aspect ratio of 9.0, a taper ratio of 2.5:1.0, no sweepback, twist, or dihedral, and a tip having the dimensions given in table I. The effective span of the model wing is 37.8 inches; the root chord is 6 inches, and the tip chord is 2.4 inches. Ordinates of the NACA 65-210 airfoil section are given in table II. A complete description of the model and tunnel setup is given in reference 1. The aileron chord is 20 percent of the wing chord and the aileron span is 37.5 percent of the wing semispan, with the inboard end of the aileron at the 60-percent-semispan station (fig. 2). Two hinges located approximately 25 percent of the aileron span from either end of the aileron supported the aileron. The ailerons are of straight sided profile with a trailing-edge angle of 11.1° (fig. 3).

Twenty static-pressure orifices were placed at each of eight stations along the wing span (fig. 4). The spanwise locations of these stations in percent of the semispan are 11, 20, 30, 43, 56, 64, 80, and 95. The four inboard stations were placed on the left half of the wing, and the four outboard stations on the right half. Pressure data at stations within the aileron span were obtained at stations 64, 80, and 95 percent of the semispan.

Normal-force, pitching-moment, and rolling-moment data were obtained from pressure-distribution measurements; and hinge-moment data were obtained by electrical-strain-gage measurements. The hinge moments were measured on the left aileron, which had no pressure stations within its span. Because of the small size of the model and the high loads encountered during these tests, it was not feasible to incorporate a seal on the left aileron where

the hinge-moment data were obtained. These data are therefore for an unsealed aileron with a gap approximately 0.003 of the wing chord. The pressure data at stations within the aileron span were obtained on the right half of the wing. The right aileron, however, was completely sealed and the coefficients derived from the pressure data are therefore for sealed-gap conditions. Aerodynamic data were obtained for angles of attack of -2°, 0°, 2°, 4°, 7°, and 10° at Mach numbers of 0.400 and 0.600 and for angles of attack of -2°, 0°, 2°, 4°, and 7° at Mach numbers of 0.760, 0.800, 0.827, 0.880, 0.907, and 0.925 (uncorrected). Tests were made at seven aileron deflections from -10° to 10° for all Mach numbers. The test Mach numbers used herein were corrected as in reference 1. A full discussion of the corrections for model constriction, wake constriction, and lift vortex interference may be found in reference 1. No corrections have been made to the rolling-moment or hinge-moment coefficient. A discussion of corrections to lateral-control coefficients is given in references 4 and 5.

The aerodynamic data show that the maximum twisting moment about a torsion axis passing through the 40-percent-chord points of the section chords occurred at a Mach number of 0.925, an angle of attack of 7°, and an aileron deflection of 9.6°. Static torsion tests of the model gave a torsional stiffness of the wing at the midspan of the aileron of 250 inch-pounds per degree; that is, a concentrated twisting moment of 250 inch-pounds applied at the wing tip would result in a twist of the wing of 1° at the midspan of the aileron. When the spanwise section-loading and section-moment data at the worst twisting conditions are used and the torsional stiffness at a section is considered to vary inversely as the cube of the distance from the plane of symmetry, the calculations indicate a maximum twist of the wing at the tip of -0.20°. No corrections have been made for the effect of twist.

RESULTS

Effects of Reynolds Number

In these tests the Reynolds number varied from 900,000 at a Mach number of 0.400 to 1,400,000 at a Mach number of 0.900 with the Reynolds number based on the mean aerodynamic chord of the wing. Some idea of the effects of

Reynolds number at subcritical Mach numbers can be obtained from the two-dimensional tests of the same airfoil section at Reynolds numbers of 1,000,000 and 9,000,000 corresponding to Mach numbers of 0.07 and 0.17, respectively (reference 6). The effects of Reynolds number on airfoils at supercritical Mach numbers are of secondary importance as compared to the effects of compressibility (reference 7).

Pressures

Illustrative chordwise pressure distributions at three spanwise stations within the aileron span for aileron deflections of -5.7°, 0.5°, and 5.8° and for Mach numbers up to 0.925 are presented in figures 5 to 7. Spanwise section loadings obtained from integration of the pressure data are shown in figures 8 to 14 for seven aileron deflections from -10.0° to 9.6°. Wing normal-force coefficient against aileron deflection and Mach number are given in figures 15 and 16, respectively. The data for even values of aileron deflection were obtained from cross plots. Spanwise section moments for aileron deflections from -10.0° to 9.6° are presented in figures 17 to 23. The effect of aileron deflection on spanwise section moments for several Mach numbers is shown in figure 24. Wing pitching-moment coefficients based on the wing mean aerodynamic chord are plotted against aileron deflection in figure 25 and against Mach number in figure 26. Incremental values of wing normal-force and pitching-moment coefficient resulting from aileron deflection are plotted against Mach number in figure 27.

The rolling-moment coefficients for the sealed aileron are plotted against aileron deflection in figure 28 and against Mach number in figure 29. The rate of change of rolling-moment coefficient with aileron deflection $(\Delta C_l/\Delta \delta_a)_\alpha$ for small aileron deflections ($\pm 2^\circ$) is plotted against Mach number in figure 30. A damping-moment coefficient C_{l_p} based on the experimentally determined values of $dc_n/d\alpha$ for zero aileron deflection is given in figure 31 to show the general effects of compressibility on damping in roll. The calculated rate of roll per unit aileron deflection for a rigid wing with sealed aileron in pure roll is plotted against Mach number in figure 32. The rate of roll per unit aileron deflection was obtained from the equation

$$\frac{pb/2V}{\Delta\delta_a} = \frac{\Delta C_l/\Delta\delta_a}{C_{l_p}}$$

Hinge Moments

An electrical strain gage was used to determine the hinge moments. The small size of the model necessitated the use of a small strain gage and this smallness of the gage, coupled with the severe operating conditions produced by high speeds, high temperatures, and large aileron loads impaired the accuracy of the hinge-moment measurements. An indication of the accuracy of the data can be obtained from the scatter of the test points of figure 33. The basic effects of compressibility, however, are well illustrated by the data. Figures 34 and 35, which were obtained from the data of figure 33, show the variation of the hinge-moment coefficients of the unsealed aileron with Mach number and angle of attack, respectively. In figure 36 is given the variation of the parameters $\left(\Delta C_{h_a}/\Delta\delta_a\right)_{\alpha=0^\circ}$ and $\left(\Delta C_{h_a}/\Delta\alpha\right)_{\delta_a=0^\circ}$ with Mach number. These slopes are the average values for aileron deflections from -1° to 1° and angles of attack from -1° to 1°. Data on the average resultant pressure coefficient across the aileron seal are shown for various aileron deflections and Mach numbers in figure 37.

DISCUSSION

Pressure-Distribution Diagrams

In reference 1, large variations were observed in normal-force coefficients at Mach numbers greater than 0.760 and in pitching-moment coefficients at Mach numbers greater than 0.825. These large changes in the aerodynamic characteristics are associated with the unsymmetrical effects of shock and shock movement on the upper and lower surfaces of the airfoil. At Mach numbers in the approximate range from 0.825 to 0.900, the rearward movement of shock on the lower surface of the airfoil predominated in affecting the aerodynamic characteristics and resulted in a reduction of normal-force coefficients, an increase in pitching-moment coefficients

in a positive direction (except at large angles of attack), and generally, as the present tests showed, a positive increase in hinge-moment coefficients (except for the large angles of attack at positive aileron deflections). At Mach numbers greater than 0.900 a greater increase in the negative direction of the pressures on the rear half of the upper surface as compared with those on the lower surface reversed the direction of the changes just noted at Mach numbers less than 0.900. These pressure phenomena are illustrated by the chordwise pressure distributions of figures 5 to 7, which are for spanwise stations within the aileron span.

Normal-Force Characteristics

The data showing the effects of compressibility on spanwise loading for various aileron deflections (figs. 8 to 14) are quite similar to the data for zero deflection (reference 1) which, at the higher speeds, show irregular load distributions, an outboard movement of the lateral center of load for positive lifts, and rapid changes in the angle of zero lift. At the highest Mach numbers, positive aileron deflections are more effective in producing lift than negative deflections (fig. 15). When the flow over an airfoil is largely supersonic, a control surface becomes relatively ineffective in controlling the supersonic flow ahead of it (reference 8). This loss in control effectiveness at such speeds is illustrated by the data of figure 16. At positive angles of attack, a positive deflection of the control changes the lower-surface pressures to values of negative pressure coefficient that are low enough to escape the full effects of compression shock on the lower surface for speed conditions corresponding to those of these tests (figs. 6 and 7) so that the control surface still retains some control on the flow over the lower surface. As is to be expected, an increase in angle of attack increases the ability of the control at positive deflections to modify the flow over the lower surface. The schlieren photographs of reference 8 for a 19-percent-thick wing section show separated flow associated with compression shock off both surfaces ahead of the control surface at supercritical Mach numbers and explain the lack of effectiveness of the control as a result of this separation. The reduced effectiveness at supercritical Mach numbers for negative aileron deflections noted for the 10-percent-thick wing used in the present tests is probably the result of similar separation off the upper surface, which is more disposed toward separation than the lower surface because of the 0.2 camber of the section

and the positive angles of attack at which the sections operate. At an angle of attack of 7° and at Mach numbers of 0.907 and 0.925, however, it is to be noted that for aileron deflections up to -3° the aileron shows some control of the flow. The data for an angle of attack of 4° at a Mach number of 0.907 also shows some control of the flow for deflections up to -5°. A study of the chordwise pressure distributions for these negative deflections and angles of attack reveals that the aileron has a noticeable effect on the lower-surface flow and also to some extent on the upper-surface flow. This discussion is also generally applicable in the analysis of changes in wing pitching-moment coefficients and rolling-moment coefficients at these high Mach numbers. Aileron deflection had relatively little effect on the Mach number at which the force break occurred (fig. 16). Noticeable increases in normal-force coefficient at Mach numbers greater than 0.900 were obtained for all aileron deflections as well as for zero deflection (fig. 16).

Pitching-Moment Characteristics

Large, somewhat irregular variations occur in the spanwise values of the section moment factor $c_m b^2 c^2/S^2$ at high Mach numbers for all aileron deflections (figs. 17 to 23). Increments of $c_m b^2 c^2/S^2$ due to aileron deflection show similar variations (fig. 24). At the higher Mach numbers, the positive aileron deflections generally have a greater effect on wing pitching-moment coefficient than the negative deflections (fig. 25), as was the case for the effect of aileron deflection on wing normal-force coefficient. General compressibility effects as regards unsymmetrical effects of shock movement over the upper and lower surfaces are the same for all aileron deflections (fig. 26). The effects of compressibility on the changes in wing normal-force coefficient and wing pitching-moment coefficient due to aileron deflection presented in figure 27 show somewhat more clearly than figures 15 and 25 the effect of aileron deflection on these characteristics.

Rolling-Moment Characteristics

The data of figures 28 to 30 show that compressibility produces no great losses in aileron rolling-moment coefficient for Mach numbers up to and including 0.825, which is well above the wing critical Mach number of 0.730 (wing normal-force coefficient of 0.2). Positive aileron deflections are shown to give rolling control at all speeds for

positive lifts and improvement in control with increase in angle of attack. At low angles of attack the negative deflections are ineffective at Mach numbers greater than 0.825 but, with an increase in angle of attack, the effectiveness improves so that at an angle of attack of 7° the ailerons are effective for positive and negative deflections. At an angle of attack of -2° an actual reversal occurs in aileron effectiveness between Mach numbers of 0.885 and 0.925 (figs. 28, 29, and 30); but the normal-force coefficient for these conditions is approximately -0.18 so that an airplane with this wing-aileron combination would not fly at an angle of attack of -2° at these high Mach numbers under all normal maneuvers. The discussion made in the preceding sections concerning the effect of aileron deflection on air flow over the airfoil applies also in the analysis of compressibility effects on rolling-moment coefficient.

The general effects of compressibility on damping-moment coefficient (fig. 31) parallel, as is to be expected, the effects of compressibility on the parameter $dC_N/d\alpha$ presented in reference 1. By use of the low-speed section data of reference 6 and the methods of reference 9, a damping-moment coefficient of 0.52 was obtained for the wing with round tips assumed and of 0.55 for the wing with square tips assumed. The variations of the damping-moment coefficient are largely reflected in the rolling effectiveness per unit aileron deflection $\frac{pb/2V}{\Delta\delta_a}$ for a rigid wing with sealed aileron at two altitudes (fig. 32) and this rolling effectiveness is seen to decrease with increasing Mach number up to a Mach number of 0.760, then to increase abruptly to a Mach number of 0.800, and then generally to decrease again as the Mach number is further increased. At Mach numbers greater than 0.850 the rolling effectiveness increases with altitude because of the improvement in rolling-moment coefficient resulting from the increase in angle of attack at altitude for level-flight conditions. For an actual airplane in flight, wing twist and yaw would appreciably reduce the rigid-wing effectiveness.

The data on the rolling-moment coefficient indicate that the ailerons are satisfactory for producing rolling moments on an airplane with this wing-aileron combination and designed to operate at maximum level-flight speeds in the Mach number range from 0.760 to 0.830. In dives in which the airplane would operate at higher Mach numbers the ailerons still produce some rolling moment at zero and positive lifts up to the maximum test Mach number of 0.925 although, at these higher Mach numbers, their effectiveness is decreased.

Hinge-Moment Characteristics

The hinge-moment data of these tests are for an unsealed aileron. The general compressibility effects, however, can be expected to apply also for a sealed aileron. For Mach numbers through 0.830 the data on the hinge-moment coefficient for the unsealed aileron show no unusual compressibility effects (figs. 33 and 34) but, at higher Mach numbers, marked changes occur in hinge-moment coefficient associated with rearward movement of shock. A possibility exists of flexibility-induced aileron snatch (reference 10) as a result of the positive slopes of $dC_{h_a}/d\delta_a$ (overbalance conditions) noted in the data for some of the test conditions. Flexibility-induced aileron snatch will occur if the change in aerodynamic hinge moment per degree change of aileron deflection $dH_a/d\delta_a$ exceeds the stiffness of the control system expressed in terms of resisting hinge moment developed per degree twist of aileron. The maximum value of $dC_{h_a}/d\delta_a$ resulted at a Mach number of 0.880 and an angle of attack of 2° and amounted to 0.021. (See fig. 33(c).) In order to avoid elastic instability, the aileron-control stiffness when expressed in this same form must exceed the value of 0.021.

No large variation of hinge-moment coefficient with angle of attack occurred for Mach numbers less than 0.850. At Mach numbers greater than 0.850, however, erratic behavior results (fig. 35). The conventional hinge-moment parameters $\left(\Delta C_{h_a}/\Delta\delta_a\right)_\alpha$ and $\left(\Delta C_{h_a}/\Delta\alpha\right)_{\delta_a}$ show the same generally large variations previously noted at speeds exceeding a Mach number of 0.850 (fig. 36). Included in figure 36 are two-dimensional data from reference 6 for the same airfoil section and aileron (sealed gap) at a Mach number of 0.17 and with a Reynolds number of 9,000,000. Also included are data from unpublished tests of a 24-inch-chord NACA 66,1-115 airfoil section with a 0.20-chord plain aileron (0.002-chord gap). The general effects of compressibility on the hinge-moment parameters for the NACA 66,1-115 airfoil in two-dimensional flow are shown to be very similar to the results obtained in three-dimensional flow with the wing of the present tests.

No tests were made to determine the effect on the aerodynamic characteristics of fixing transition on the airfoil. Unpublished data obtained in the Langley 8-foot high-speed tunnel on a three-dimensional model of a horizontal tail of low-drag section and having roughness at 0.10 chord on both surfaces showed that fixing transition made the parameter $\left(dC_h/d\alpha\right)_\delta$ more negative, the parameter $\left(dC_h/d\delta\right)_\alpha$ less negative, and lessened the severity of the compressibility effects on both these parameters. Lifts were reduced but the general effects of compressibility on lift were the same.

The data on the resultant pressure coefficient ΔP across the aileron seal (fig. 37) are useful for determining the amount of balance of internally balanced aileron systems. The curve of ΔP against aileron deflection is seen to be approximately linear for positive aileron deflections but the slope of the curve decreases for negative deflections. At supercritical speeds, smaller seal-pressure coefficients would be expected at negative deflections as a result of the general ineffectiveness of the ailerons at these deflections. At subcritical speeds, however, these data are in variance with the low-speed ($M = 0.17$) two-dimensional data of reference 6 and with the data from unpublished low-speed ($M = 0.21$) tests made in the Langley stability tunnel of a three-dimensional model of a horizontal tail, both of which show a linear variation of resultant seal pressure for both positive and negative aileron deflections. Tests of a partly sealed aileron (reference 11) show that negative aileron deflections are somewhat less effective in modifying seal pressures than positive deflections at Mach numbers from 0.3 to 0.7.

From the hinge-moment data, no serious compressibility effects on hinge-moment characteristics are indicated for an airplane with the wing-aileron combination tested and designed to operate at maximum level-flight Mach numbers up to 0.830. At higher Mach numbers (approx. 0.880) comparable to those obtained in dives, a possibility of flexibility-induced aileron snatch exists for an airplane having an aileron control system of inadequate stiffness.

Wing-Torsional Consideration

From the high-speed aerodynamic data of these tests, some calculations of the effect of wing twist on the rolling characteristics have been made for an airplane of 104.5-foot span. The torsional stiffness of the wing was assumed to vary inversely as the cube of the distance from the wing center line (reference 12). The spanwise distribution of wing twist resulting from the spanwise distribution of pitching moment due to aileron deflection was thus obtained and the opposing rolling moment due to wing twist could then be determined by use of the section twist, the experimentally determined rate of change of section normal-force coefficient with angle of attack $dc_n/d\alpha$, and the distance to the spanwise station from the center line. The calculations indicated that in order for the airplane with an assumed wing span of 104.5 feet to retain at least 25 percent of the rigid-wing rolling effectiveness (fig. 32) at a Mach number of 0.880 and sea-level conditions, a wing with a minimum torsional stiffness at the midspan of the ailerons of 6,400,000 foot-pounds per radian must be obtained. The required torsional stiffness for the same rolling effectiveness for similar wings on airplanes of different size varies as the cube of the wing span (reference 12) and conversion of the torsional requirements from one airplane to another is therefore straightforward.

The rate of change of pitching-moment coefficient with aileron deflection was found in these tests to vary approximately as the factor $1/\sqrt{1 - M^2}$ up to a Mach number of 0.880. Calculations of the torsional stiffness, obtained for a Mach number of 0.880 by the method of reference 12 from the low-speed data of reference 6 and extended to a Mach number of 0.880 by the factor $1/\sqrt{1 - M^2}$, indicated that a minimum torsional stiffness of the wing at the aileron midspan of 6,080,000 foot-pounds per radian is required to retain 25 percent of the rigid-wing rolling effectiveness. Beyond a Mach number of 0.880, an abrupt decrease occurs in the rate at which the pitching-moment coefficient varies with aileron deflection so that at a Mach number of 0.900 the rate is only about one-fourth that at a Mach number of 0.880. The present tests show, therefore, that the low-speed aerodynamic data for this wing can be satisfactorily extended for wing-twist calculations by

the factor $1/\sqrt{1 - M^2}$ up to the Mach number where the break in rate of change of pitching-moment coefficient with aileron deflection occurs but at Mach numbers beyond this break where, for example, wing reversal speeds are to be determined, actual experimental data should be used.

CONCLUSIONS

Tests at high speeds were made in the Langley 8-foot high-speed tunnel of a wing of high aspect ratio with straight-sided-profile 0.20-chord plain ailerons of 37.5 percent wing semispan. For an airplane with this particular wing-aileron combination, the wind-tunnel data indicate the following conclusions.

1. The ailerons are satisfactory for producing rolling moment on an airplane designed to operate at maximum level-flight Mach numbers up to 0.830. In dives at which the airplane would operate at higher Mach numbers the ailerons still produce some rolling moment at zero and positive lifts up to the maximum test Mach number of 0.925, although, at these higher Mach numbers, their effectiveness is decreased.

2. No serious compressibility effects are indicated on the aileron hinge-moment characteristics for level-flight Mach numbers up to 0.830. At higher Mach numbers (approx. 0.880) comparable to those obtained in dives, flexibility-induced aileron snatch is possible for an airplane having an aileron control system of inadequate stiffness.

Langley Memorial Aeronautical Laboratory
National Advisory Committee for Aeronautics
Langley Field, Va.,

REFERENCES

1. Whitcomb, Richard T.: Investigation of the Characteristics of a High-Aspect-Ratio Wing in the Langley 8-Foot High-Speed Tunnel. NACA RM No. L6H28a, 1946.

2. Ferri, Antonio: Preliminary Investigation of Downwash Fluctuations of a High-Aspect-Ratio Wing in the Langley 8-Foot High-Speed Tunnel. NACA RM No. L6H28b, 1946.

3. Mattson, Axel T.: Investigation of Dive Brakes and a Dive-Recovery Flap on a High-Aspect-Ratio Wing in the Langley 8-Foot High-Speed Tunnel. NACA RM No. L6H28c, 1946.

4. Swanson, Robert S., and Toll, Thomas A.: Jet-Boundary Corrections for Reflection-Plane Models in Rectangular Wind Tunnels. NACA ARR No. 3E22, 1943.

5. Graham, Donald J.: Tunnel-Wall Corrections to Rolling and Yawing Moments Due to Aileron Deflection in Closed Rectangular Wind Tunnels. NACA ARR No. 4F21, 1945.

6. Underwood, William J., Braslow, Albert L., and Cahill, Jones F.: Two-Dimensional Wind-Tunnel Investigation of 0.20-Airfoil-Chord Plain Ailerons of Different Contour on an NACA 65_1-210 Airfoil Section. NACA ACR No. L5F27, 1945.

7. Ferri, Antonio: Completed Tabulation in the United States of Tests of 24 Airfoils at High Mach Numbers (Derived from Interrupted Work at Guidonia, Italy, in the 1.31-by 1.74-Foot High-Speed Tunnel). NACA ACR No. L5E21, 1945.

8. Lindsey, W. F.: Effect of Compressibility on the Pressures and Forces Acting on a Modified 65,3-019 Airfoil Having a 0.20-Chord Flap. NACA ACR No. L5G31a 1946.

9. Swanson, Robert S., and Toll, Thomas A.: Estimation of Stick Forces from Wind-Tunnel Aileron Data. NACA ARR No. 3J29, 1943.

10. Becker, John V., and Korycinski, Peter F.: Aerodynamic Tests of a Full-Scale TBF-1 Aileron Installation in the Langley 16-Foot High-Speed Tunnel. NACA ARR No. L4K22, 1944.

11. Laitone, Edmund V.: An Investigation of 0.15-Chord Ailerons on a Low-Drag Tapered Wing at High Speeds. NACA ACR No. 4I25, 1944.

12. Pearson, Henry A., and Aiken, William S., Jr.: Charts for the Determination of Wing Torsional Stiffness Required for Specified Rolling Characteristics or Aileron Reversal Speed. NACA ACR No. L4L13, 1944.

TABLE I

DIMENSIONS OF WING-TIP SHAPE

[See fig. 2]

Plan-form contour		
Distance from tip, y_t (in.)	Distance forward of 25-percent-chord line, x_f (in.)	Distance rearward of 25-percent-chord line, x_r (in.)
0	-0.360	0.360
.026	.041	.963
.053	.176	1.168
.079	.268	1.307
.105	.337	1.413
.158	.436	1.565
.236	.529	1.710
.341	.595	1.817
.473	.623	1.868

Section contour		
Distance from tip, y_t (in.)	Lower-surface ordinate, z_L (in.)	Upper-surface ordinate, z_U (in.)
0.026	0.024	0.076
.053	.041	.093
.079	.052	.105
.105	.061	.113
.158	.074	.126
.236	.086	.138
.341	.094	.147
.473	.098	.151

NATIONAL ADVISORY
COMMITTEE FOR AERONAUTICS

TABLE II

ORDINATES FOR NACA 65-210 AIRFOIL

[Stations and ordinates in percent wing chord]

Upper surface		Lower surface	
Station	Ordinate	Station	Ordinate
0	0	0	0
.435	.819	.565	-.719
.678	.999	.822	-.859
1.169	1.273	1.331	-1.059
2.408	1.757	2.592	-1.385
4.898	2.491	5.102	-1.859
7.394	3.069	7.606	-2.221
9.894	3.555	10.106	-2.521
14.899	4.338	15.101	-2.992
19.909	4.938	20.091	-3.346
24.921	5.397	25.079	-3.607
29.936	5.732	30.064	-3.788
34.951	5.954	35.049	-3.894
39.968	6.067	40.032	-3.925
44.984	6.058	45.016	-3.868
50.000	5.915	50.000	-3.709
55.014	5.625	54.986	-3.435
60.027	5.217	59.973	-3.075
65.036	4.712	64.964	-2.652
70.043	4.128	69.957	-2.184
75.045	3.479	74.955	-1.689
80.044	2.783	79.956	-1.191
85.038	2.057	84.962	-.711
90.028	1.327	89.972	-.293
95.014	.622	94.986	.010
100.000	0	100.000	0

L. E. radius: 0.687. Slope of radius through end of chord: 0.084

NATIONAL ADVISORY
COMMITTEE FOR AERONAUTICS

CONFIDENTIAL

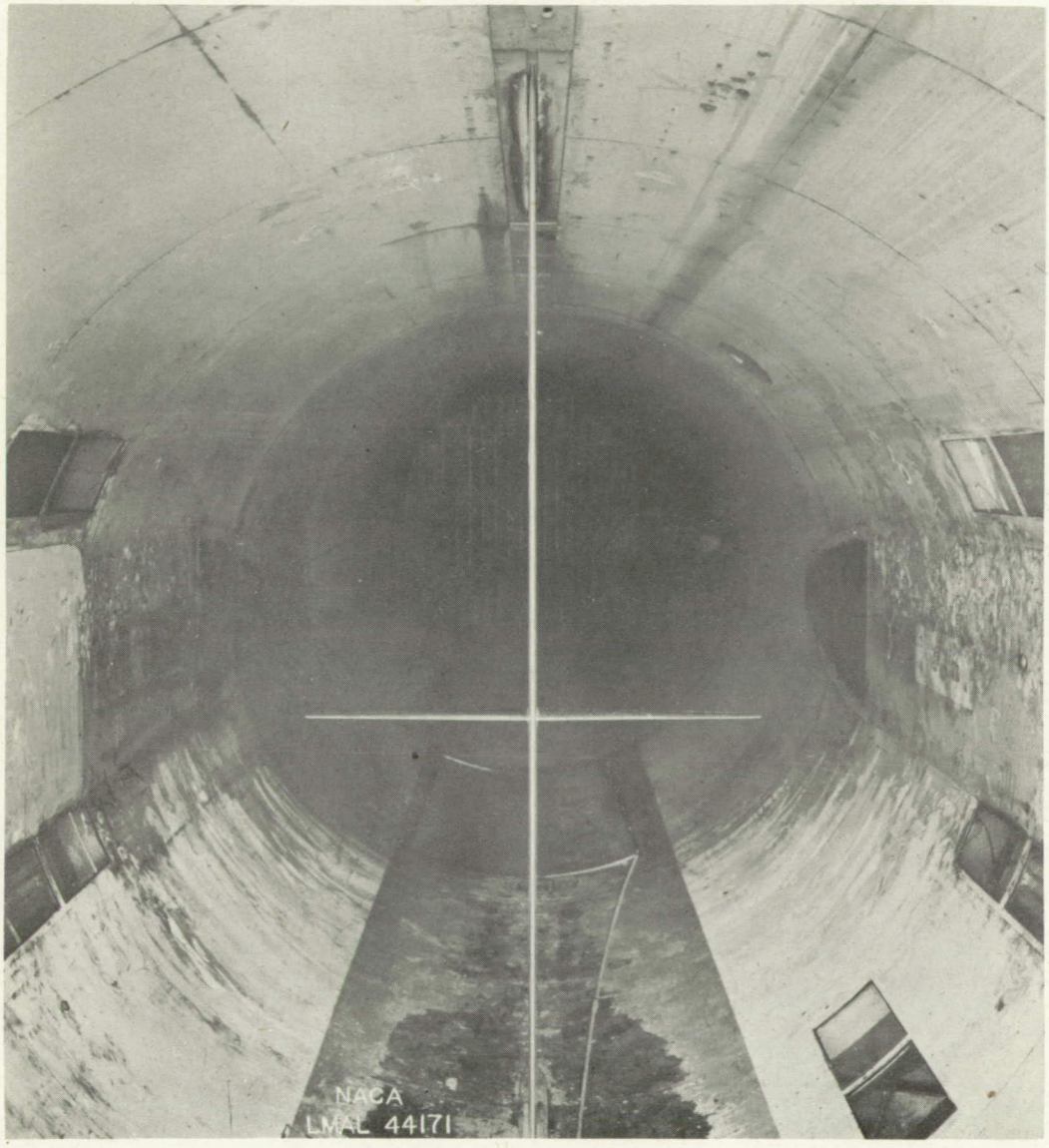

(a) Front view.

Figure 1.- Wing of high aspect ratio mounted on vertical support plate in Langley 8-foot high-speed tunnel.

CONFIDENTIAL

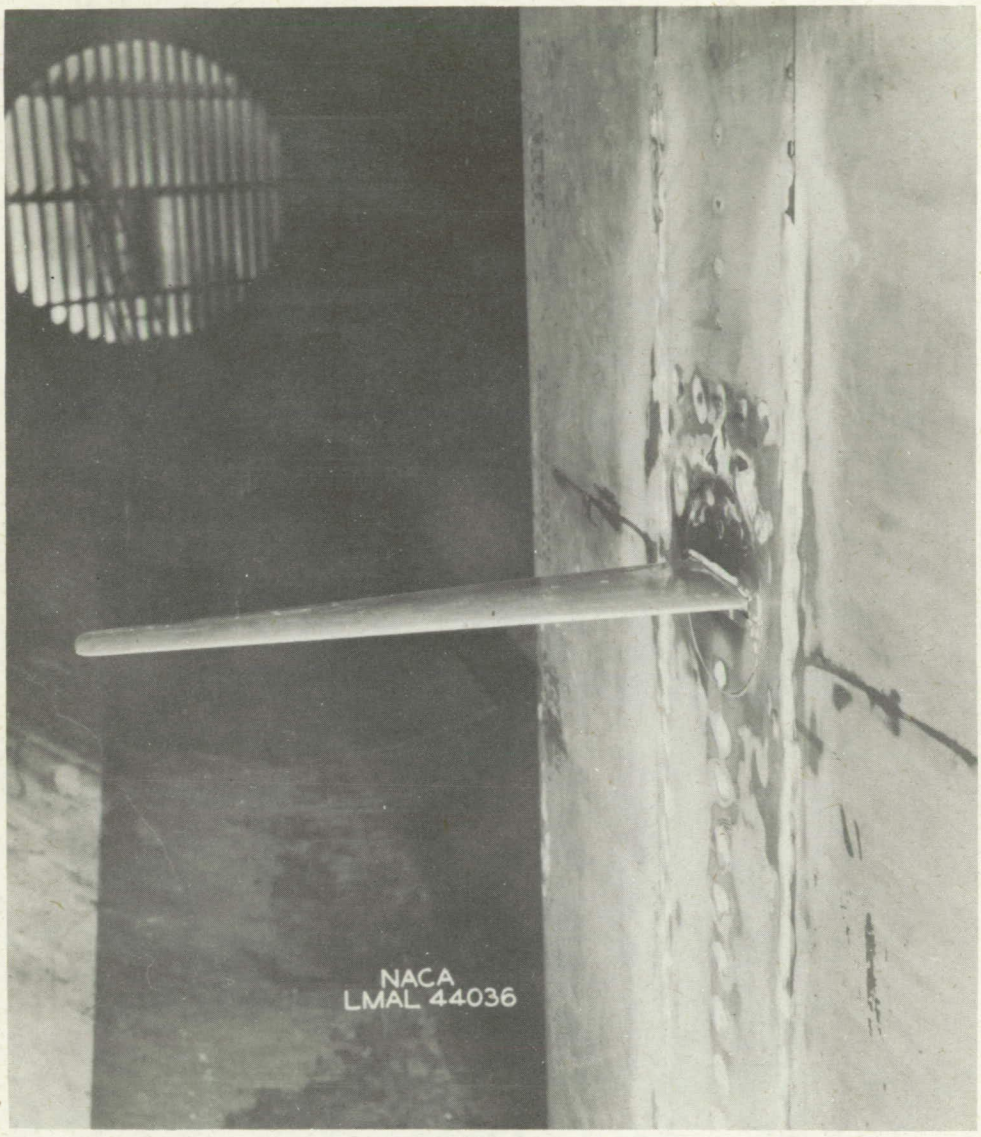

(b) Three-quarter view of right wing.

Figure 1.- Concluded.

CONFIDENTIAL

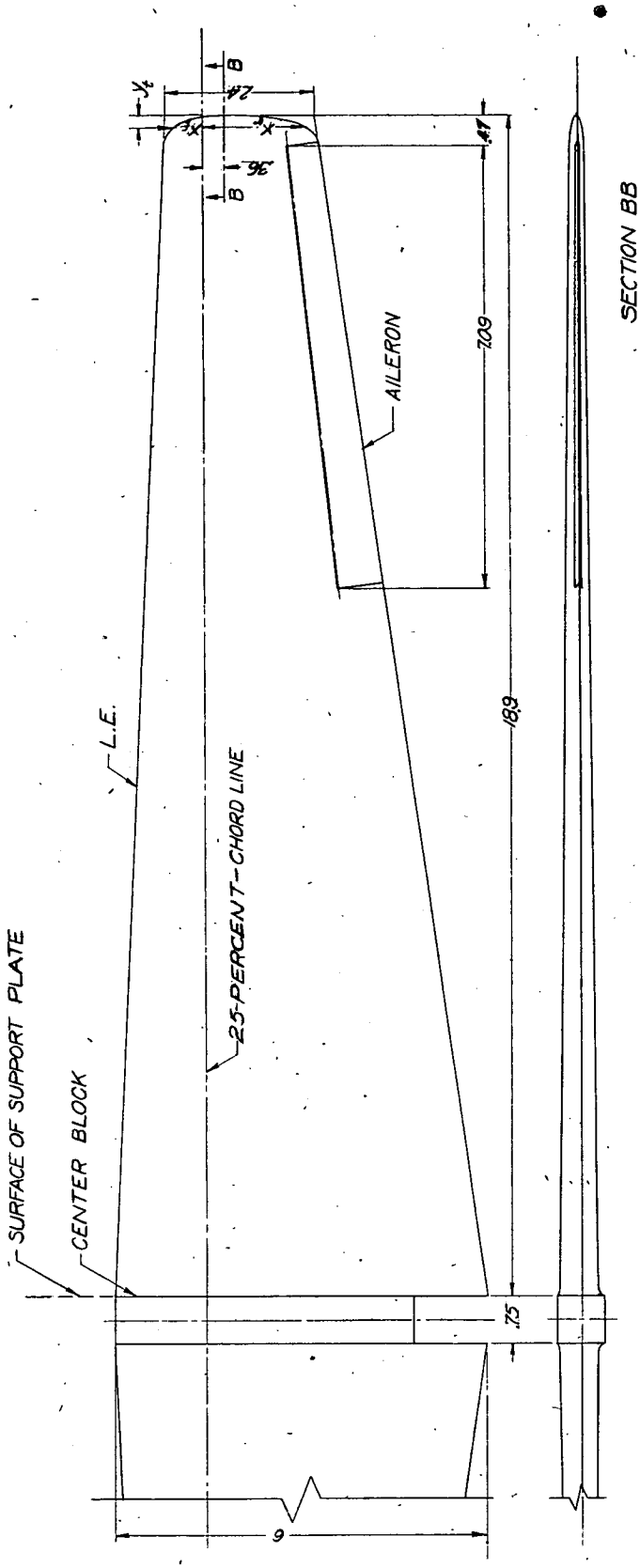

FIGURE 2.-WING DIMENSIONS.

CONFIDENTIAL

CONFIDENTIAL

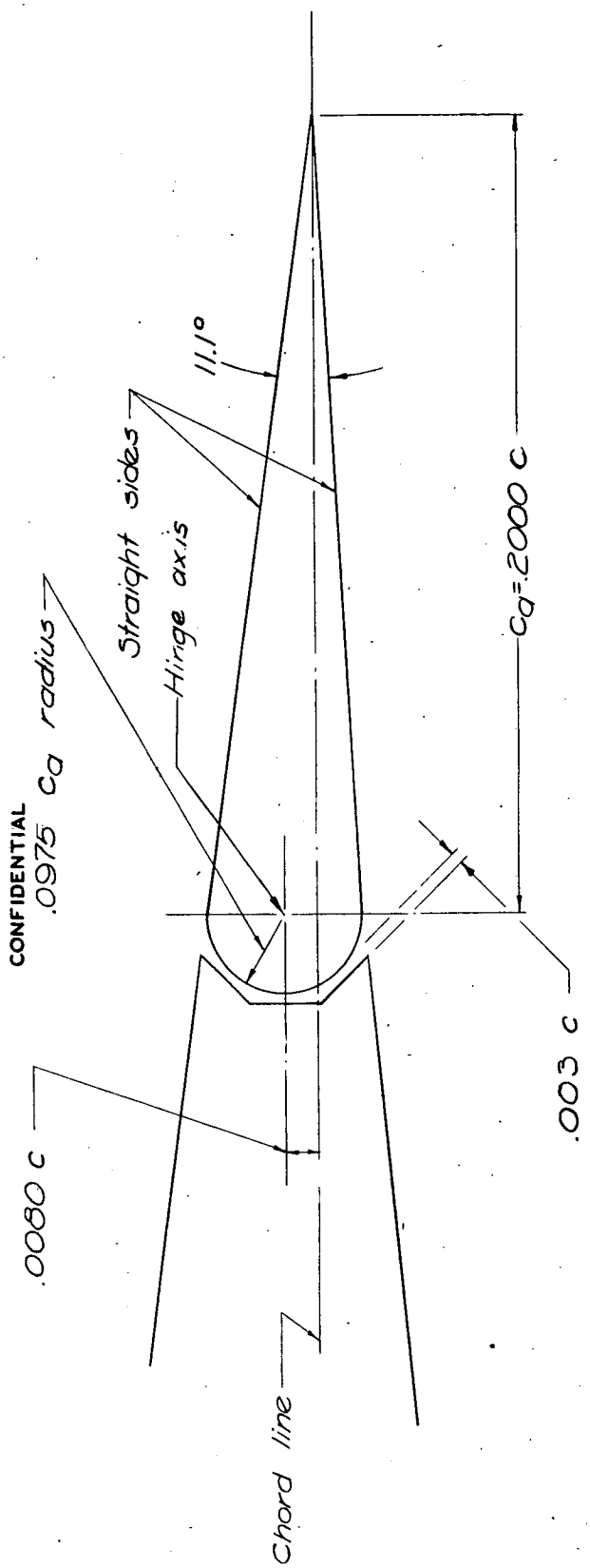

Figure 3.- Dimensions of constant-chord ailerons used on NACA 65-210 wing.

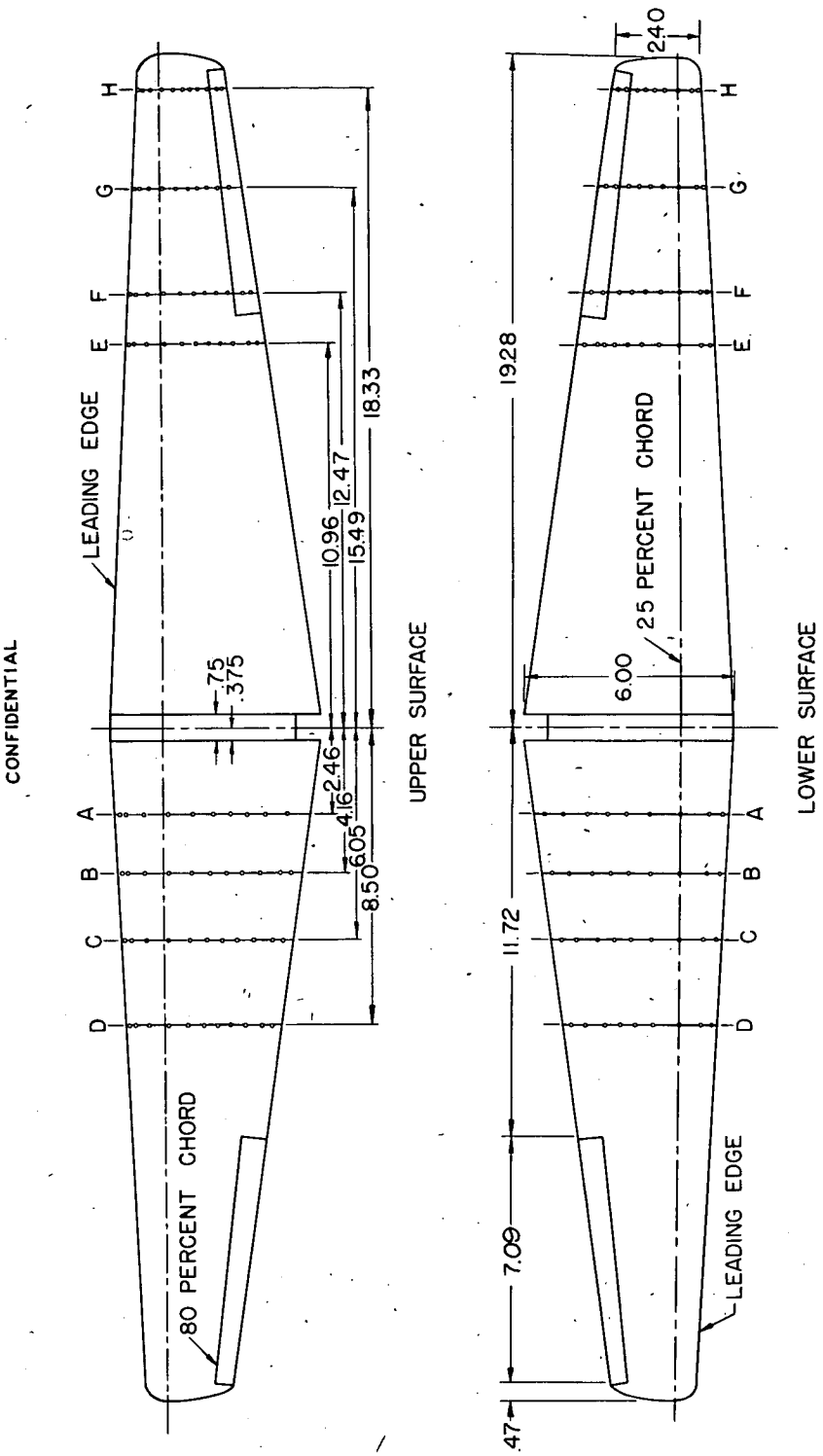

FIGURE 4.- SPAN LOCATIONS OF PRESSURE ORIFICES.
(ALL DIMENSIONS ARE IN INCHES.)

CONFIDENTIAL

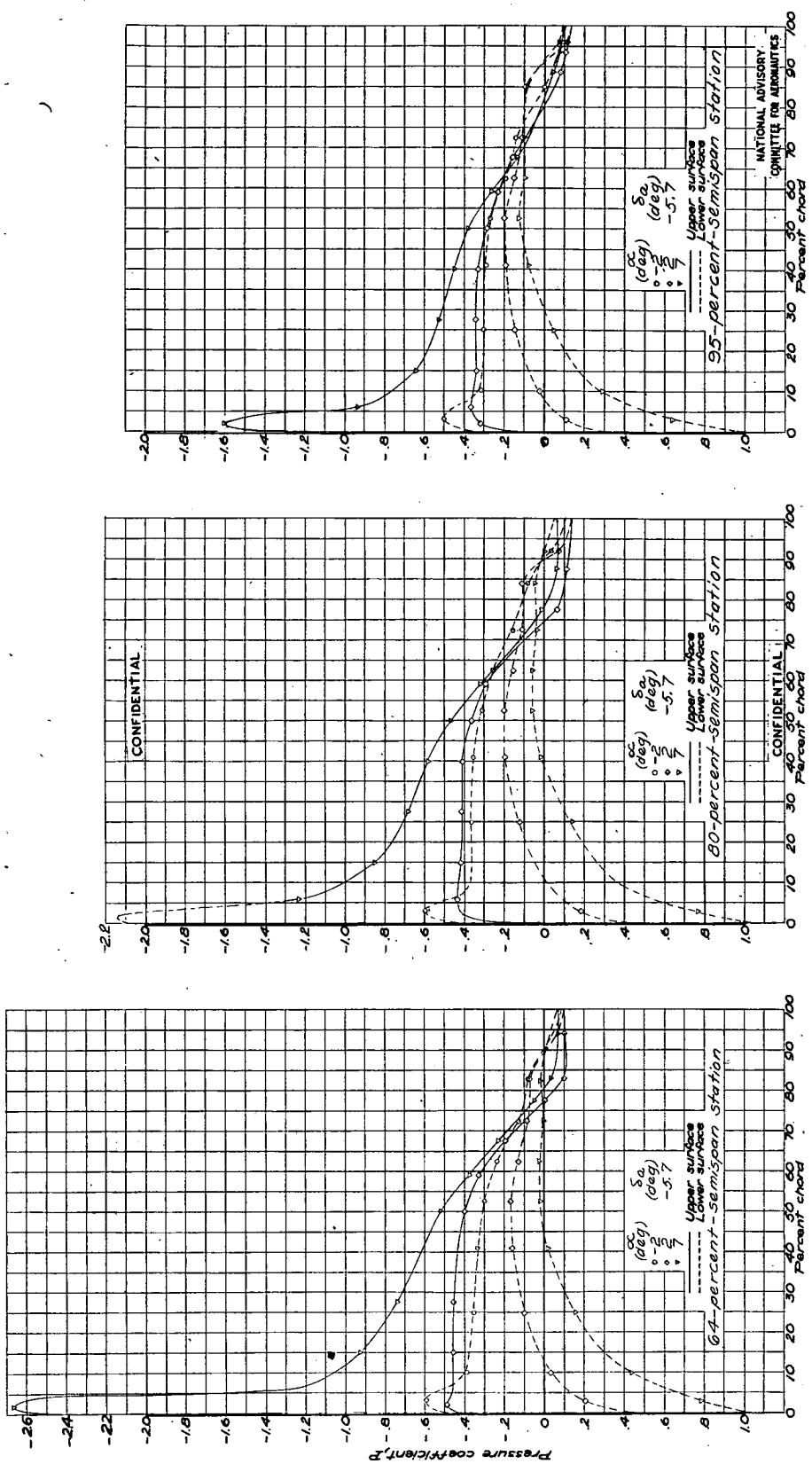

(a) $M = 0.400$.

Figure 5.- Pressure distribution about the wing and aileron at three spanwise stations. $\delta_a = -5.7°$.

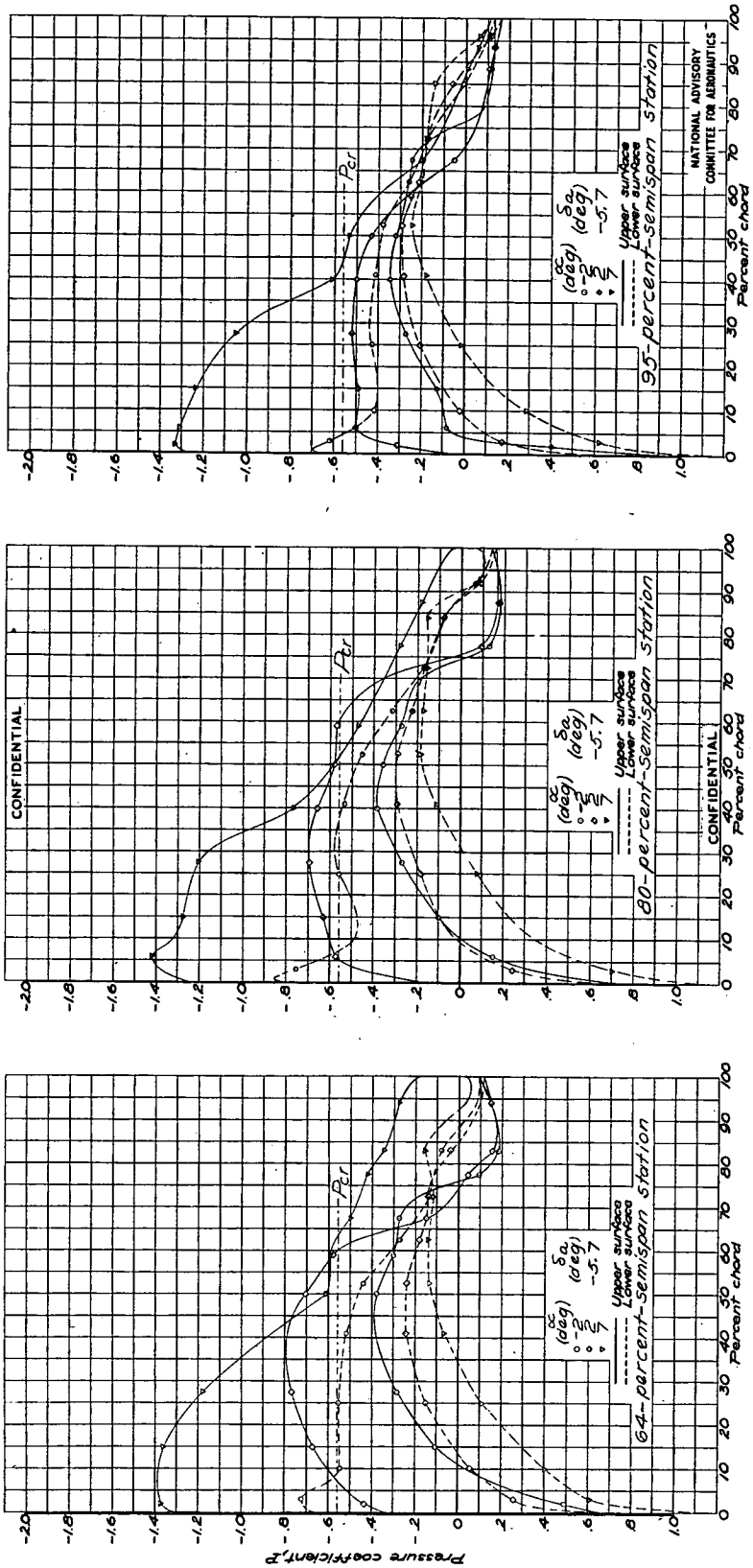

(b) M=0.760. Continued.

Figure 5.

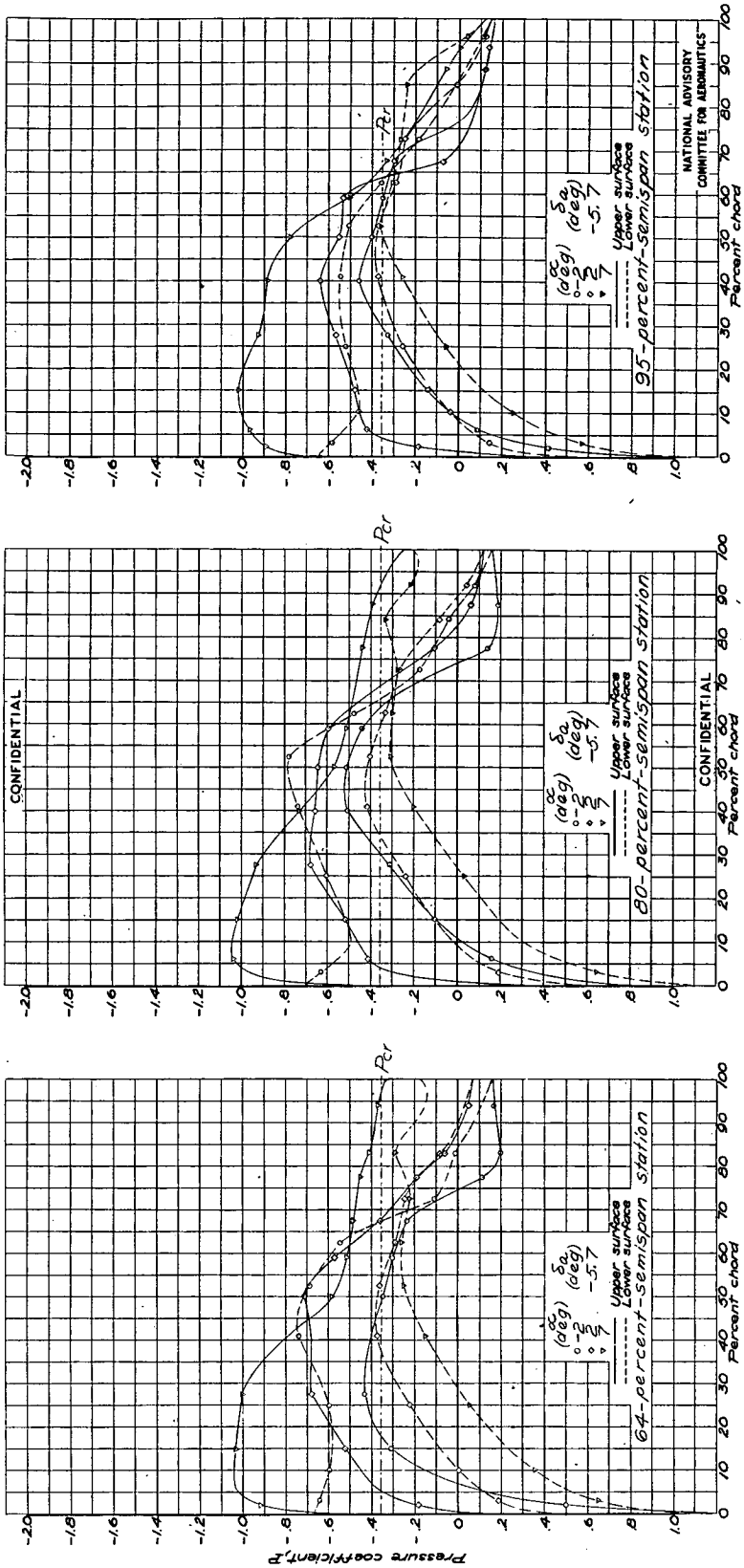

(c) $M = 0.827$.

Figure 5.- Continued.

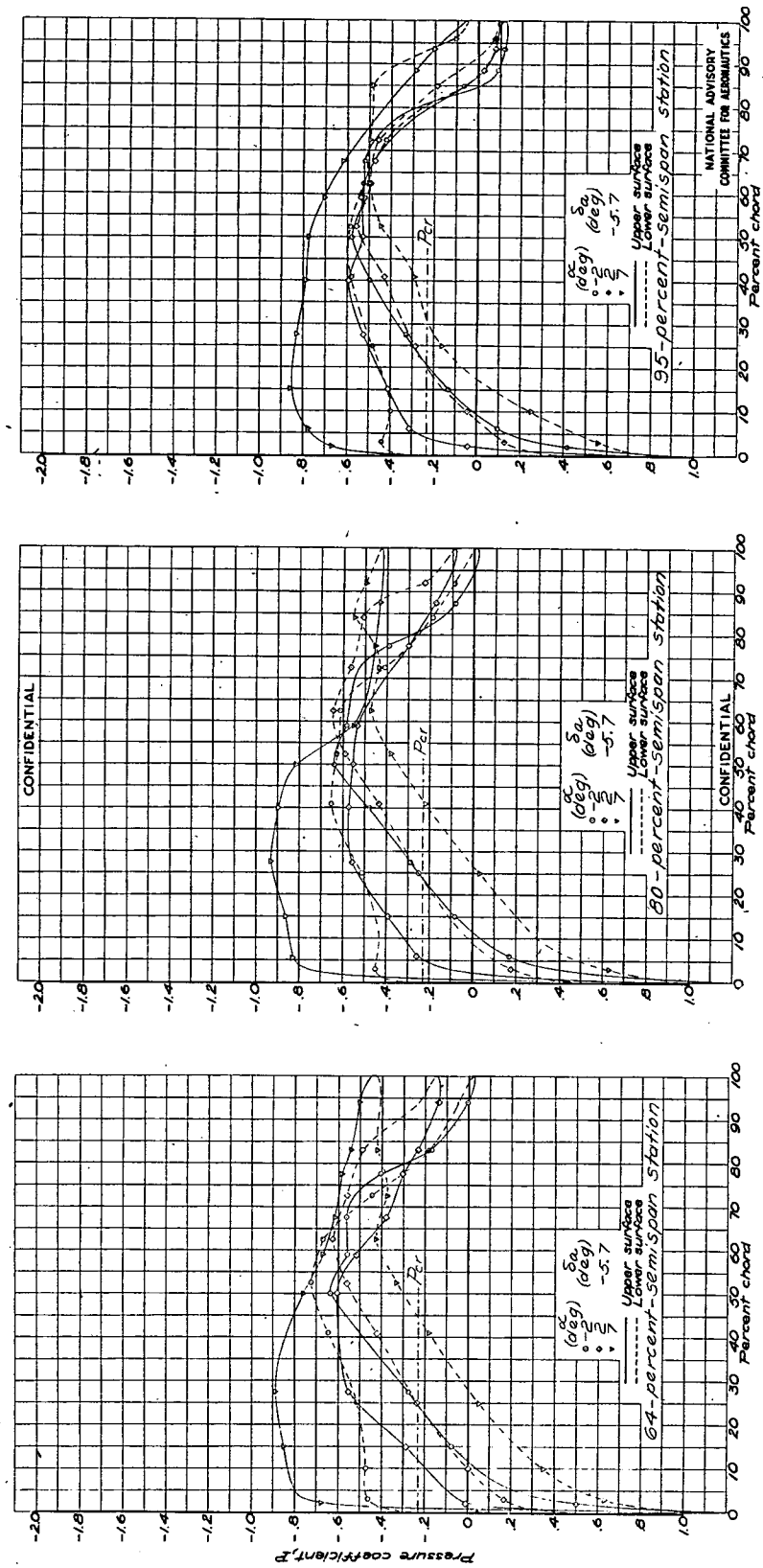

(g) $M = 0.880$.

Figure 5.- Continued.

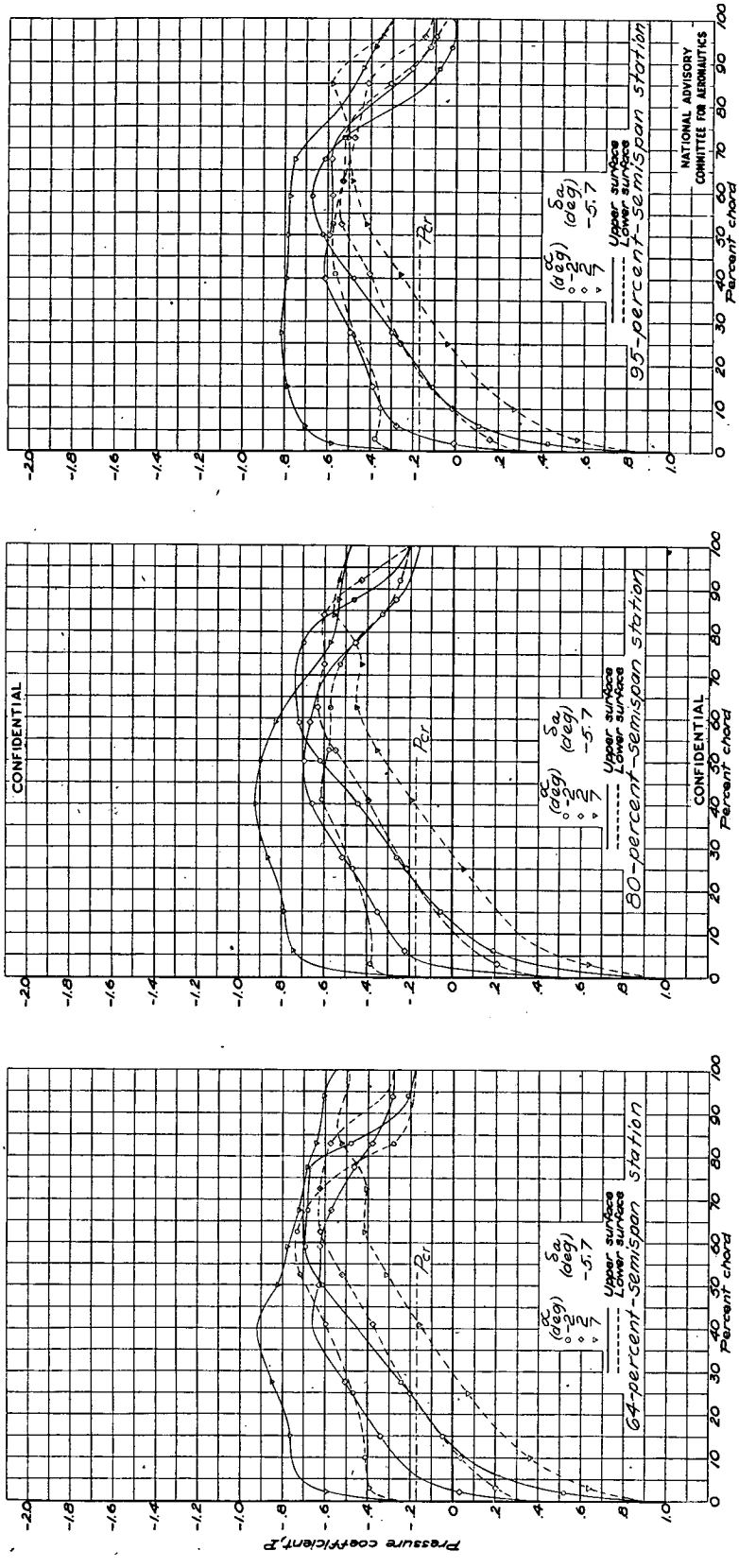

(e) M=0.907.

Figure 5.- Continued.

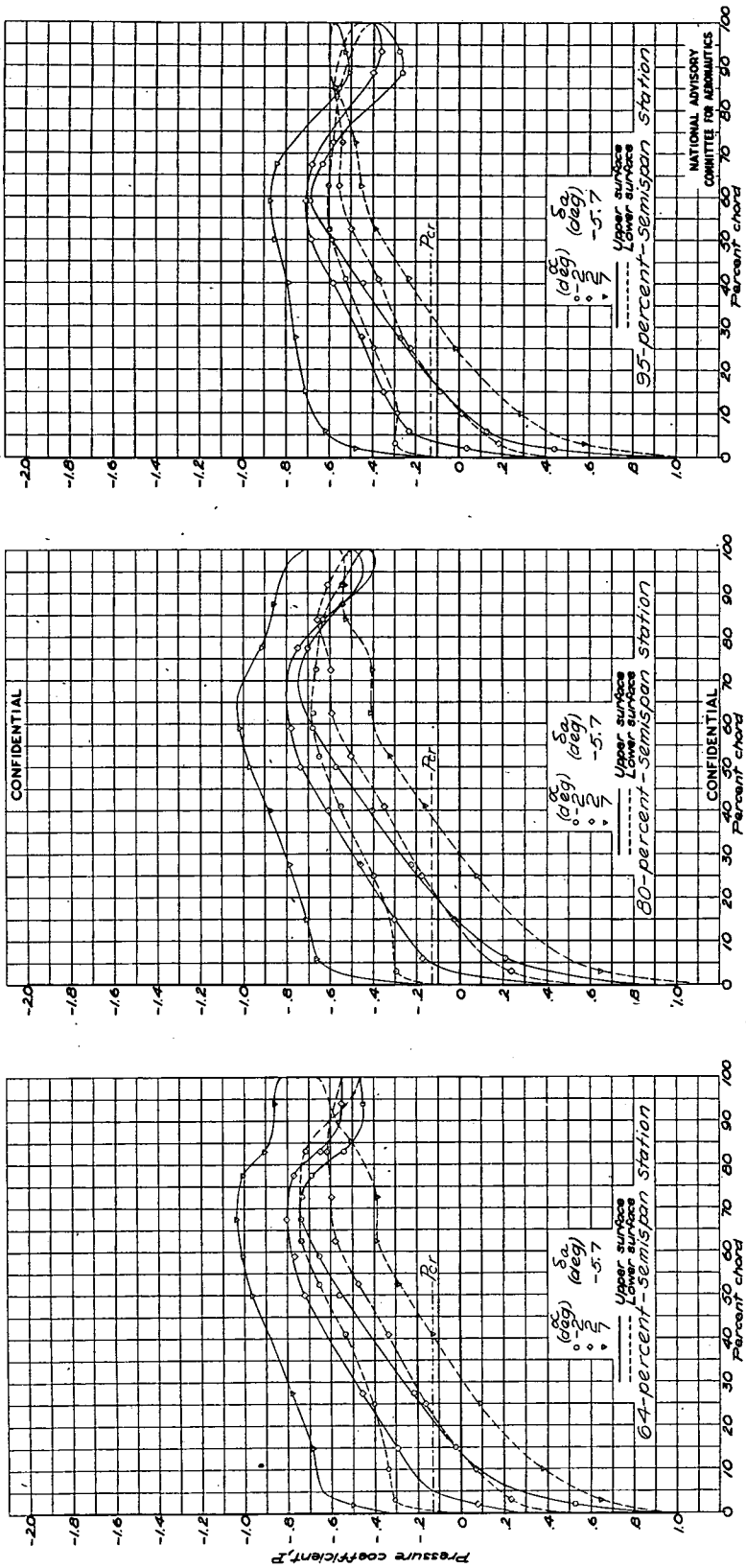

(f) $M = 0.925$ (Uncorrected)

Figure 5. - Concluded.

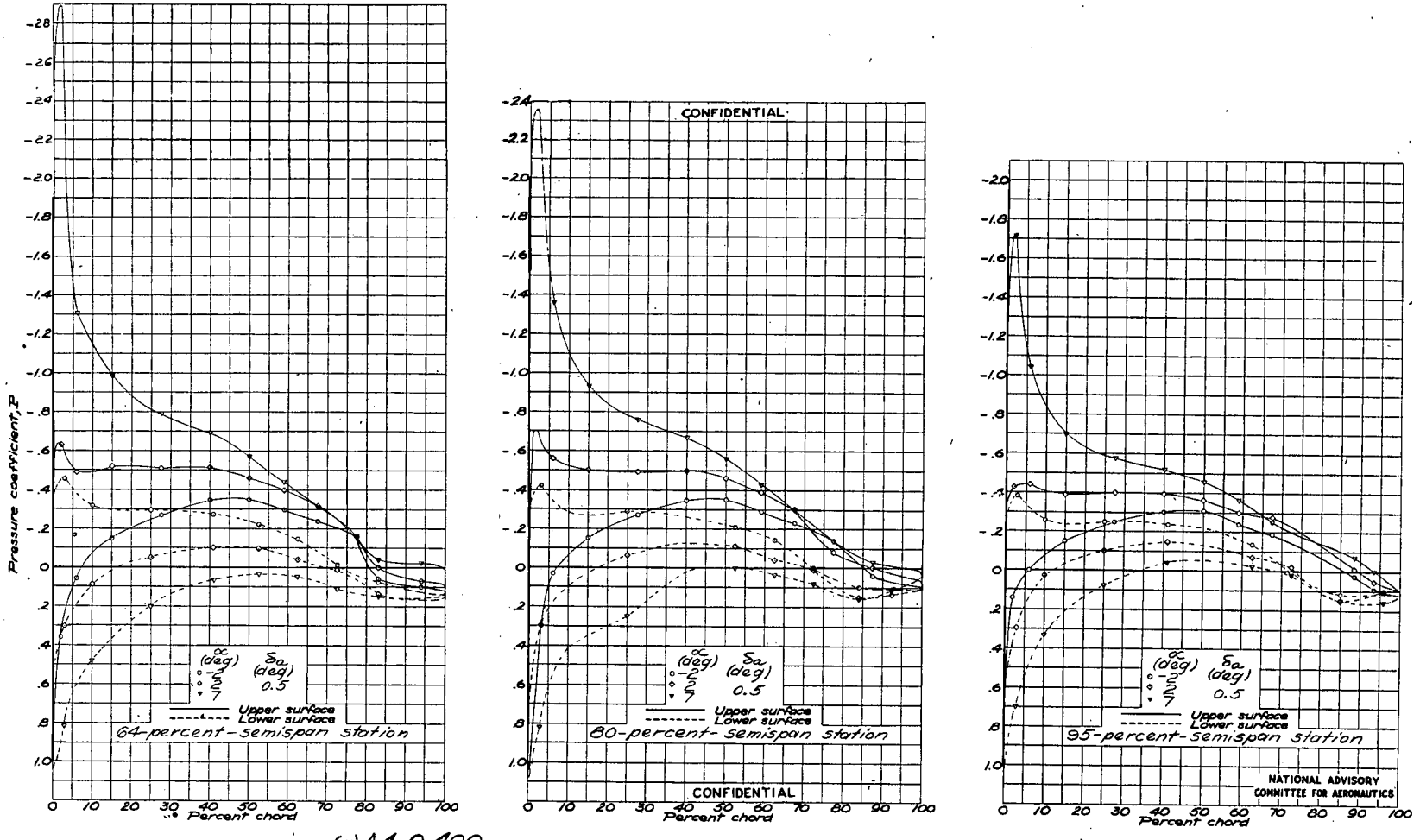

(a) $M = 0.400$.

Figure 6.- Pressure distribution about the wing and aileron at three spanwise stations. $\delta_a = 0.5°$.

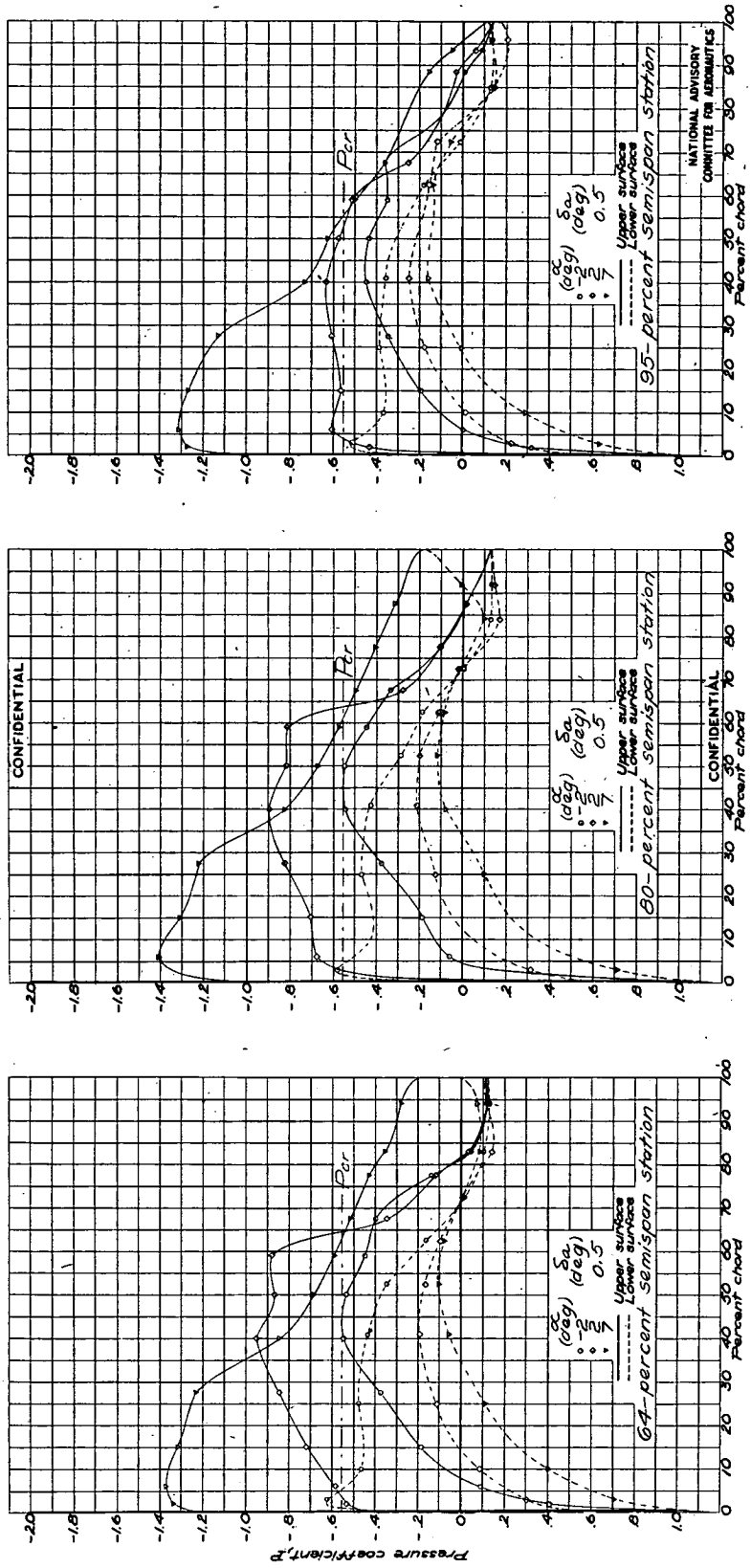

(b) M=0.760. Continued.
Figure 6.- Continued.

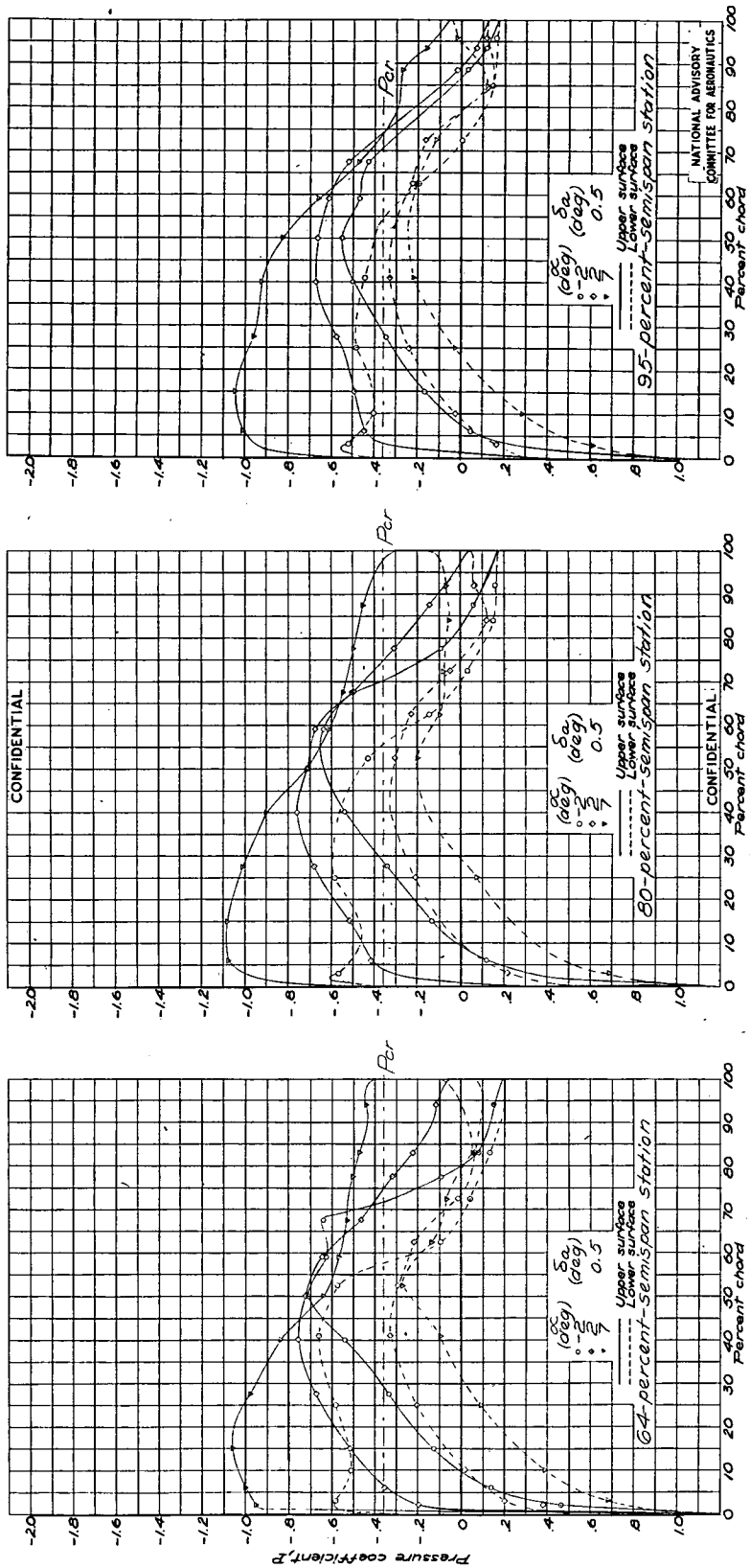

(c) M=0.827.

Figure 6. - Continued.

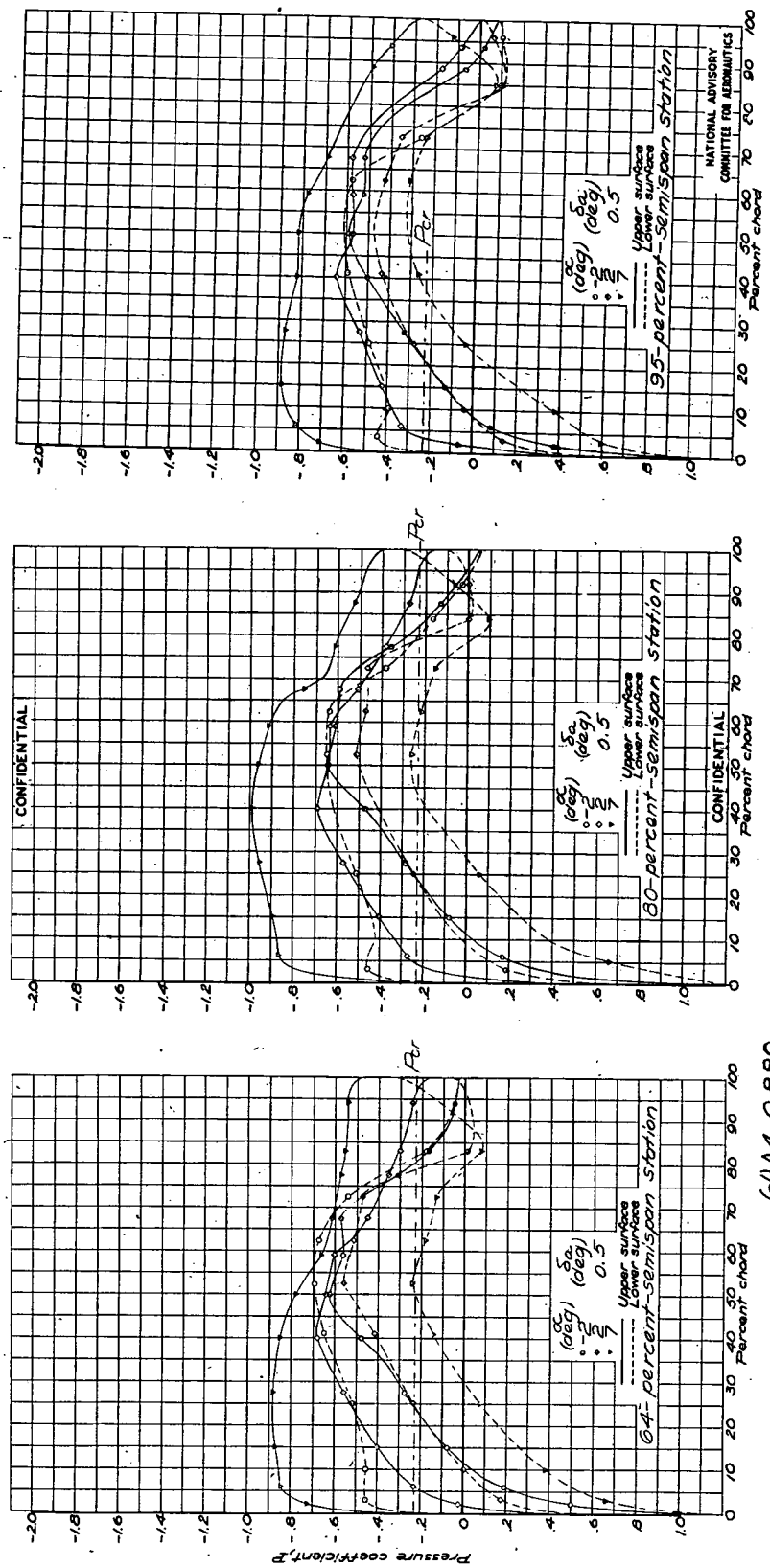

(a) $M = 0.880$.

Figure 6.- Continued.

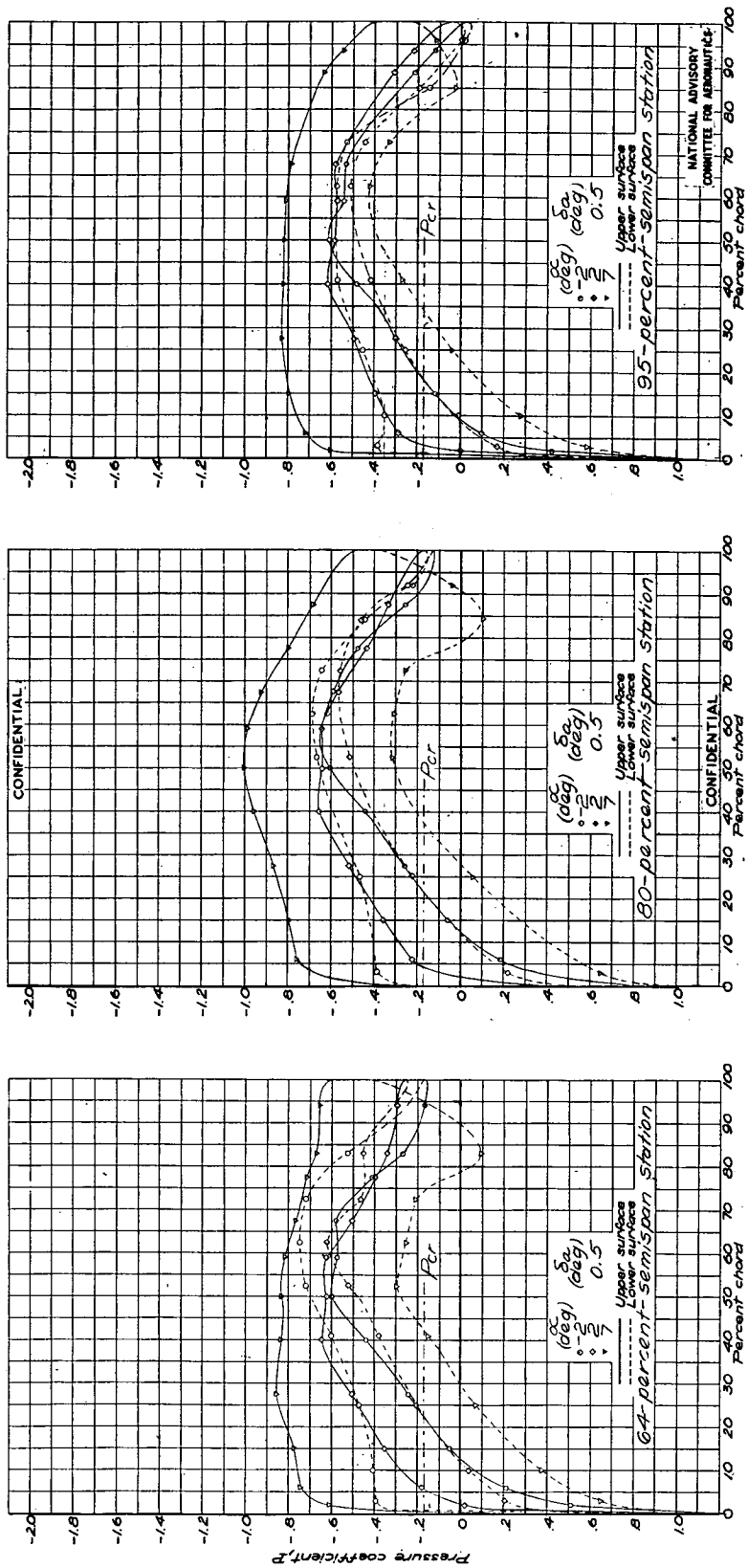

(e) M = 0.907. - Continued.

Figure 6.

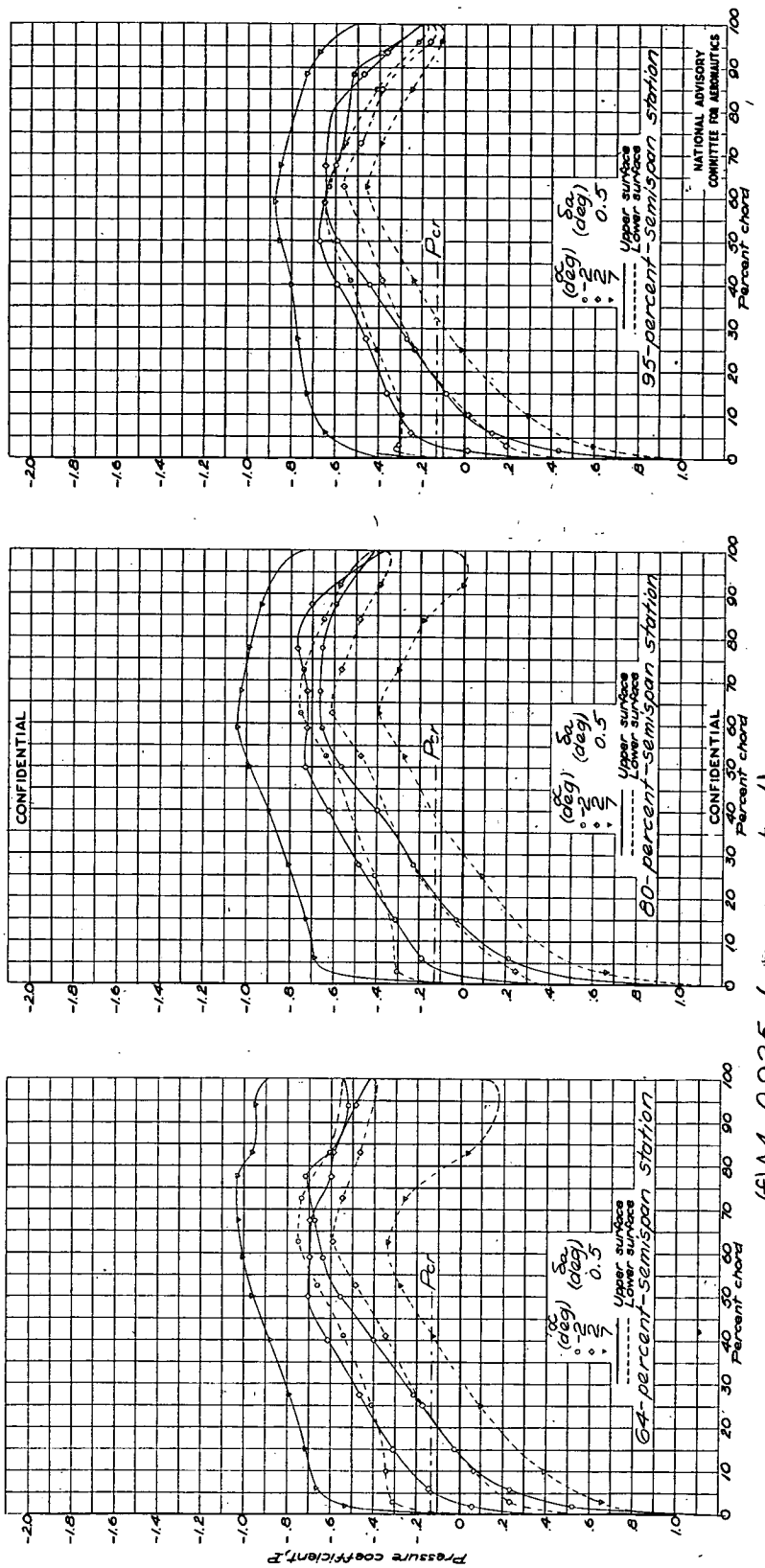

(f) $M = 0.925$ (uncorrected).

Figure 6.- Concluded.

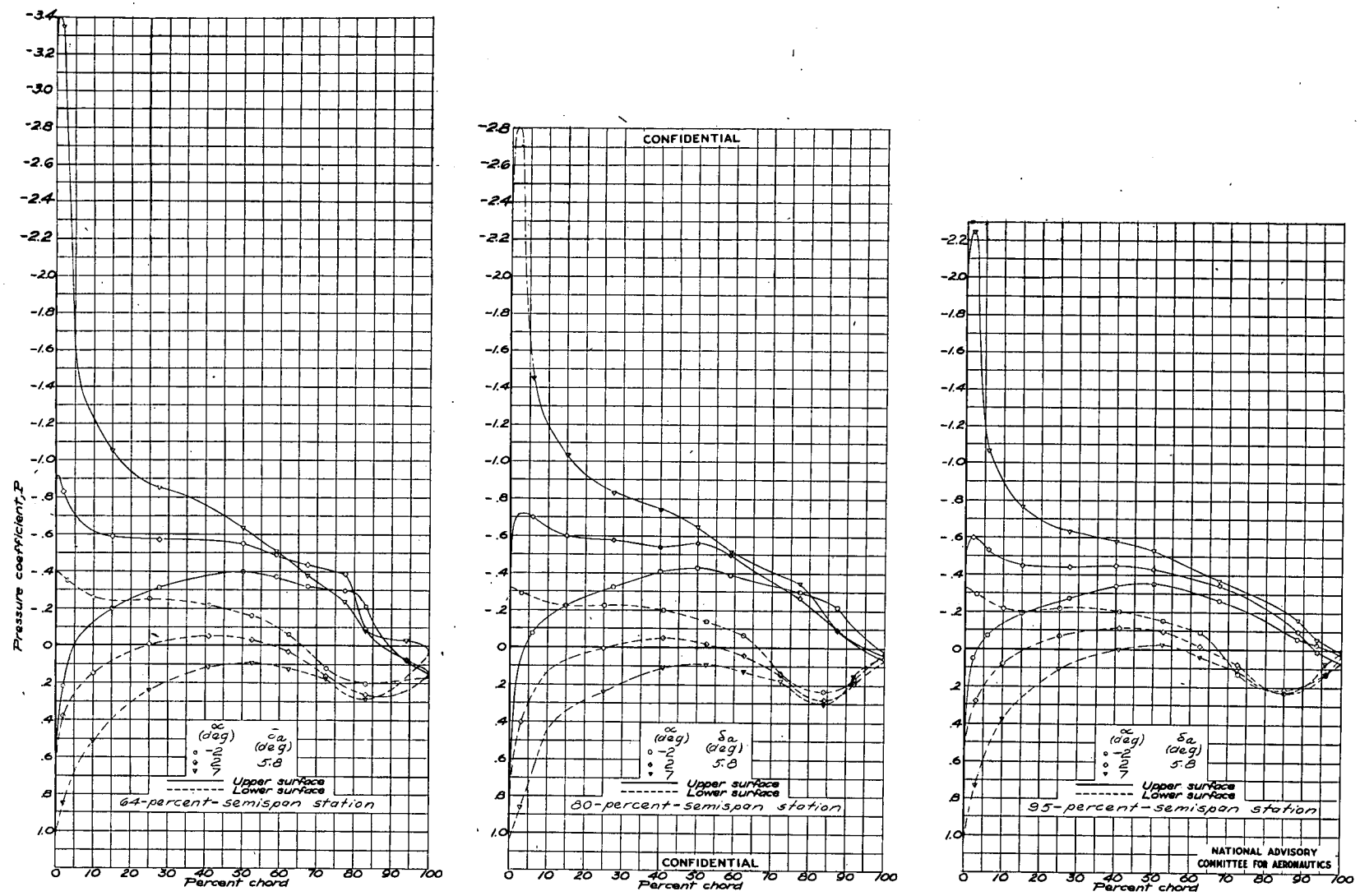

(a) M = 0.400.

Figure 7.- Pressure distribution about the wing and aileron at three spanwise stations. $\delta_a = 5.8°$.

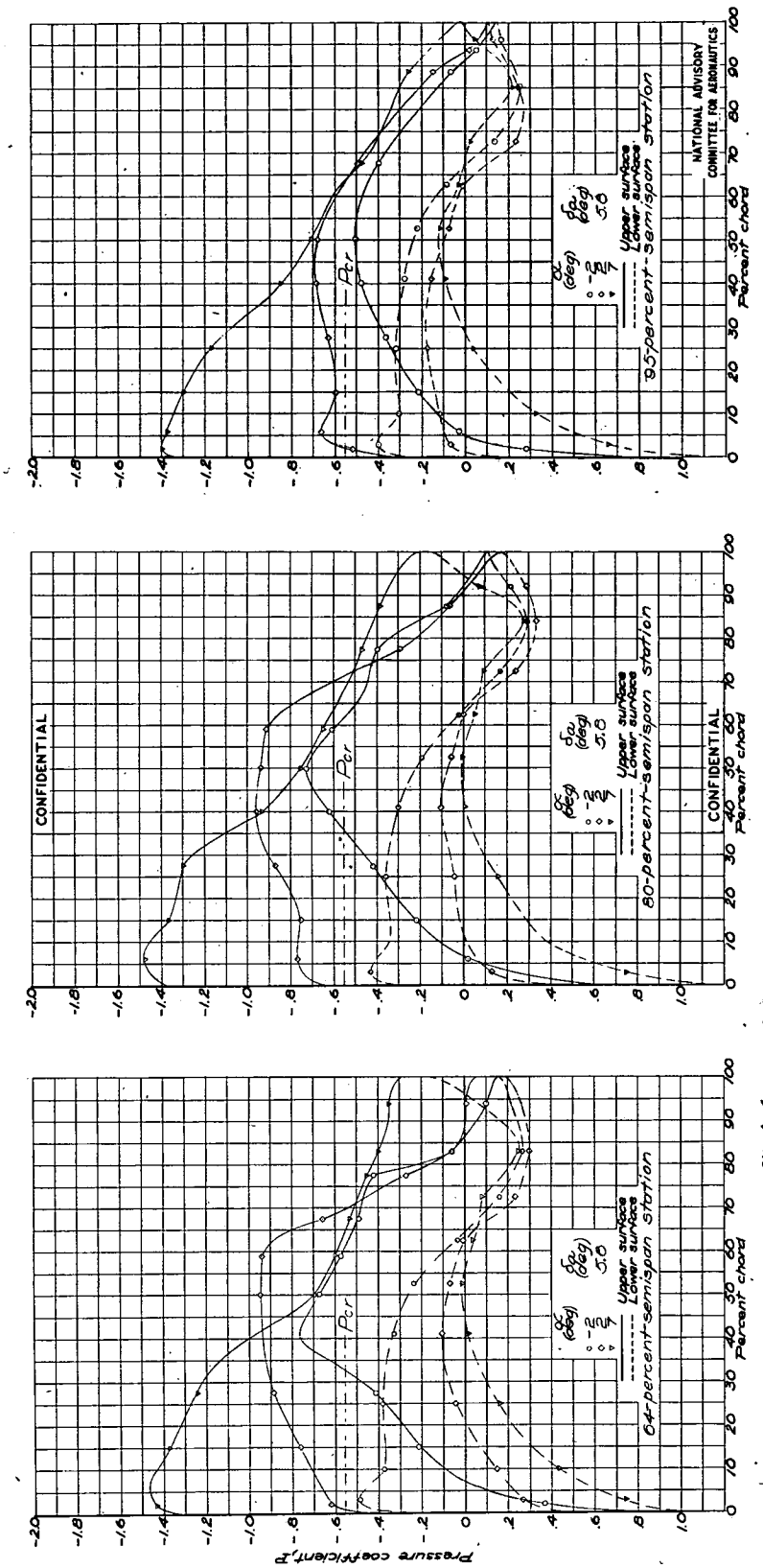

(b) M = 0.760. Continued.

Figure 7.- Continued.

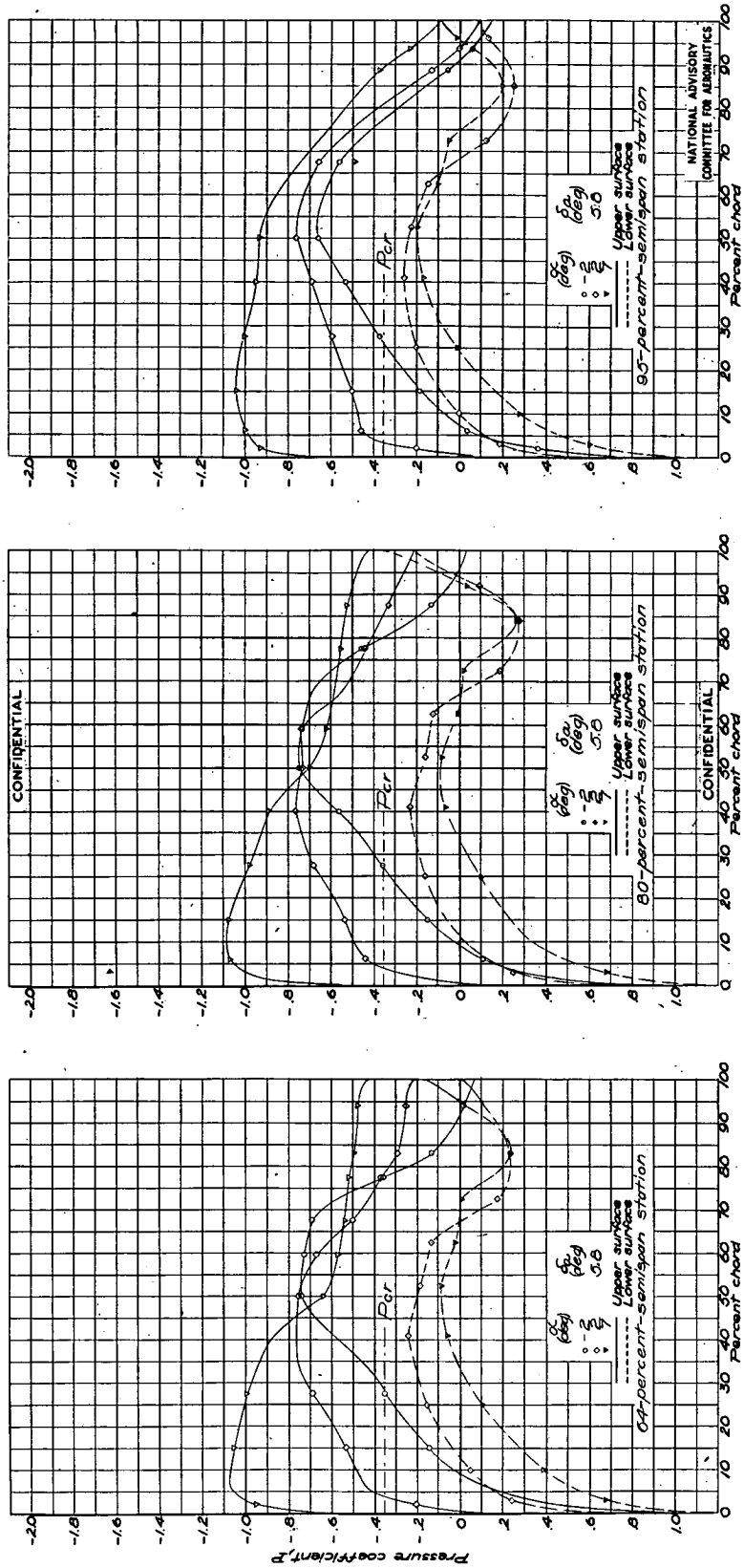

(c) M=0.827

Figure 7.- Continued.

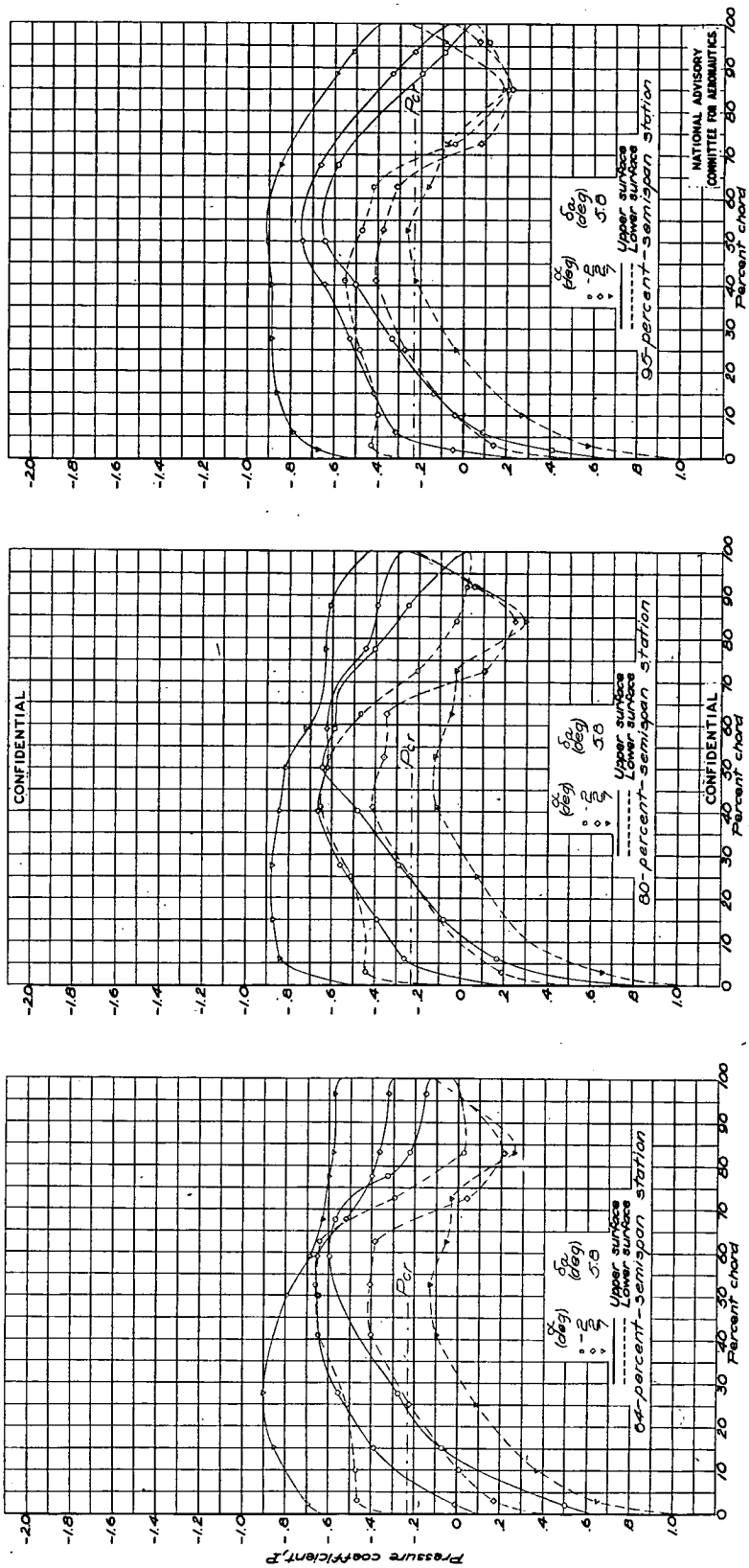

(d) M=0.880.

Figure 7. - Continued.

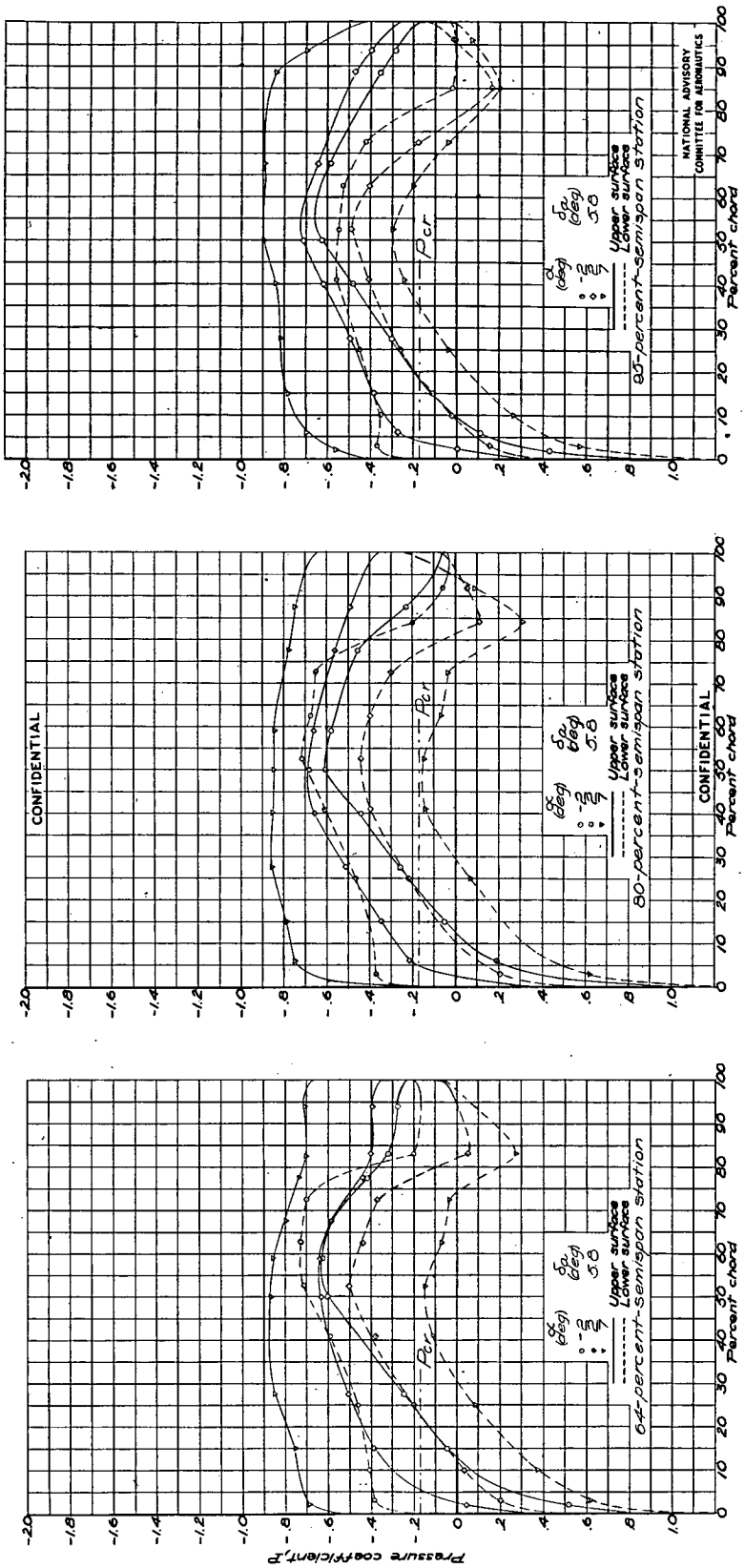

(e) $M=0.907$. Figure 7.- Continued.

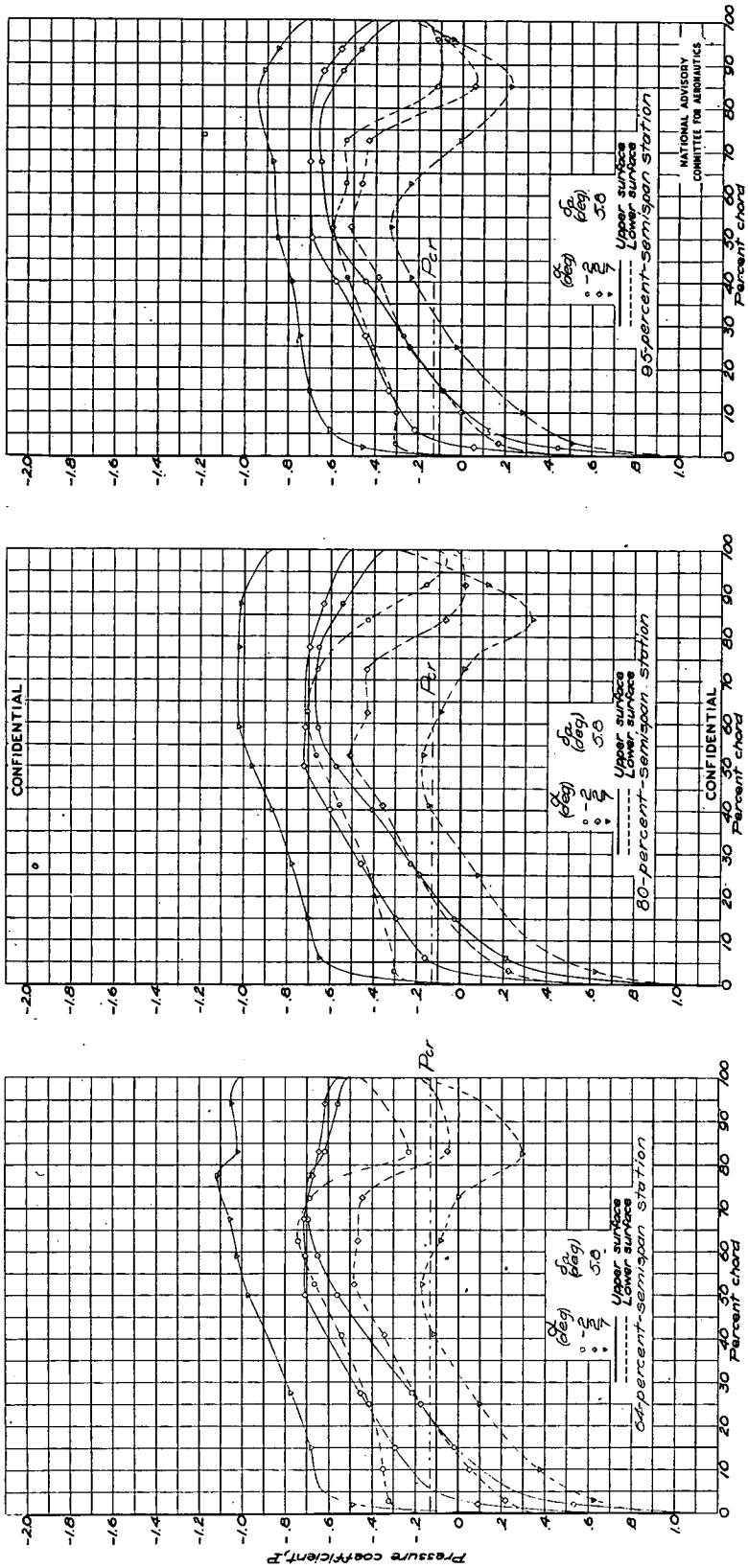

(f) M=0.925 (uncorrected).

Figure 7.- Concluded.

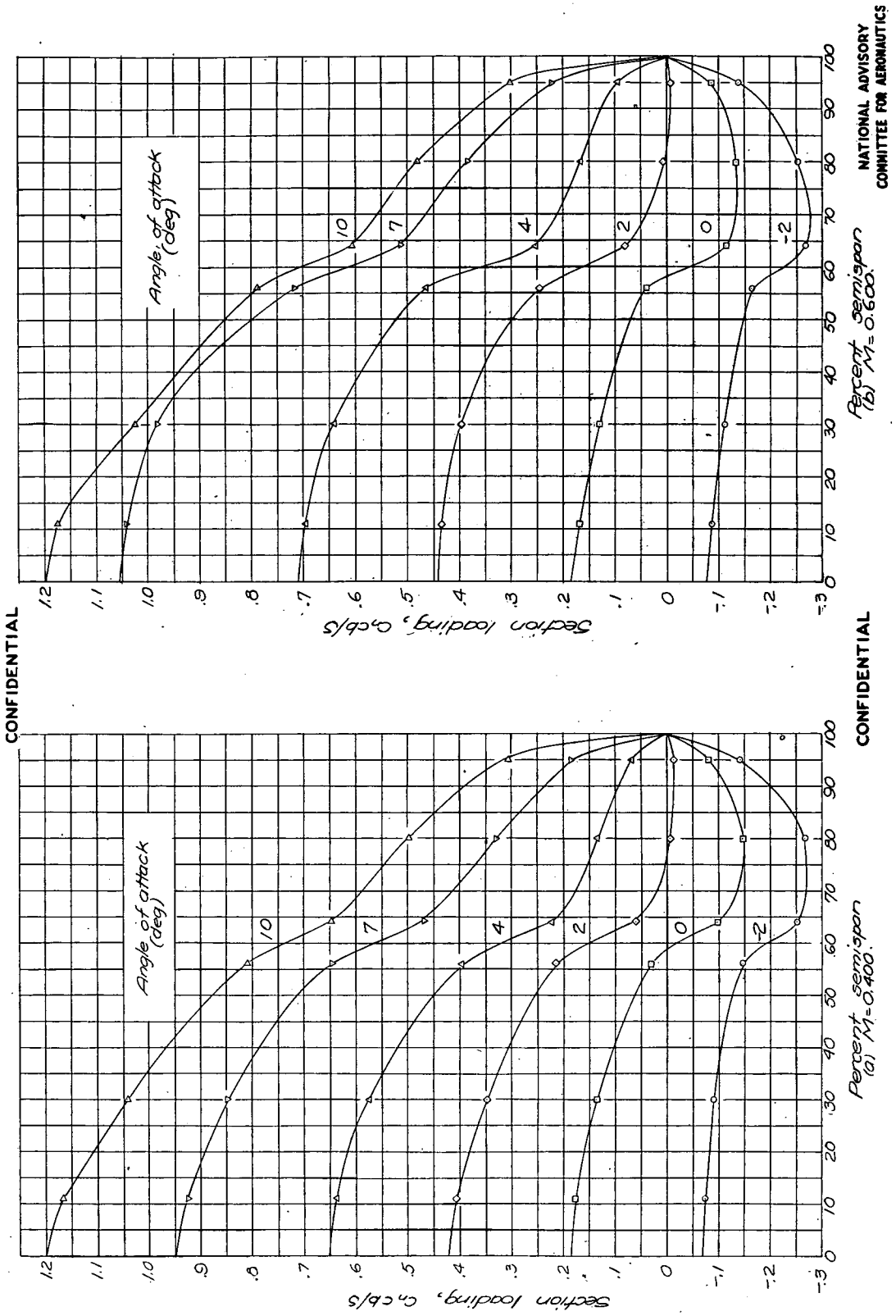

Figure 8.- Spanwise variation in section loading. δ_a=10.0°.

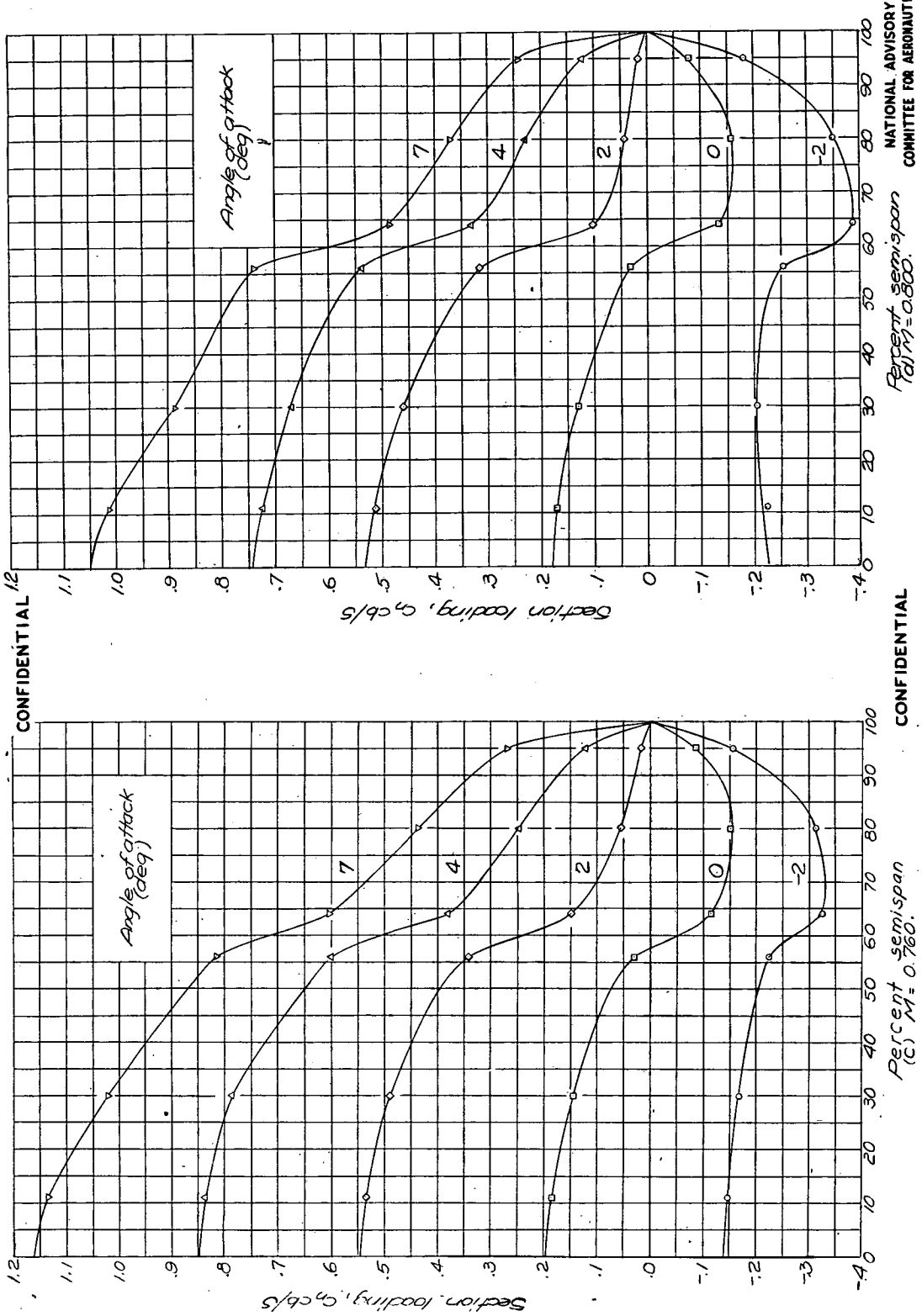

Figure 8.- Continued. $\delta_0 = -10.0°$.

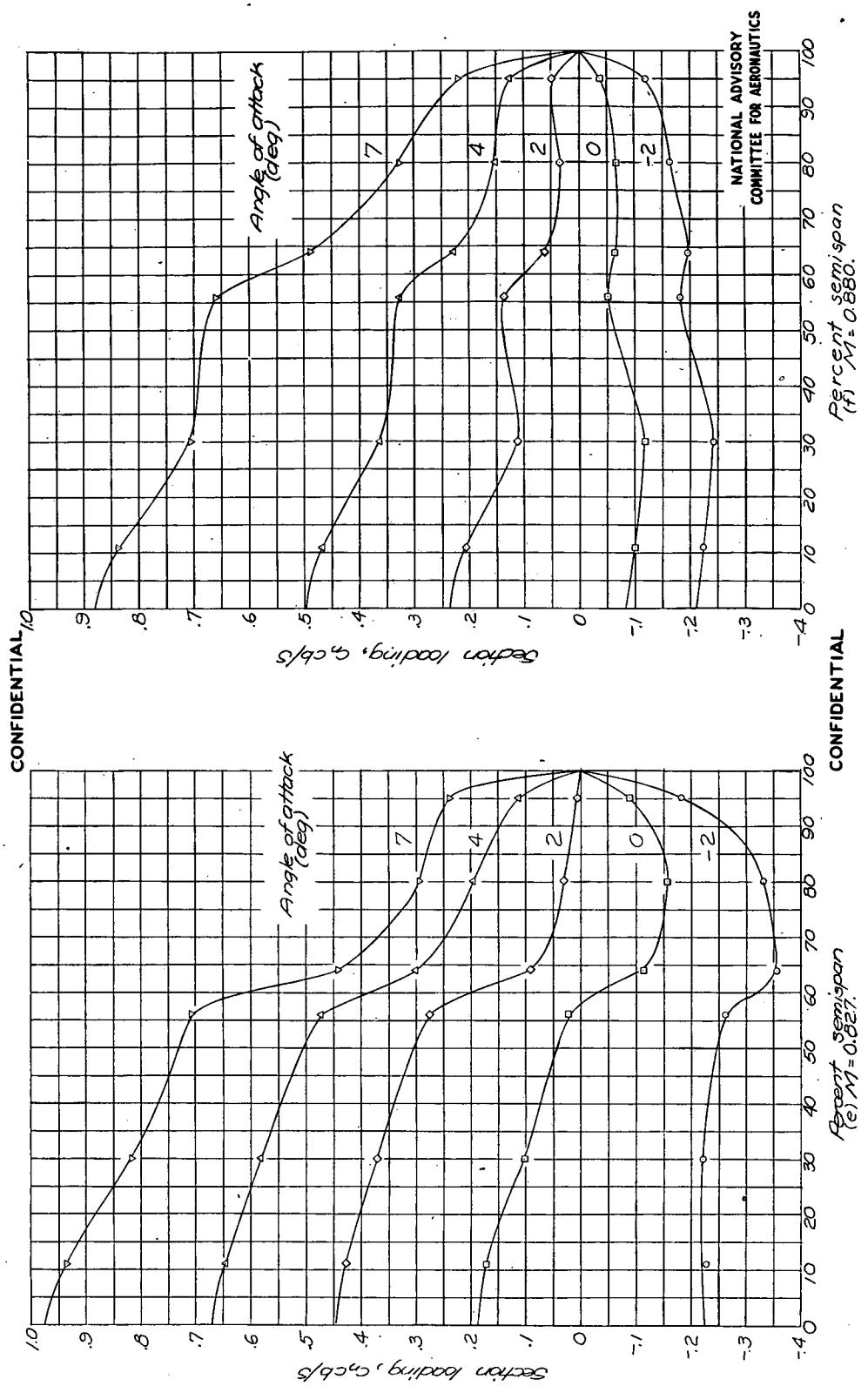

Figure 8.- Continued. $\delta_a = -10.0°$.

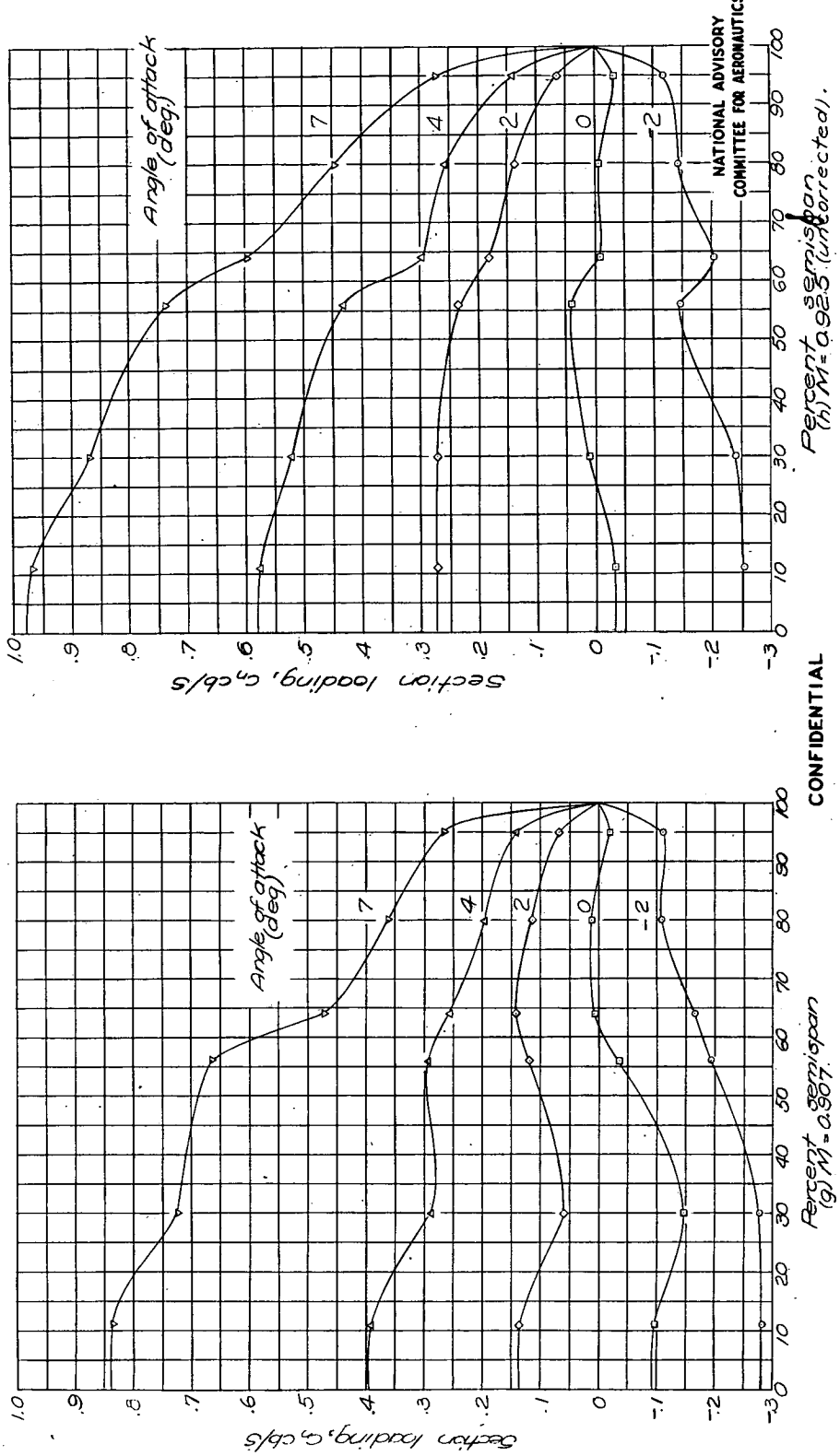

Figure 8. - Concluded. $\delta_a = -10.0°$

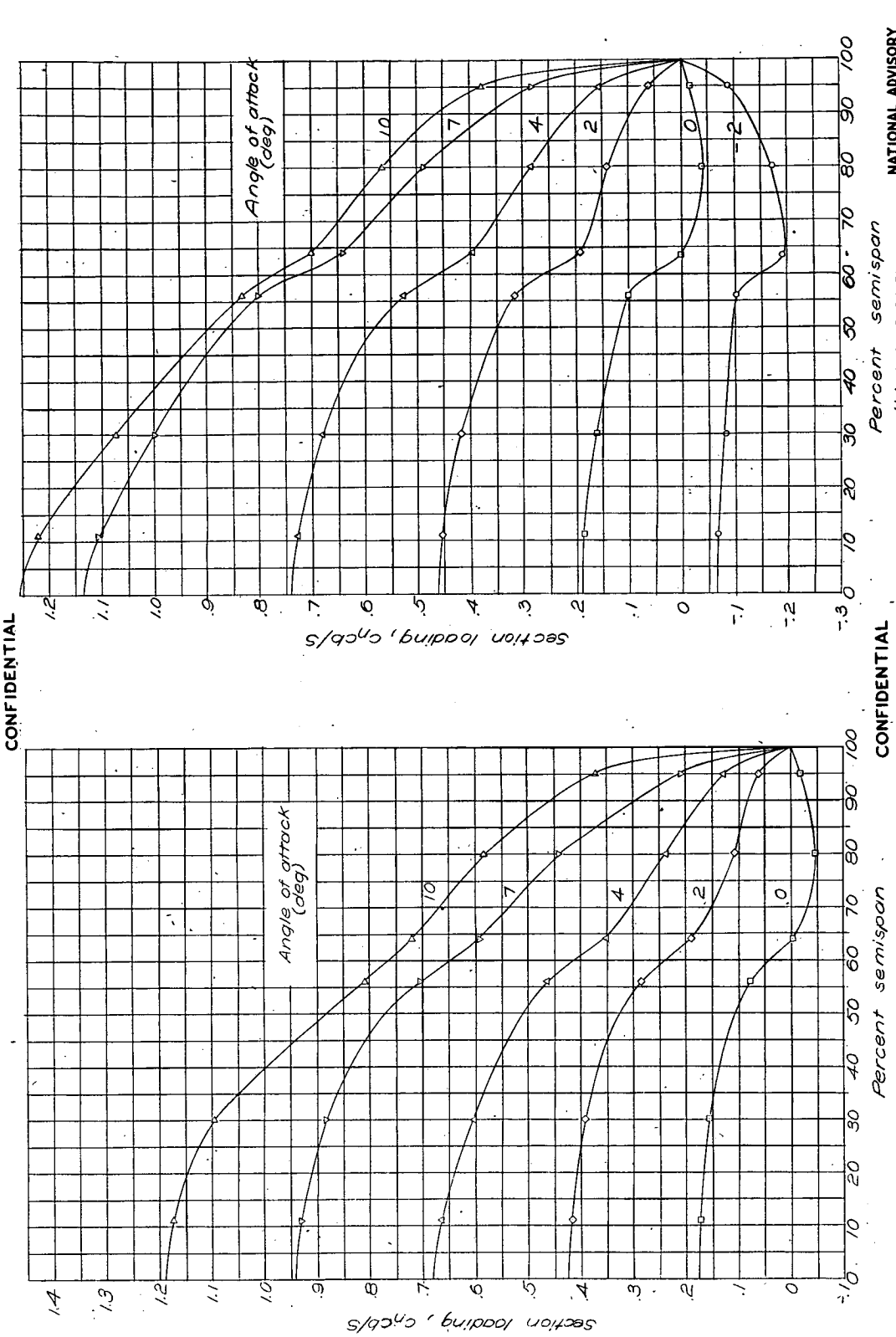

Figure 9.- Spanwise variation in section loading. $\delta_a = -5.7°$.

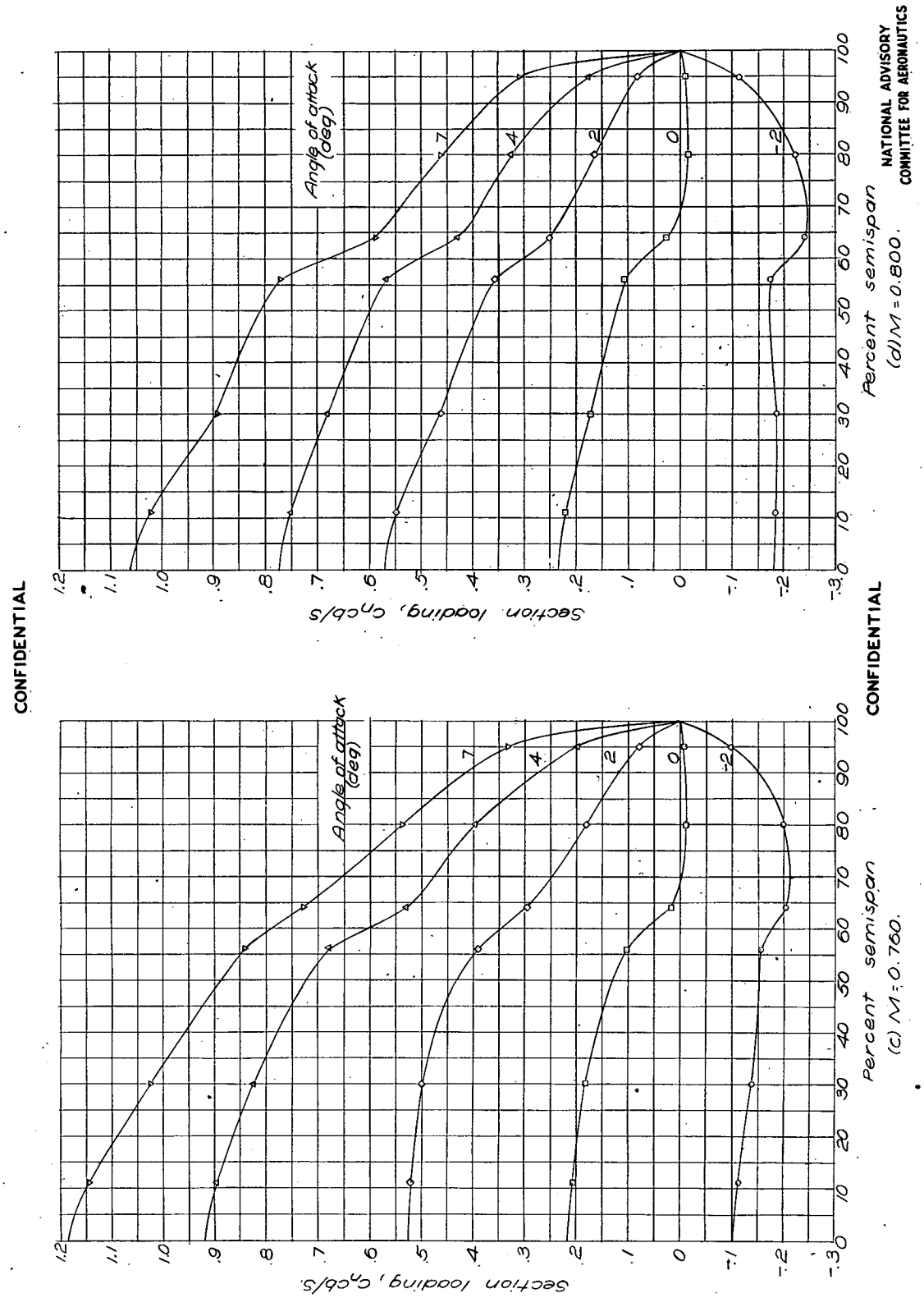

Figure 9.- Continued. $\delta_a = -5.7°$

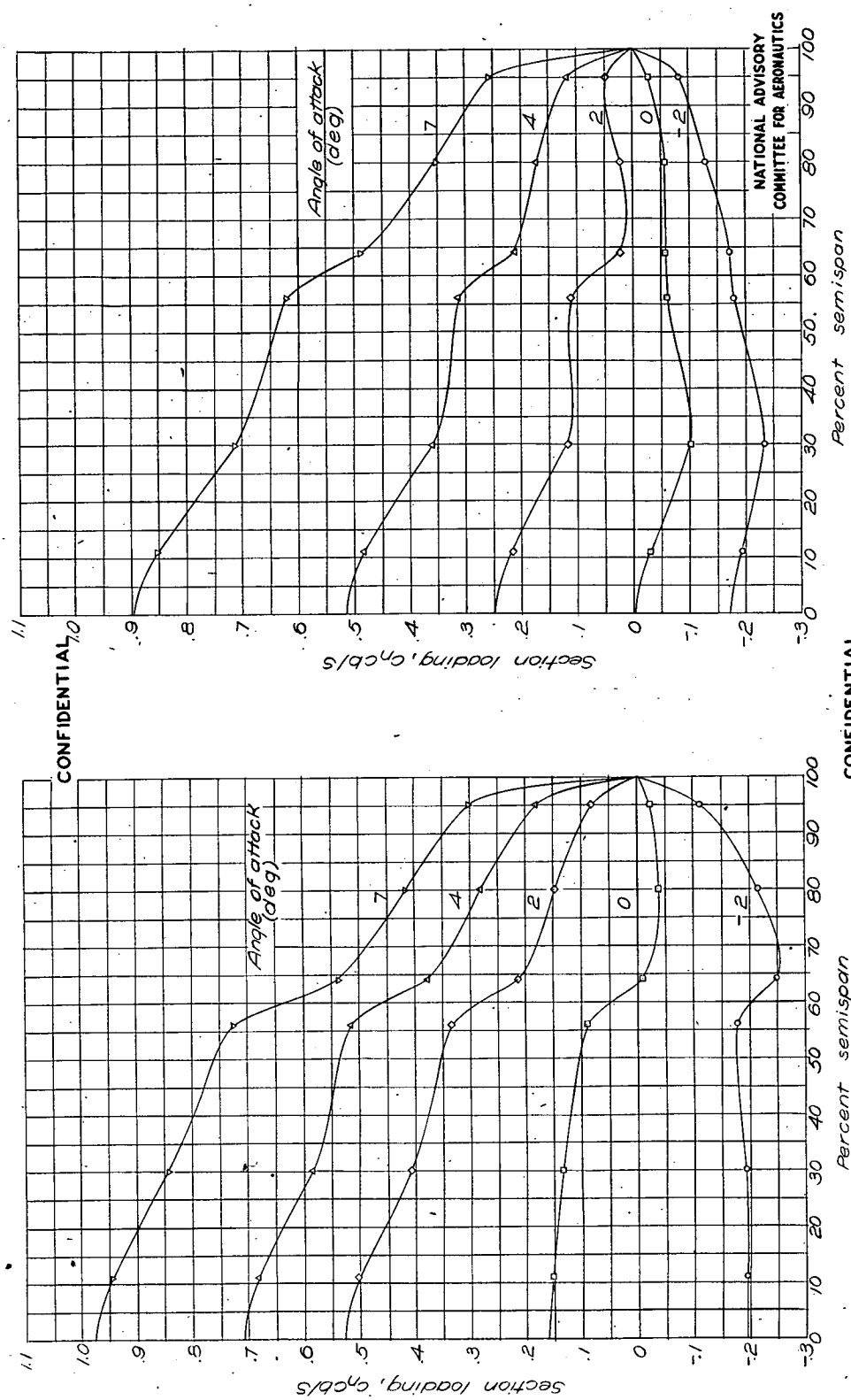

Figure 9.- Continued. $\delta_a = -5.7°$

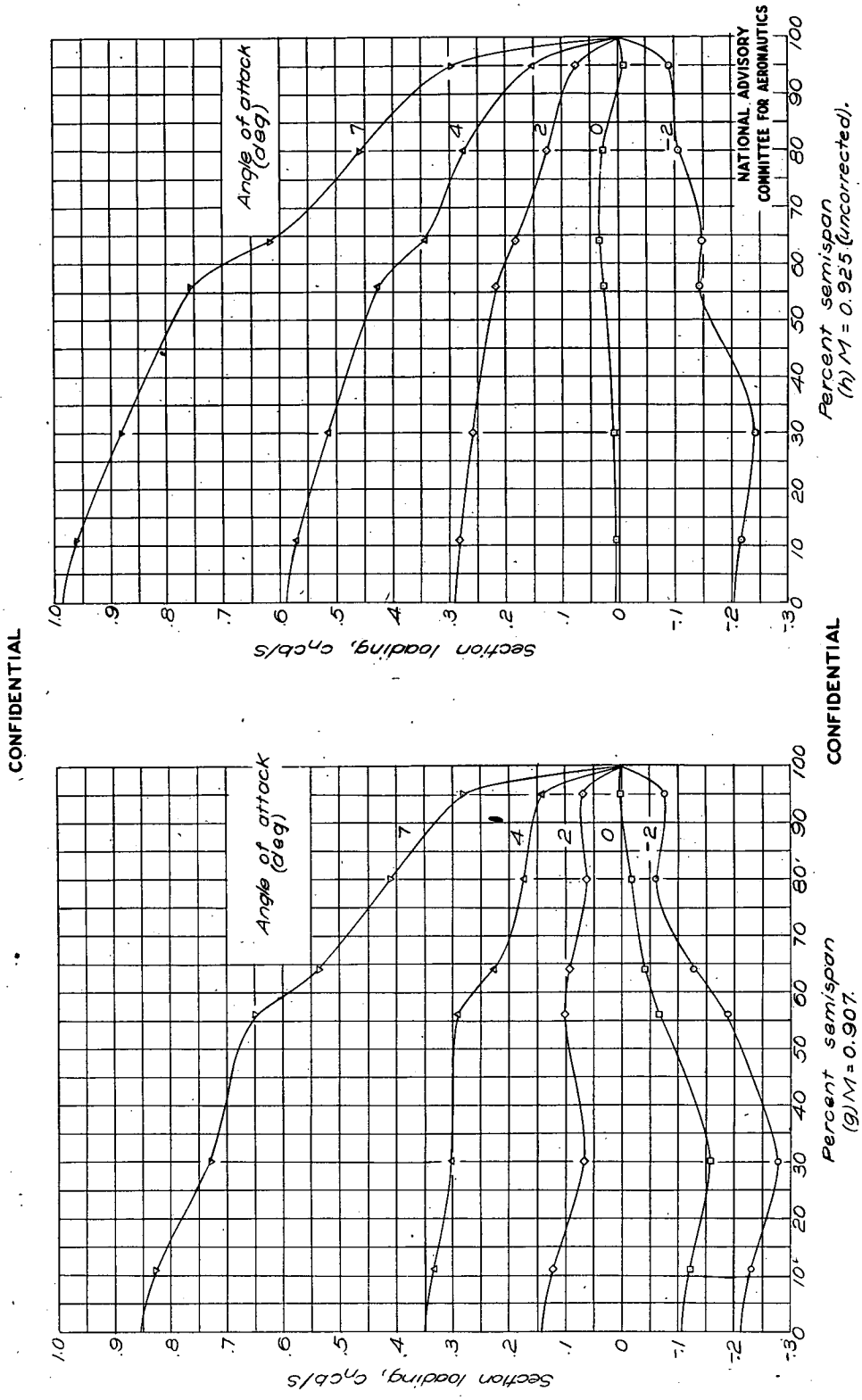

Figure 9.- Concluded. $\delta_a = -5.7°$

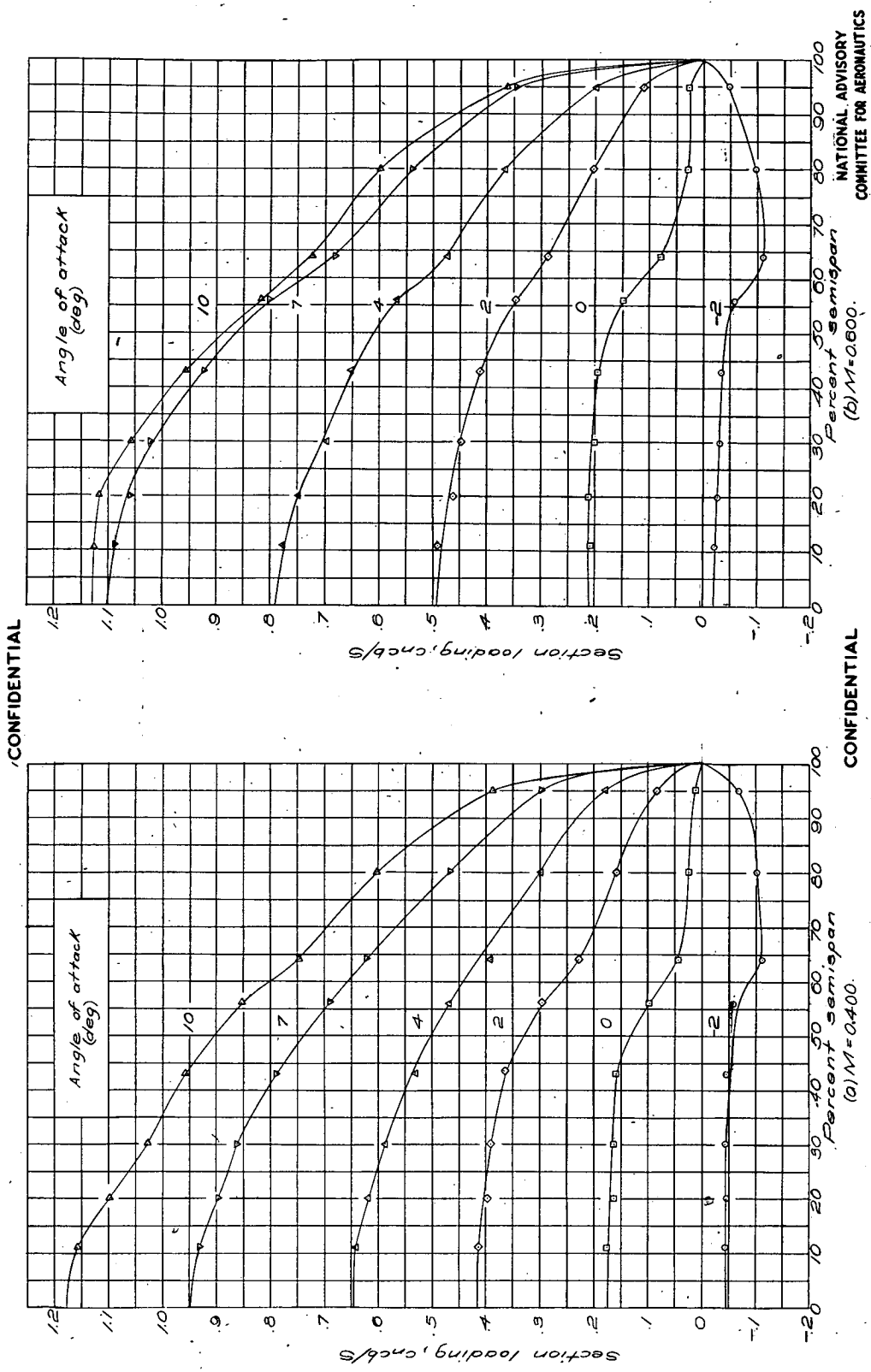

Figure 10.- Spanwise variation in section loading. $\delta_d = -3.2°$.

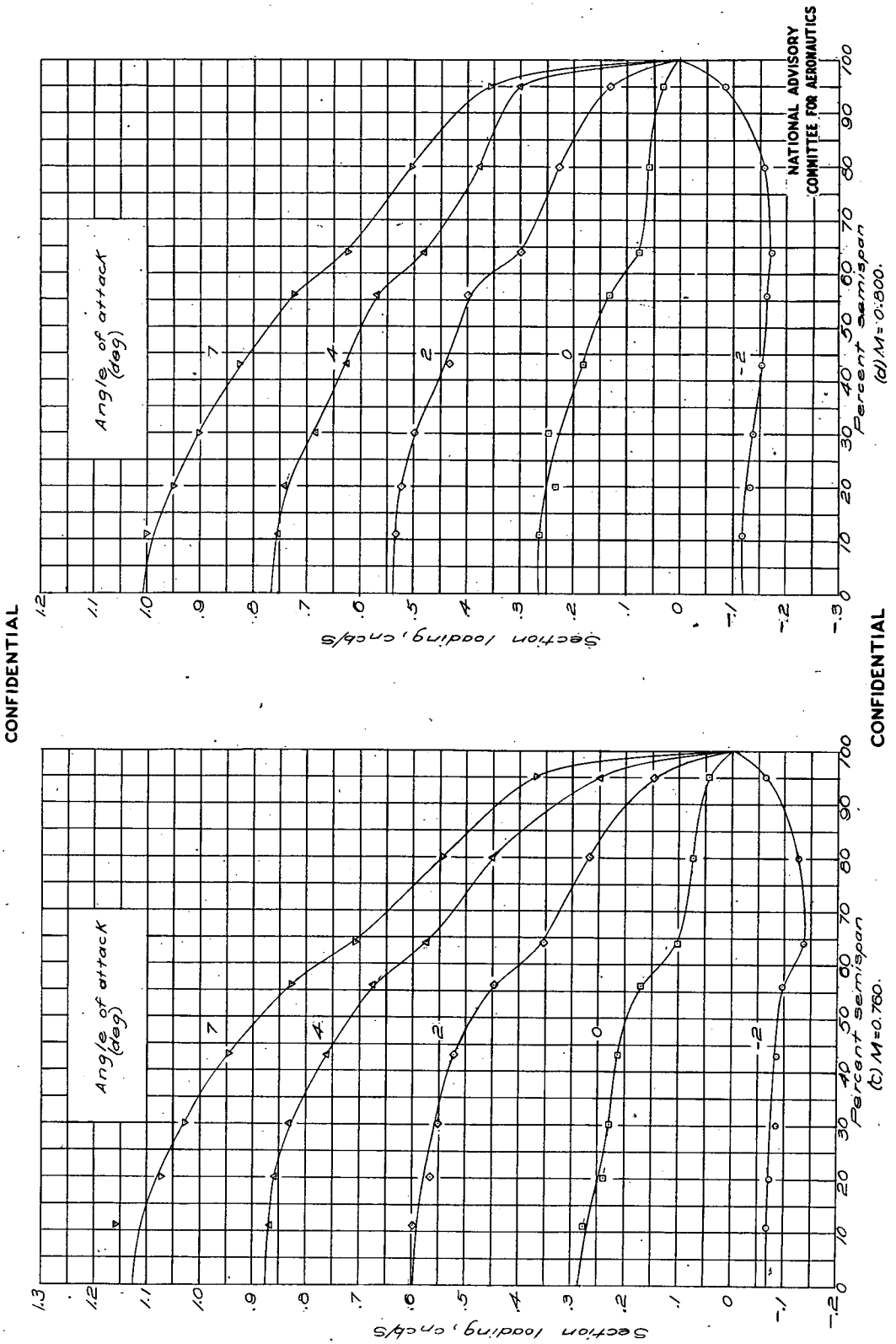

Figure 10.- Continued. $\delta_a = -3.2°$

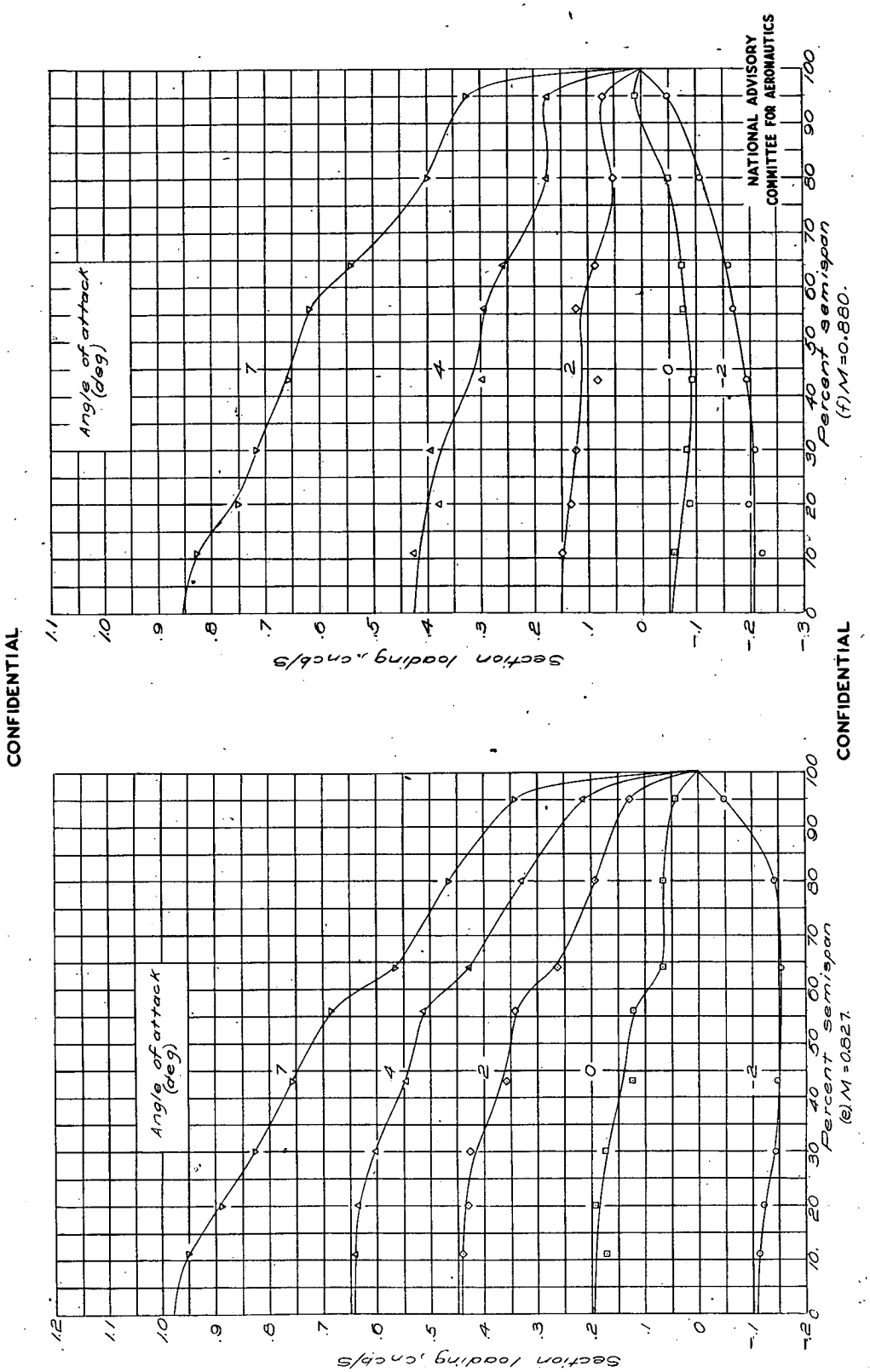

Figure 10.- Continued. $\delta_a = -3.2°$

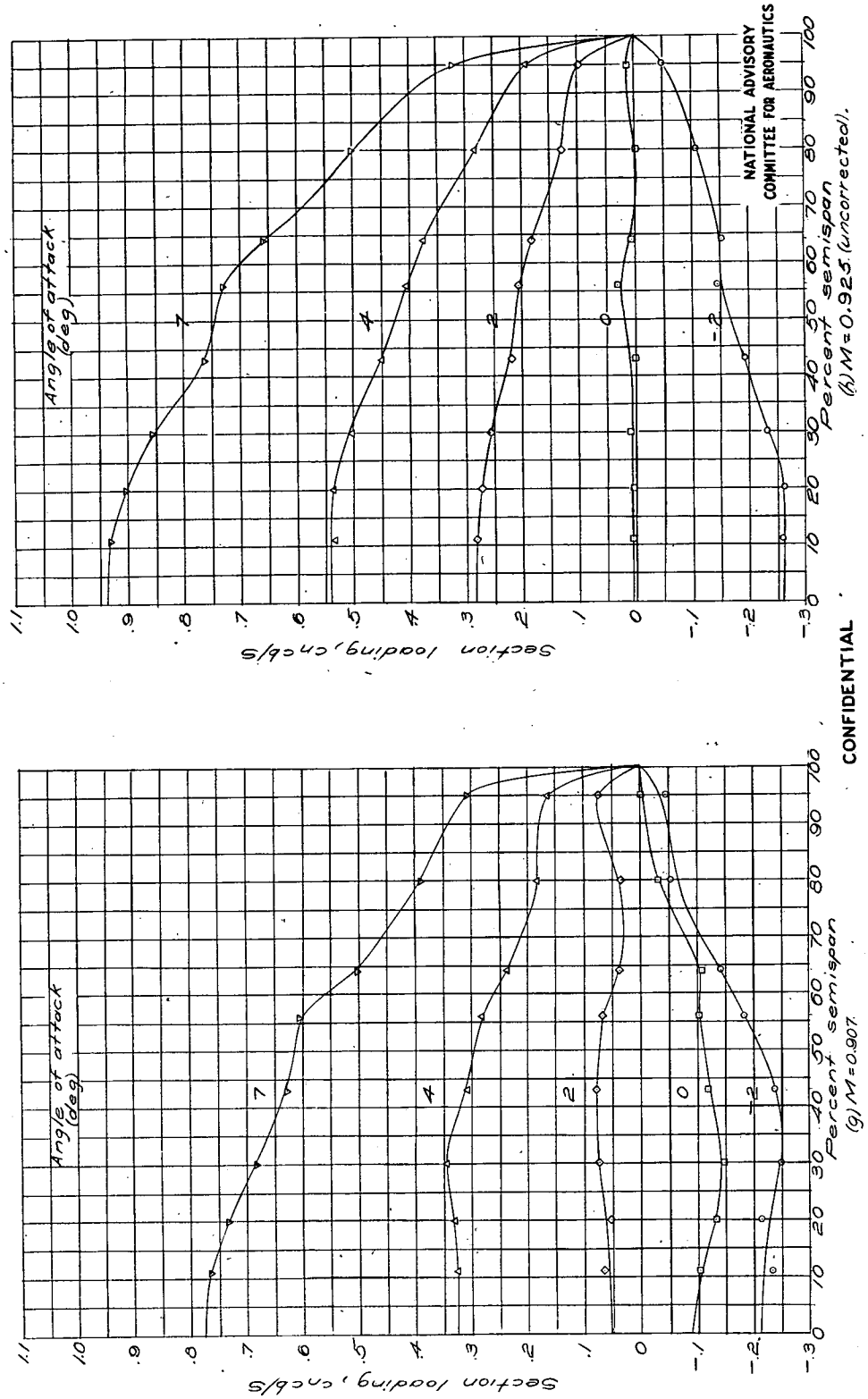

Figure 10.- Concluded. $\delta = -3.2°$

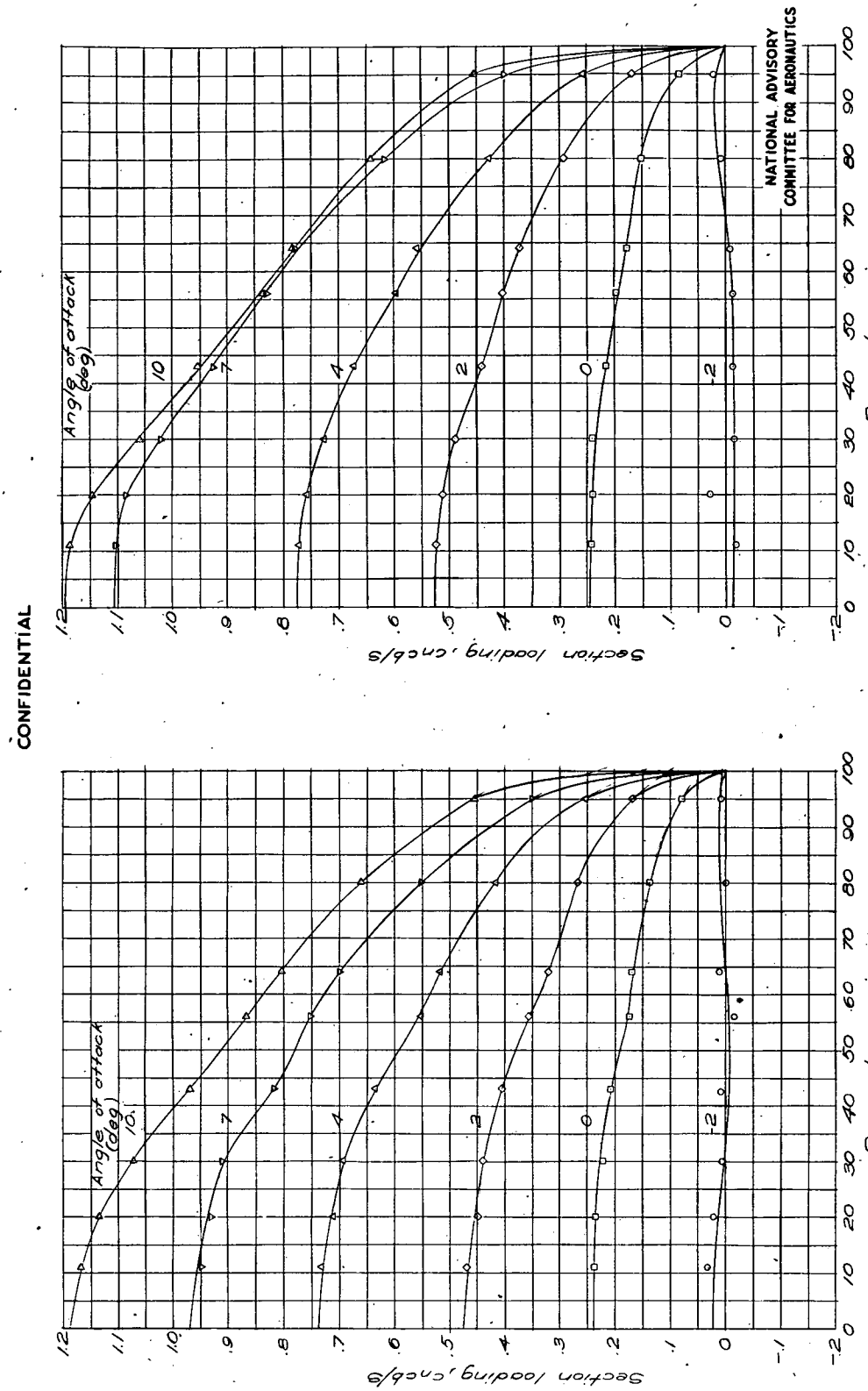

Figure 11.- Spanwise variation in section loading. $\delta_d = 0.5°$.

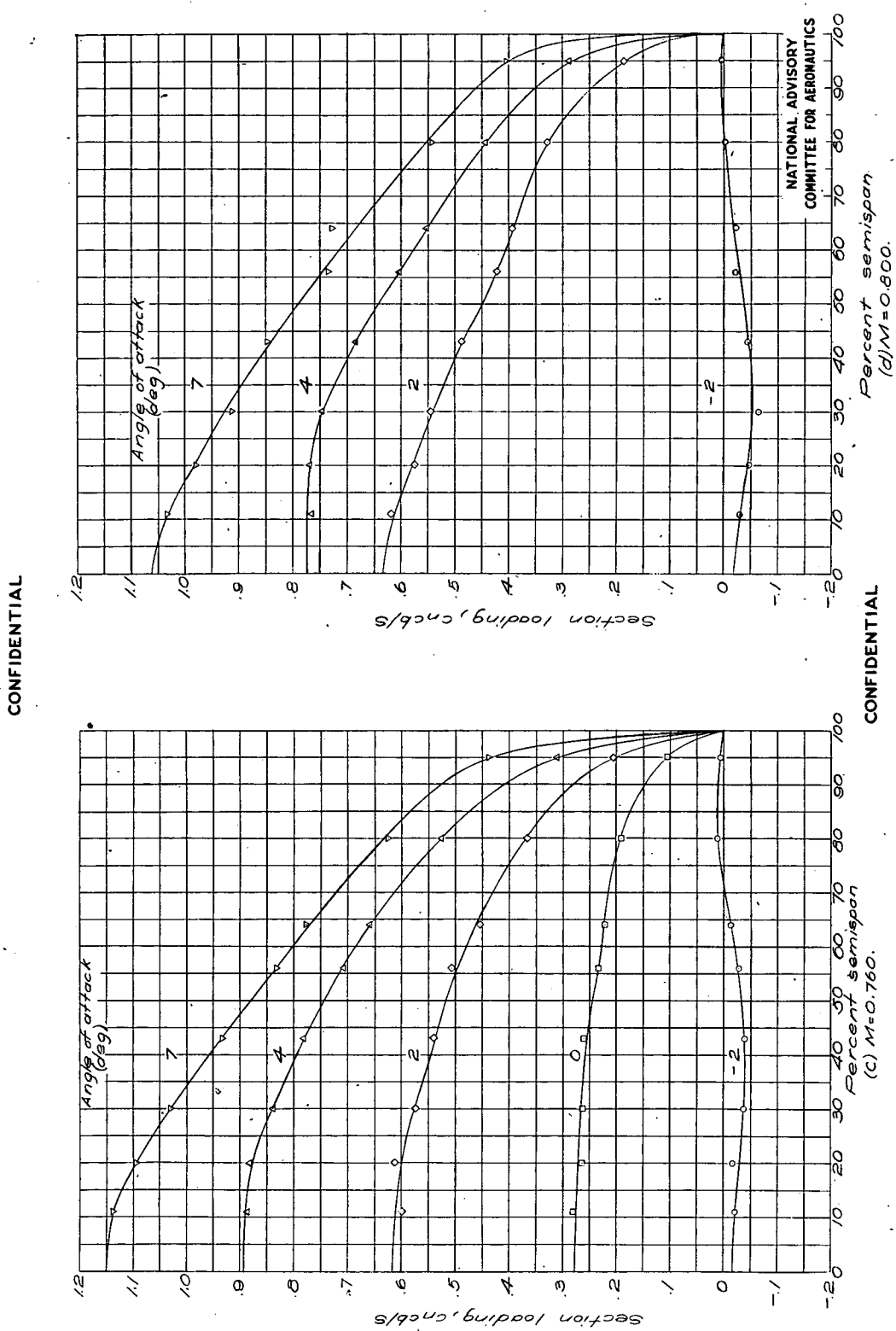

Figure 11.- Continued. $\delta_a = 0.5°$.

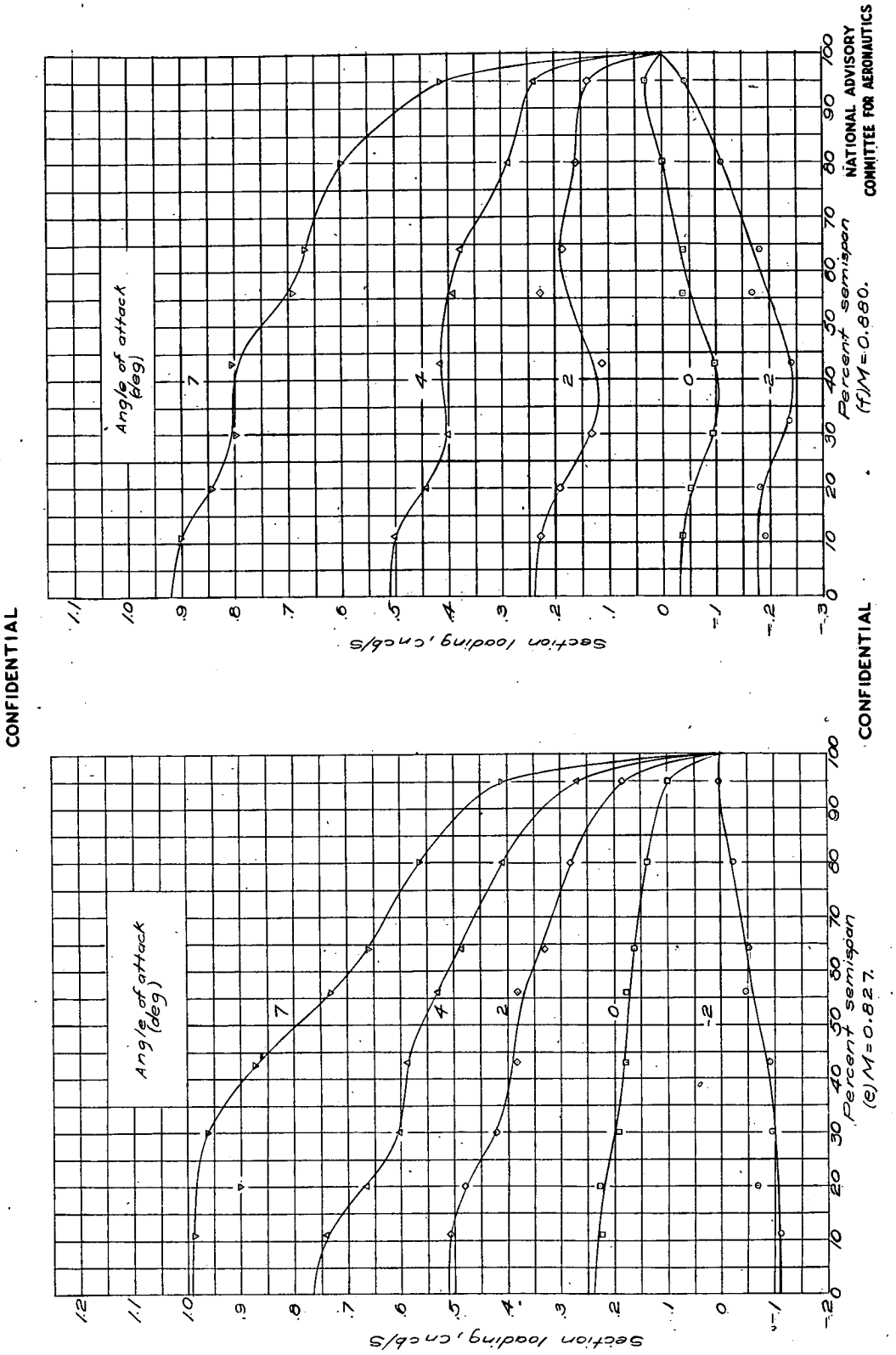

Figure 11.- Continued. $\delta_a = 0.5°$.

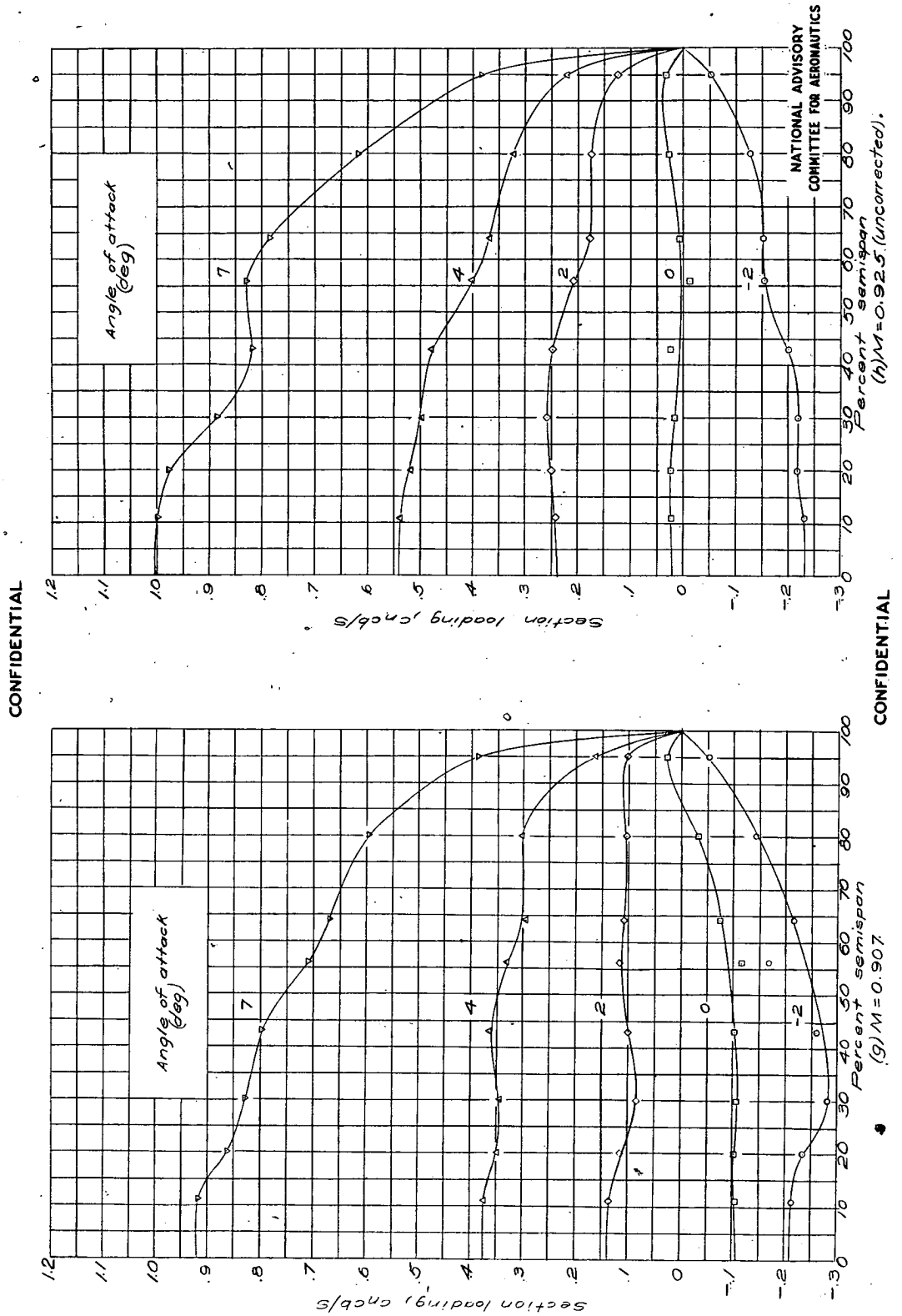

Figure 11.- Concluded. $\delta_a = 0.5°$.

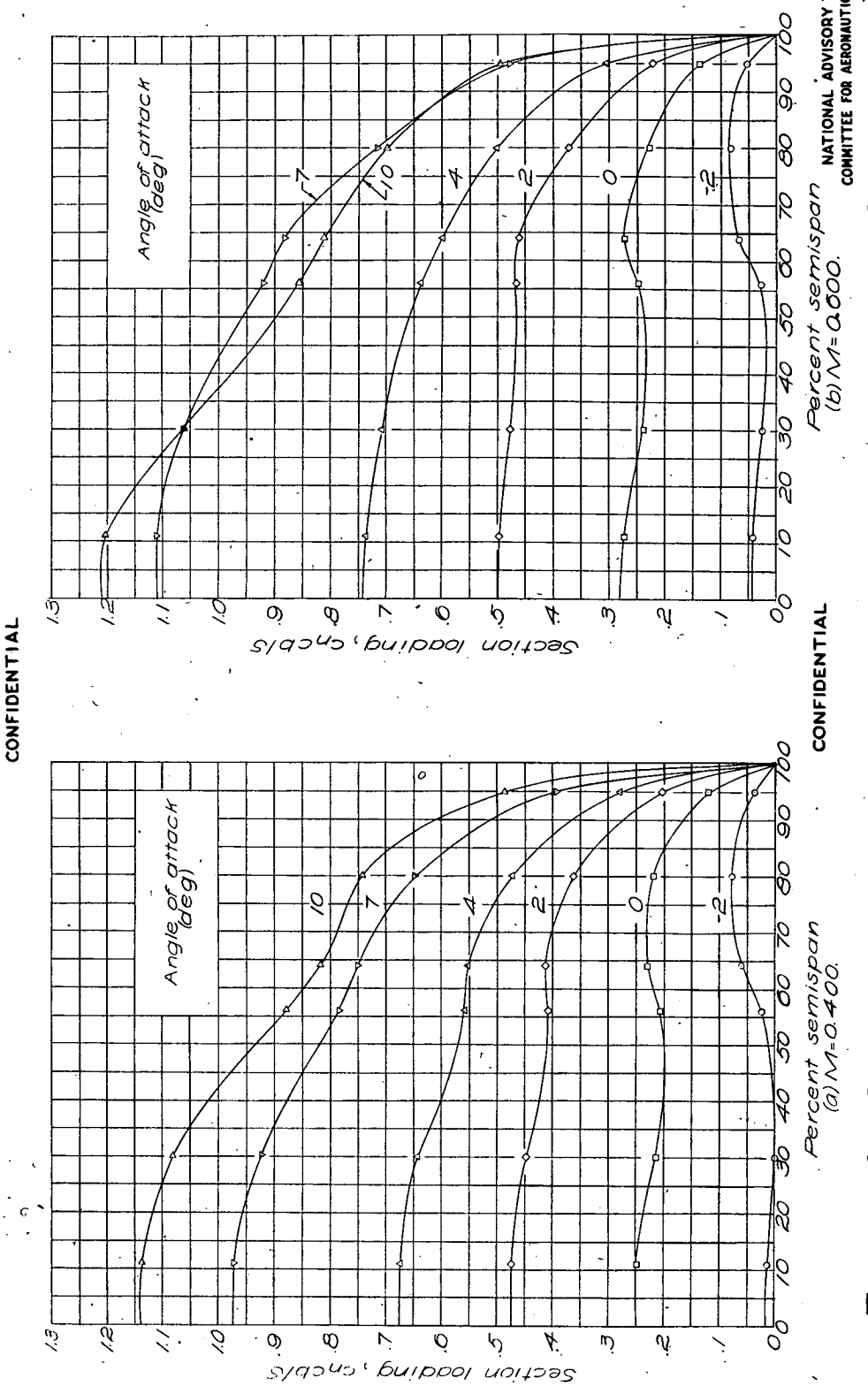

Figure 12.- Spanwise variation in section loading. $\delta_a = 2.9°$.

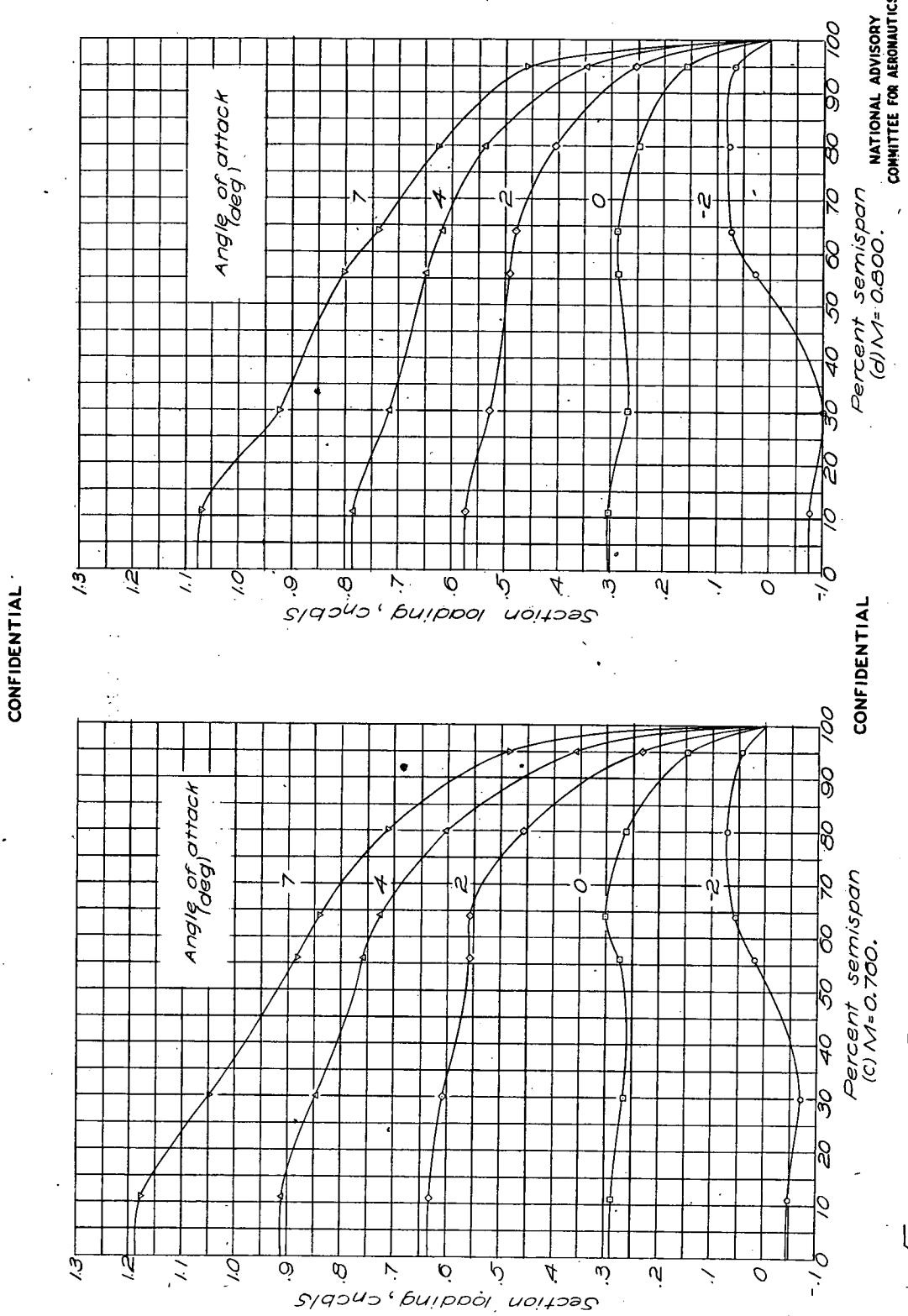

Figure 12.- Continued. $\delta_a = 2.9°$

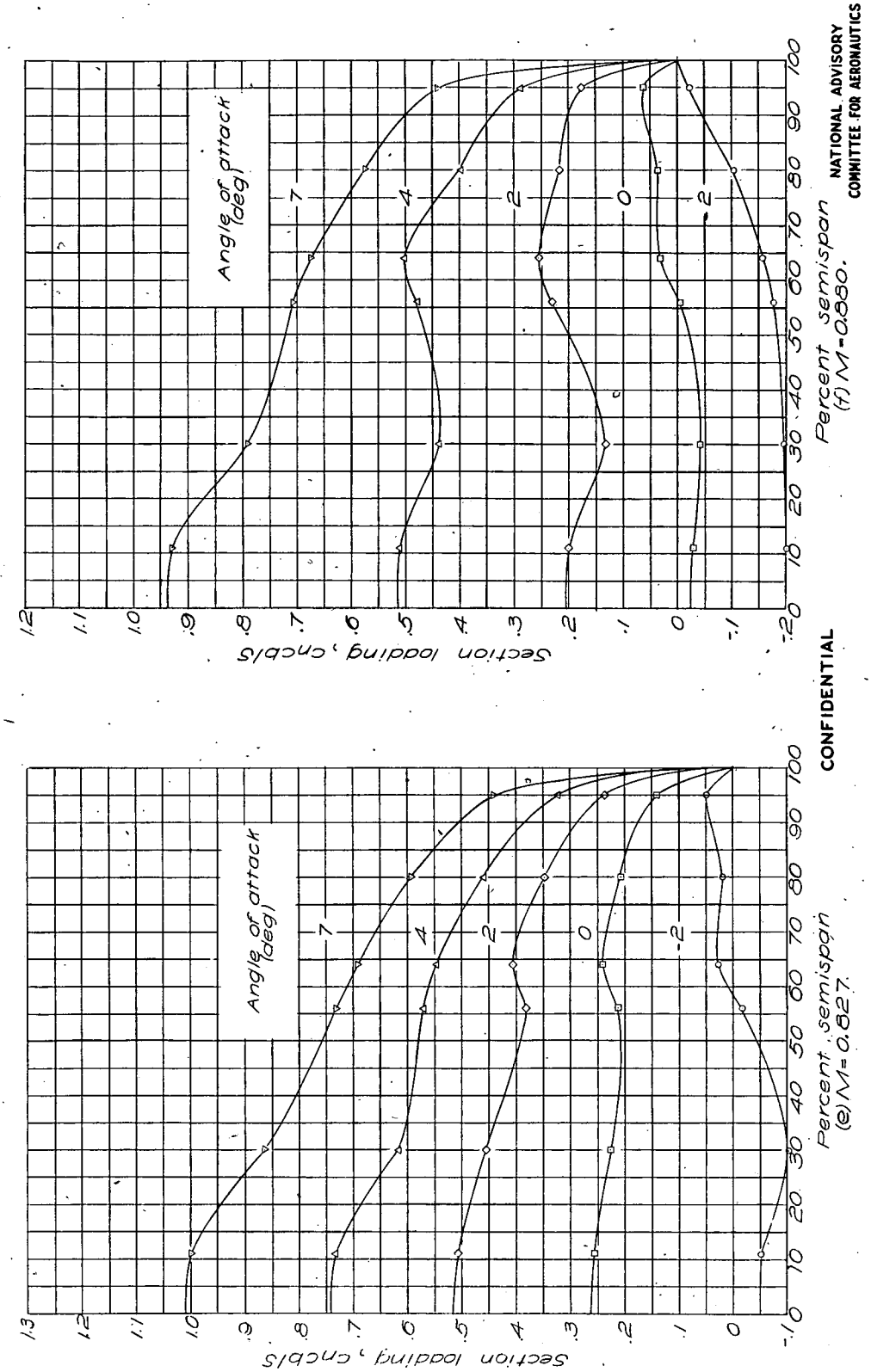

Figure 12.- Continued. $\delta_a = 2.9°$.

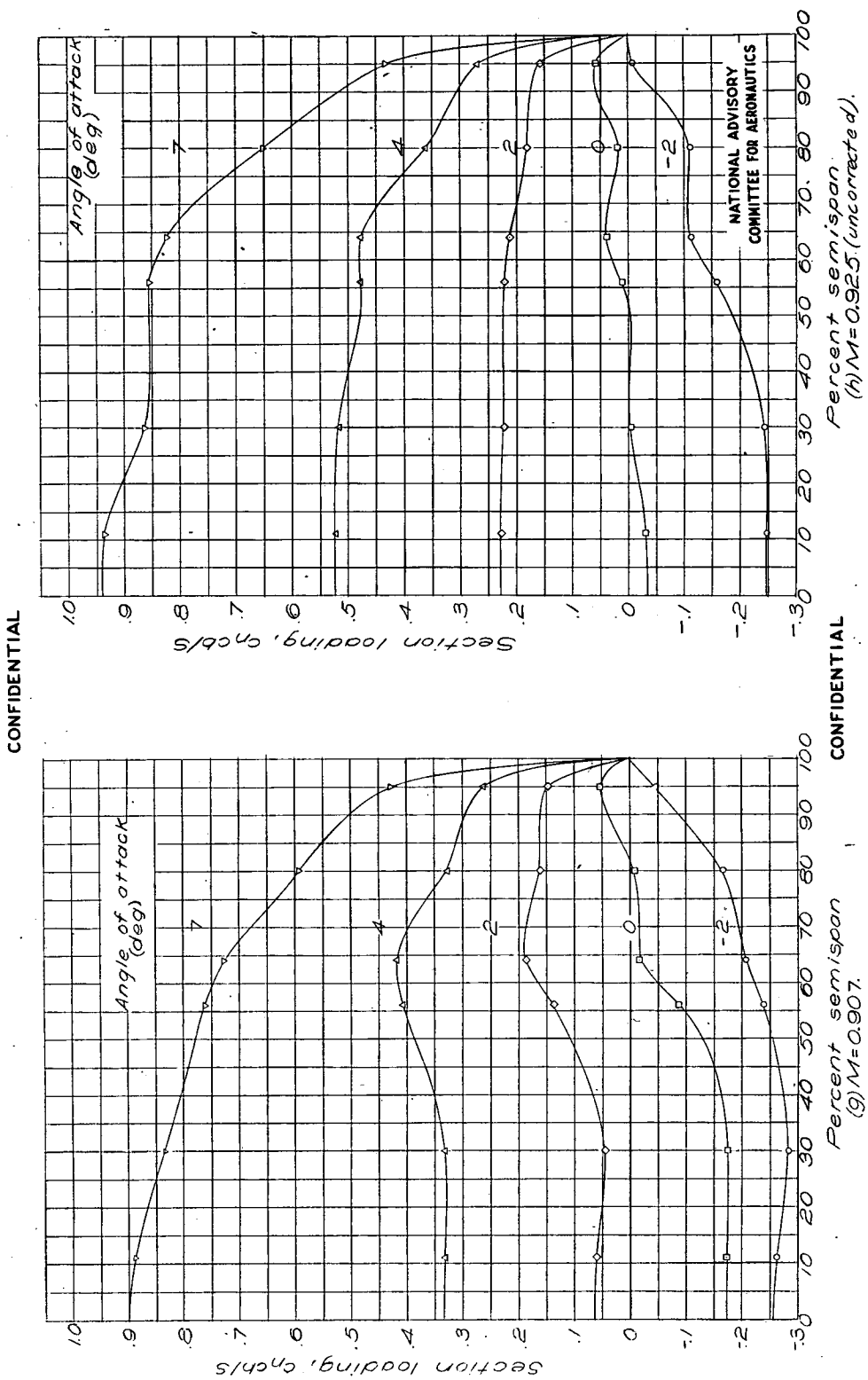

Figure 12.- Concluded. $\delta_a = 2.9°$.

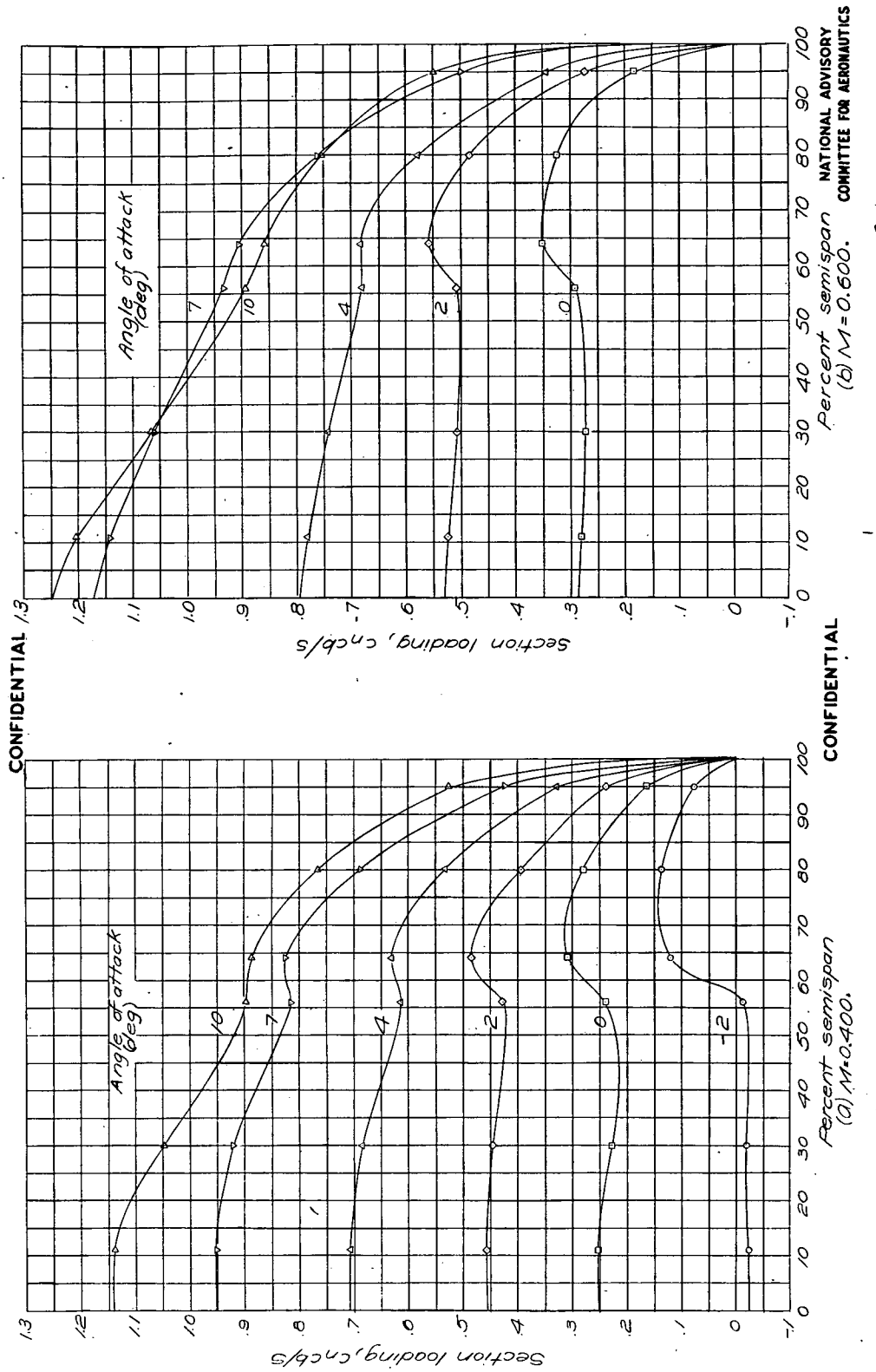

Figure 13.- Spanwise variation in section loading. $\delta_a = 5.8°$.

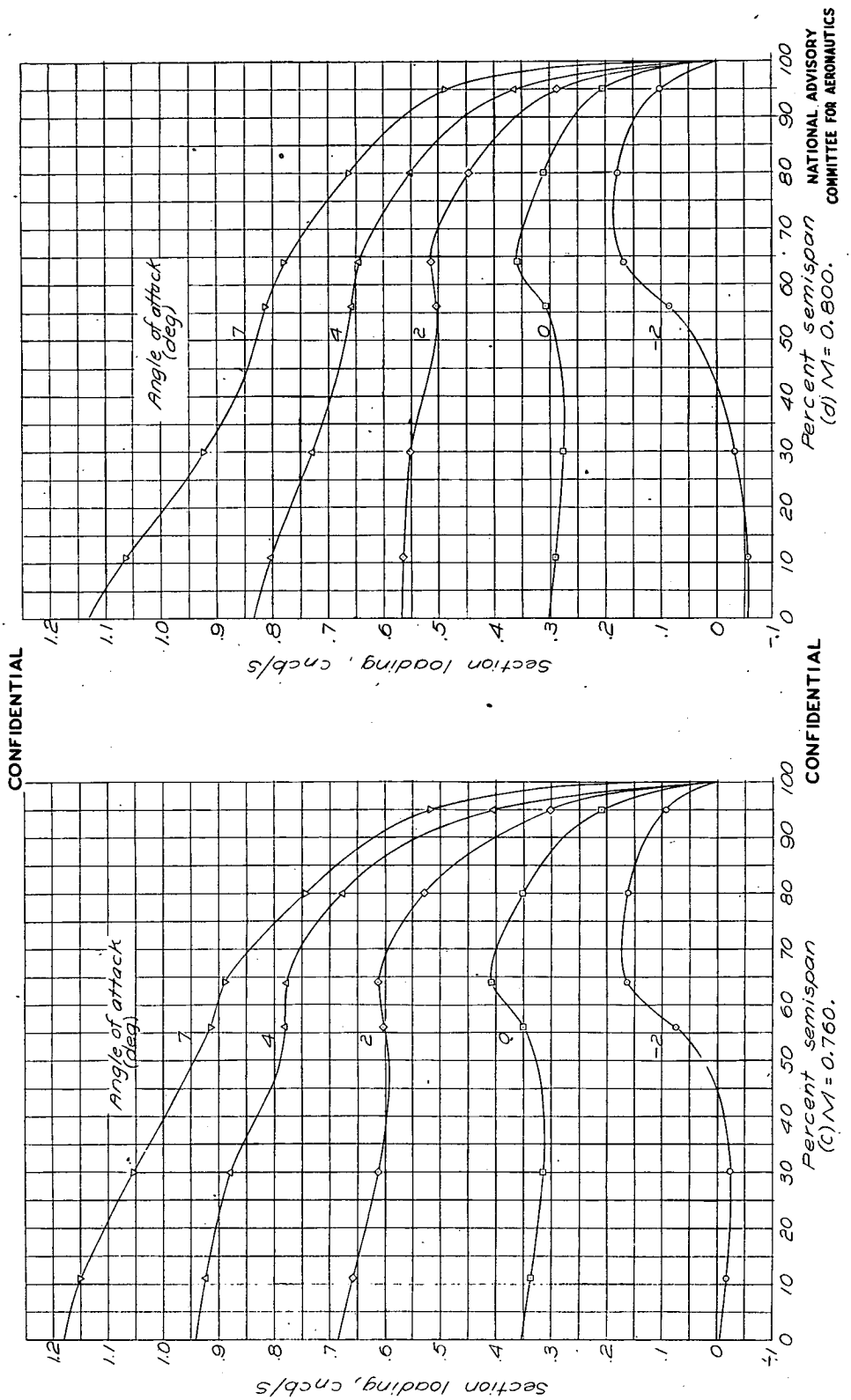

Figure 13.- Continued. $\delta_a = 5.8°$

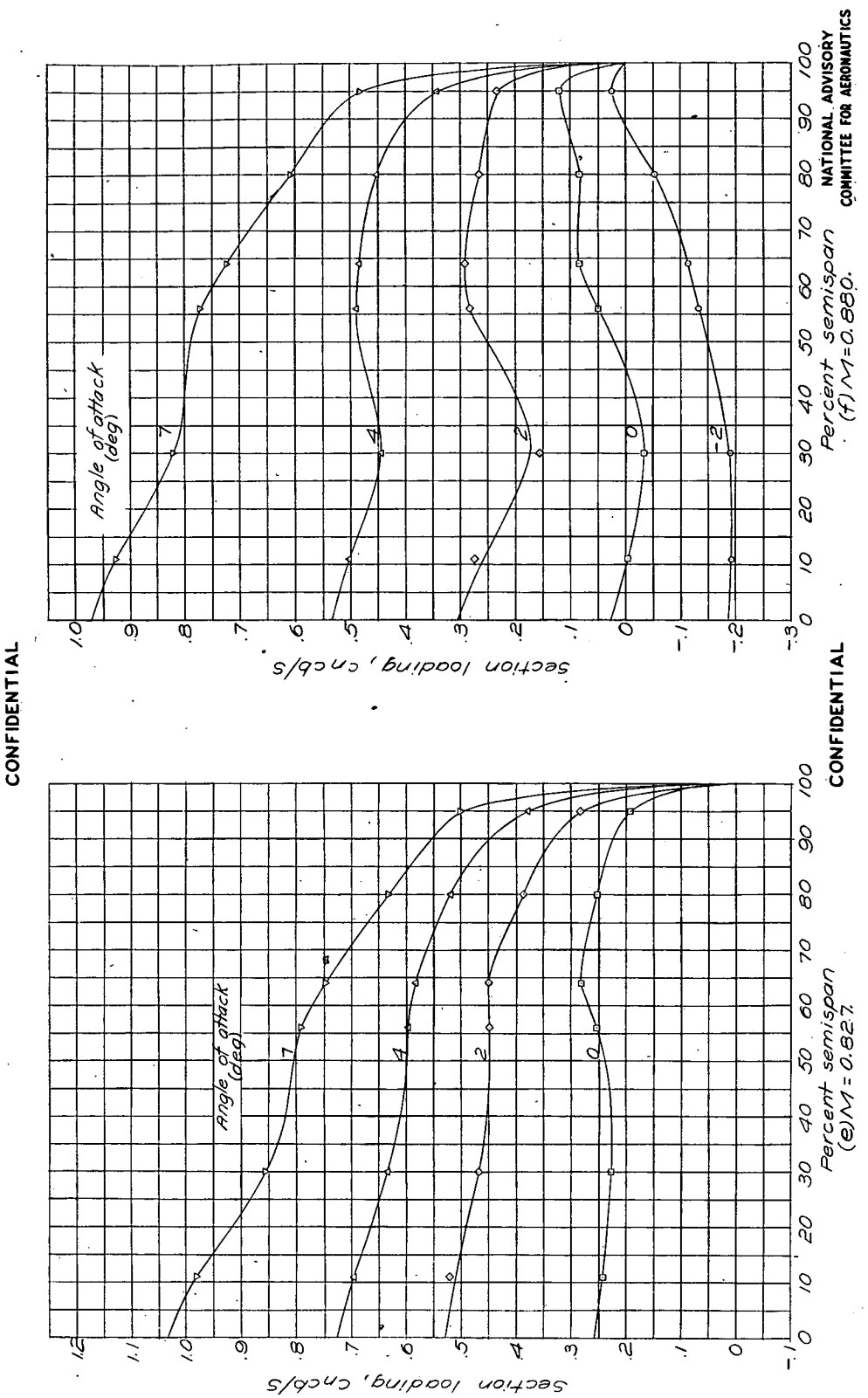

Figure 13.- Continued. $\delta_a = 5.8°$

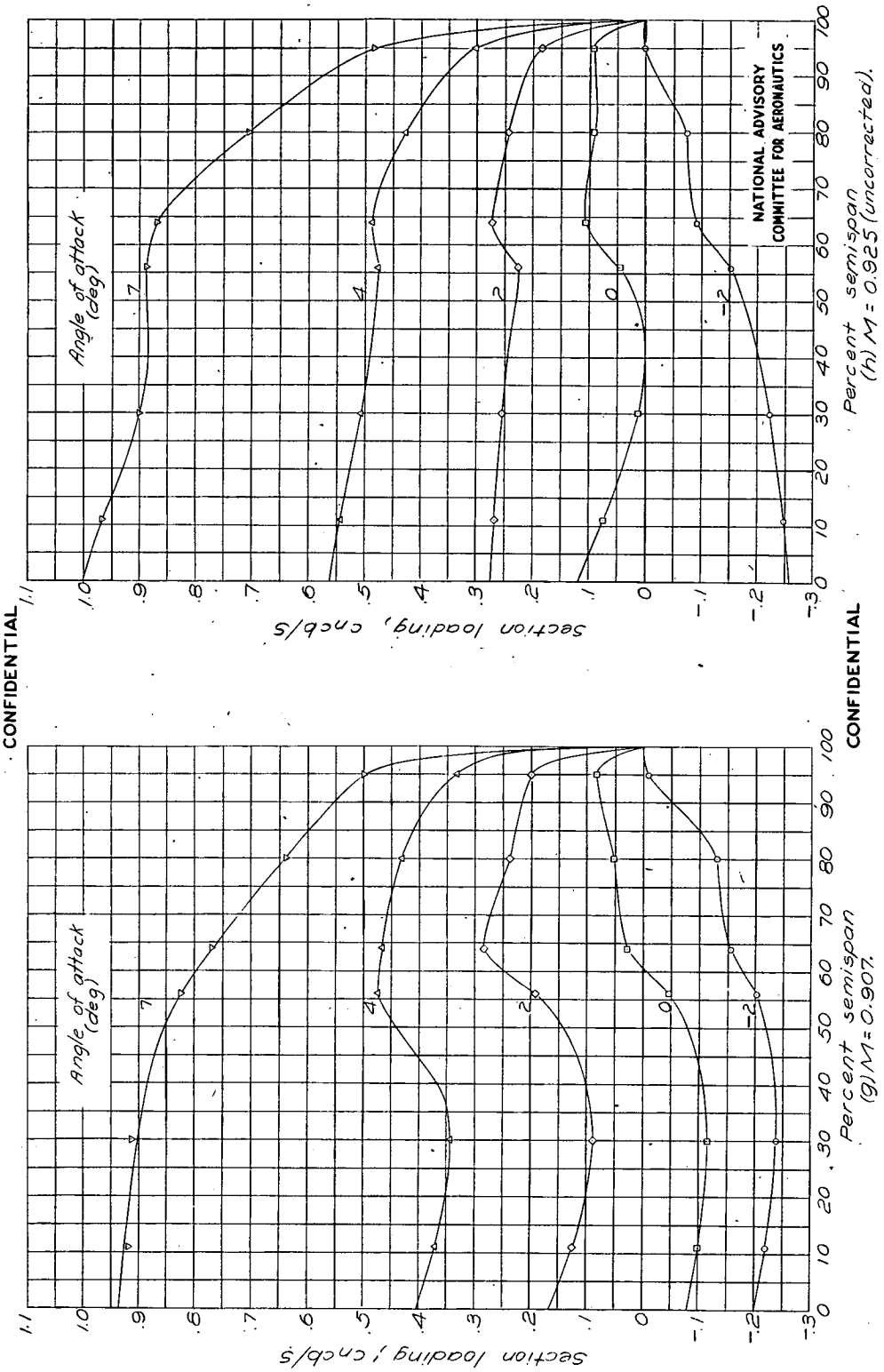

Figure 13.- Concluded. $\delta_a = 5.8°$

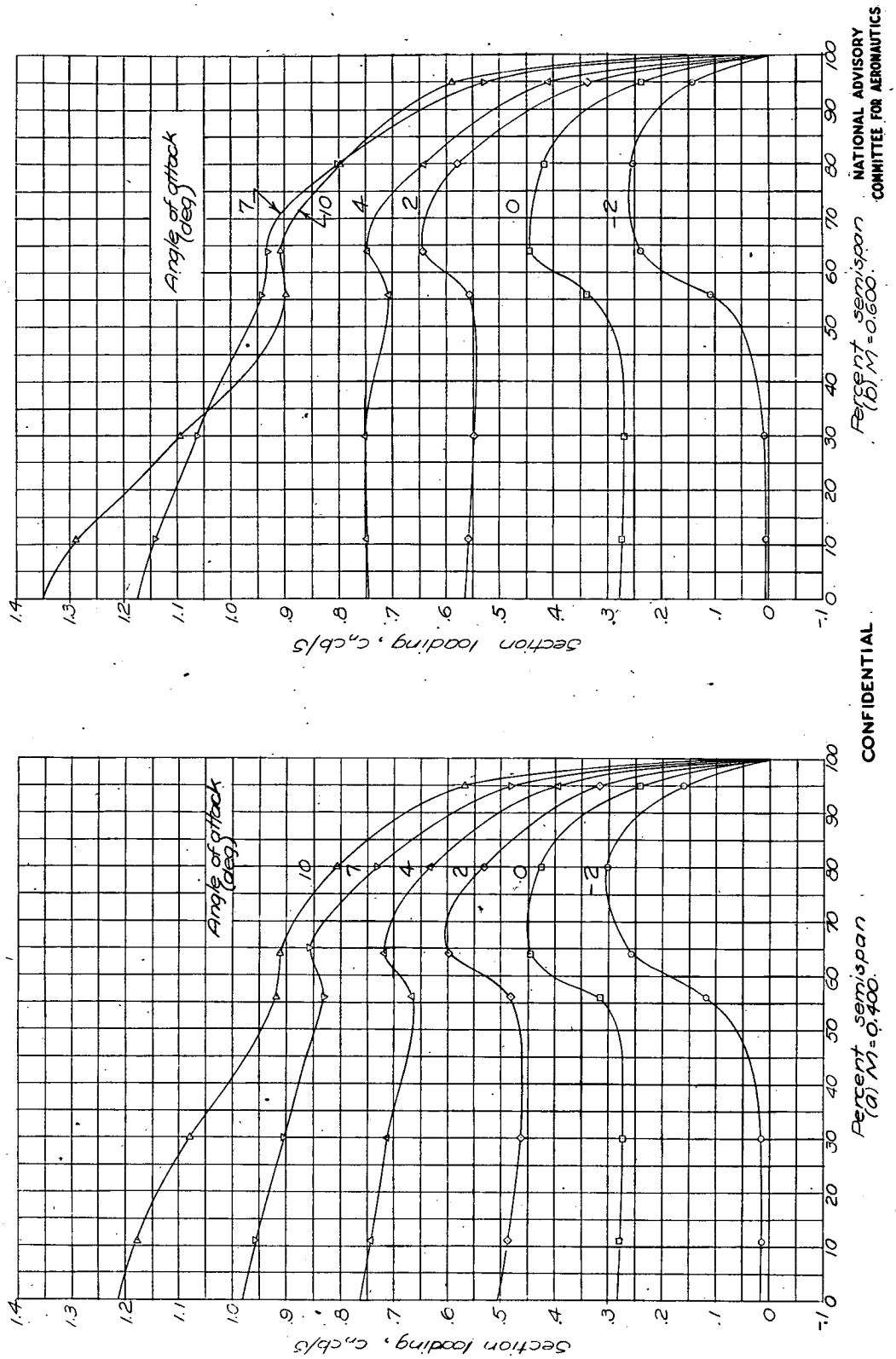

Figure 14.- Spanwise variation in section loading. $\delta_d = 9.6°$.

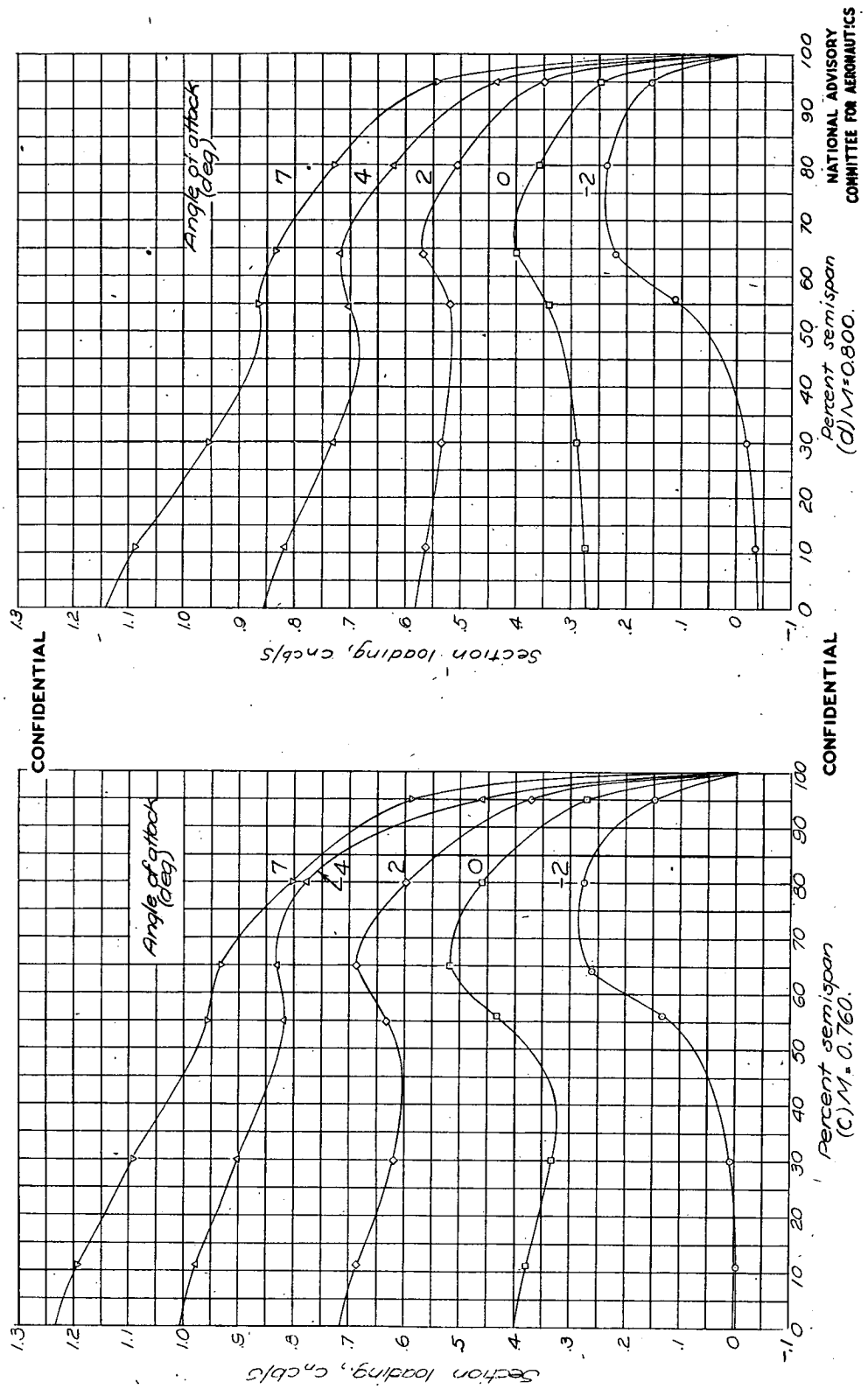

Figure 14.- Continued. $\delta_a = 9.6°$

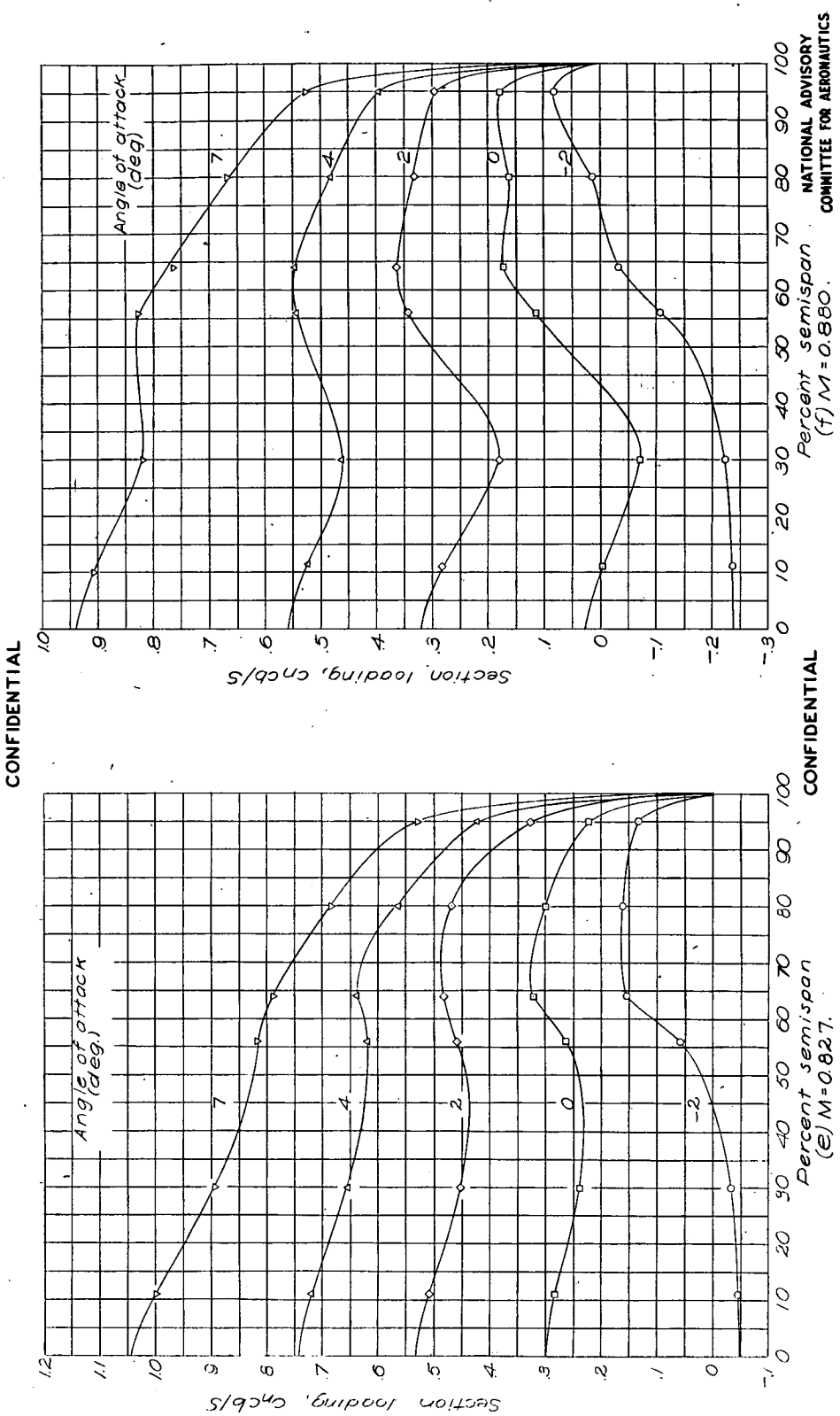

Figure 14.-Continued. $\delta_a = 9.6°$

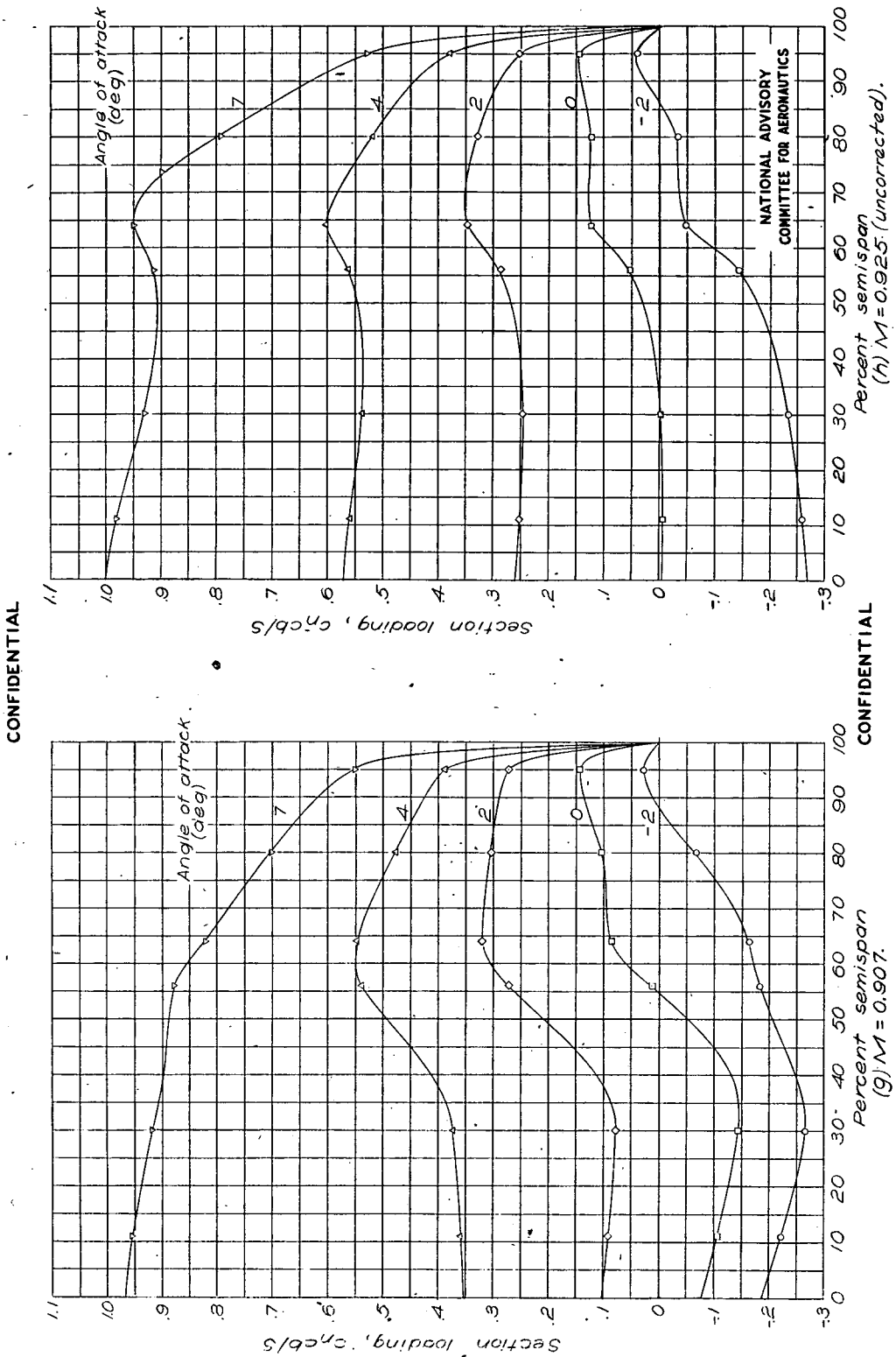

Figure 14.-Concluded. $\delta_a = 9.6°$

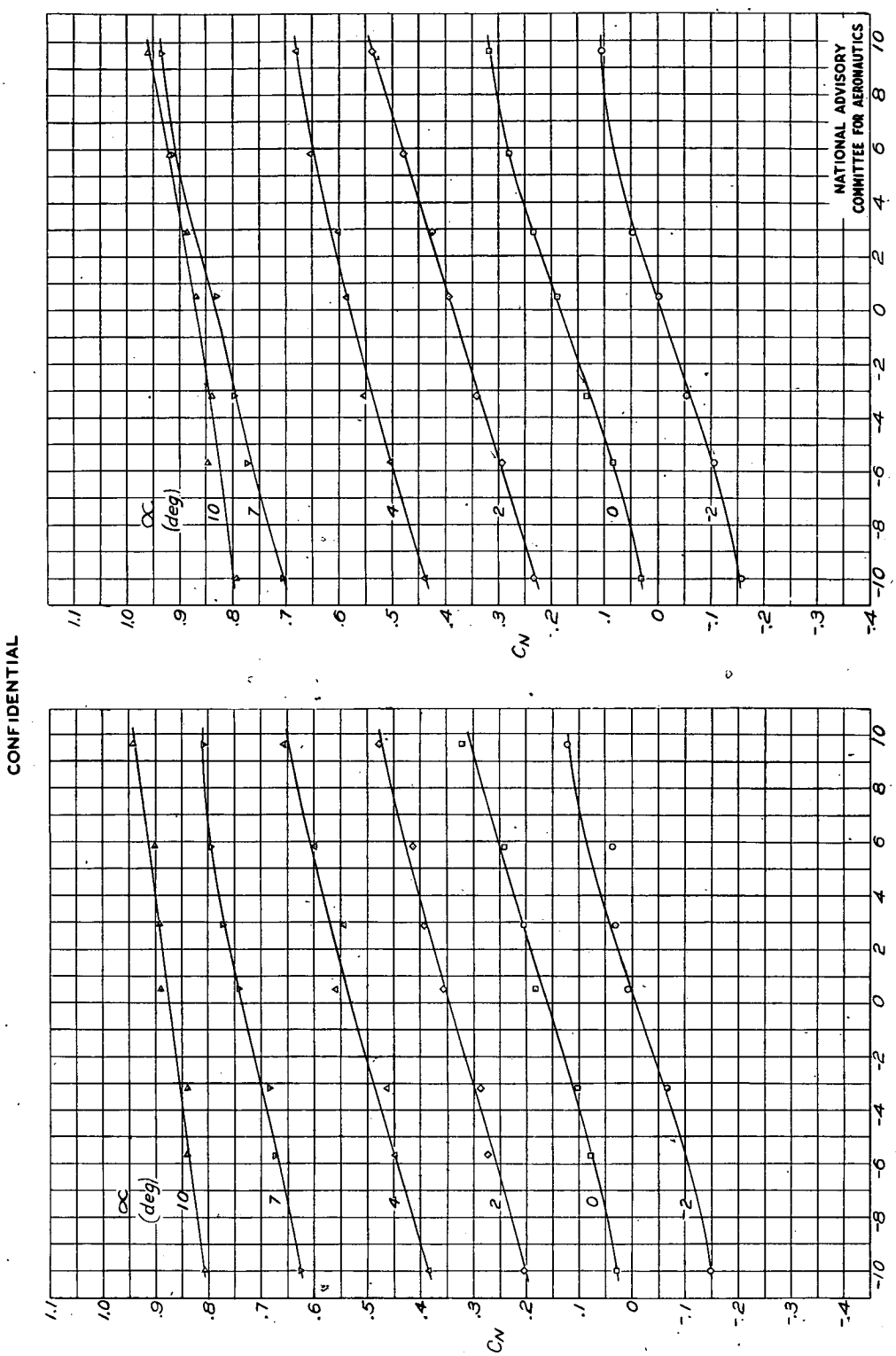

Figure 15.- Wing normal-force coefficient against aileron deflection at various angles of attack.

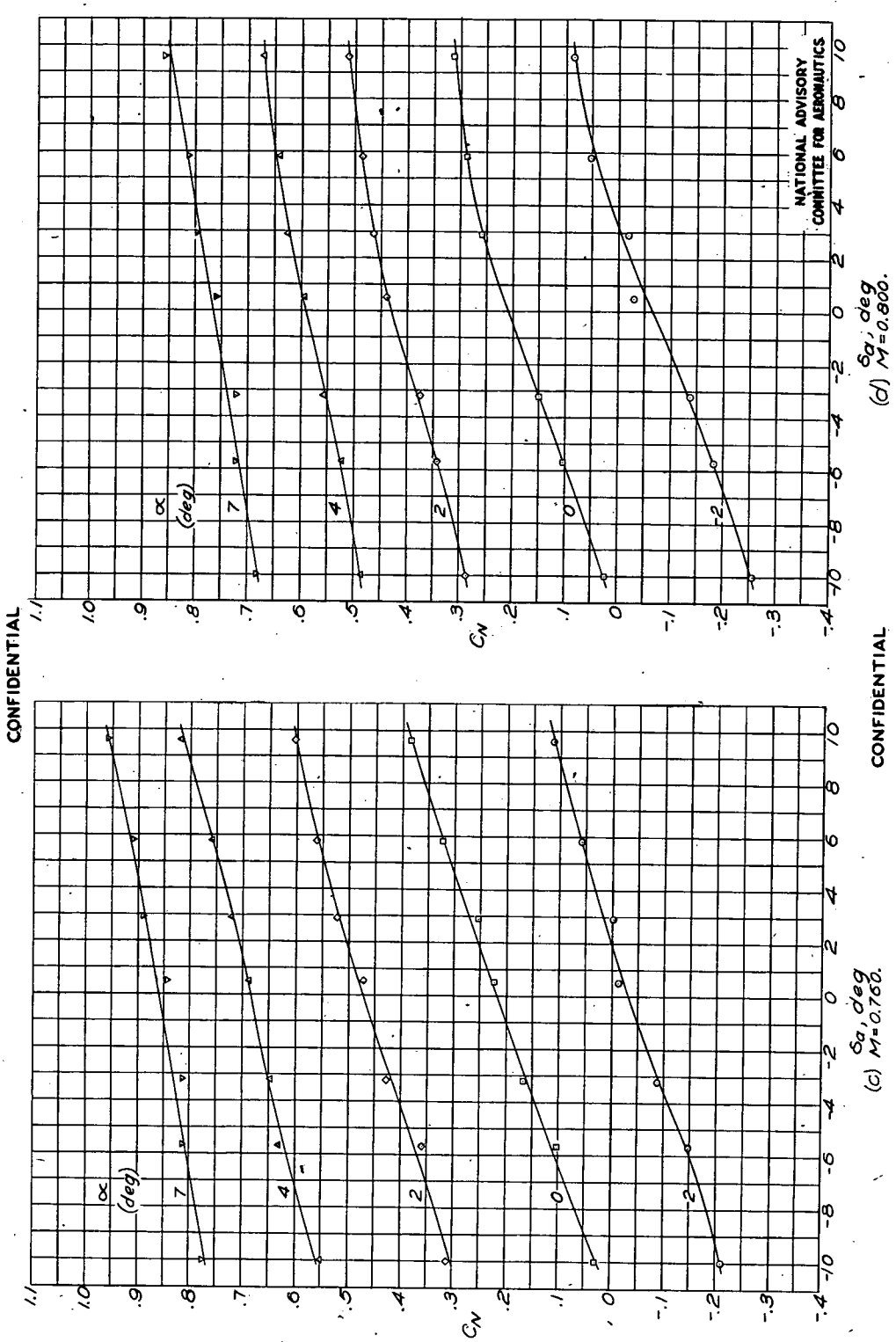

Figure 15.-Continued.

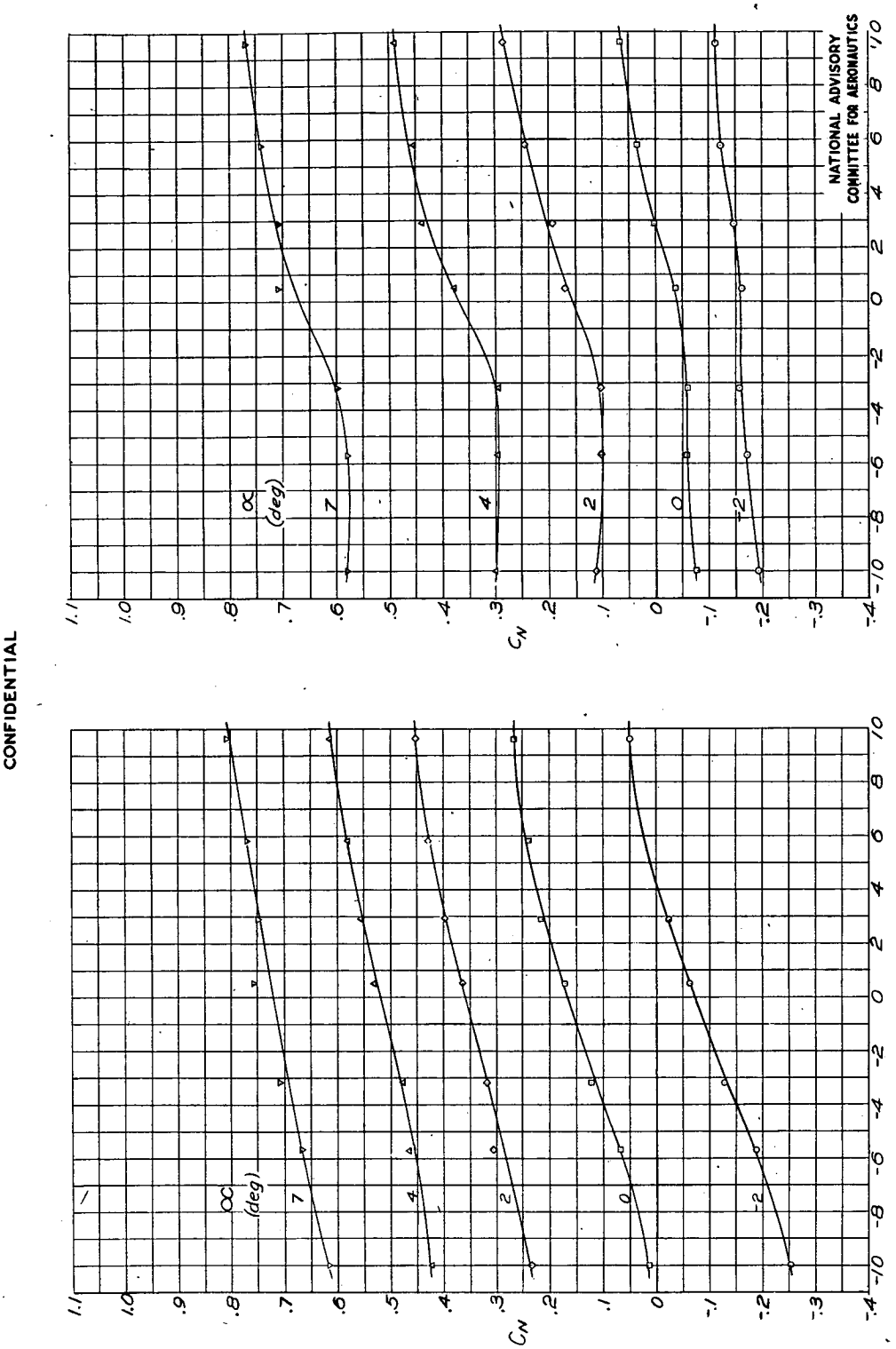

Figure 15.- Continued.

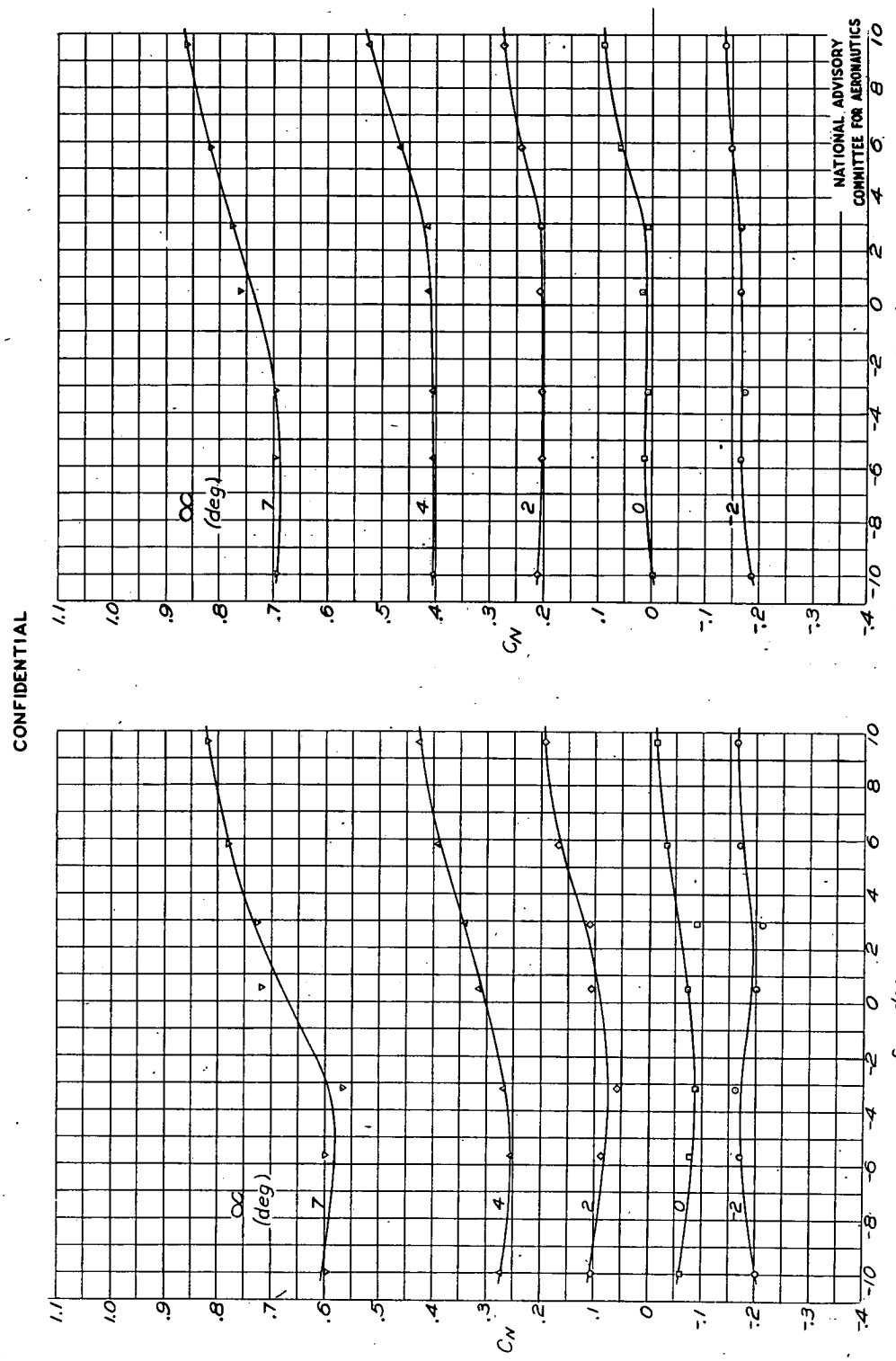

Figure 15. - Concluded.

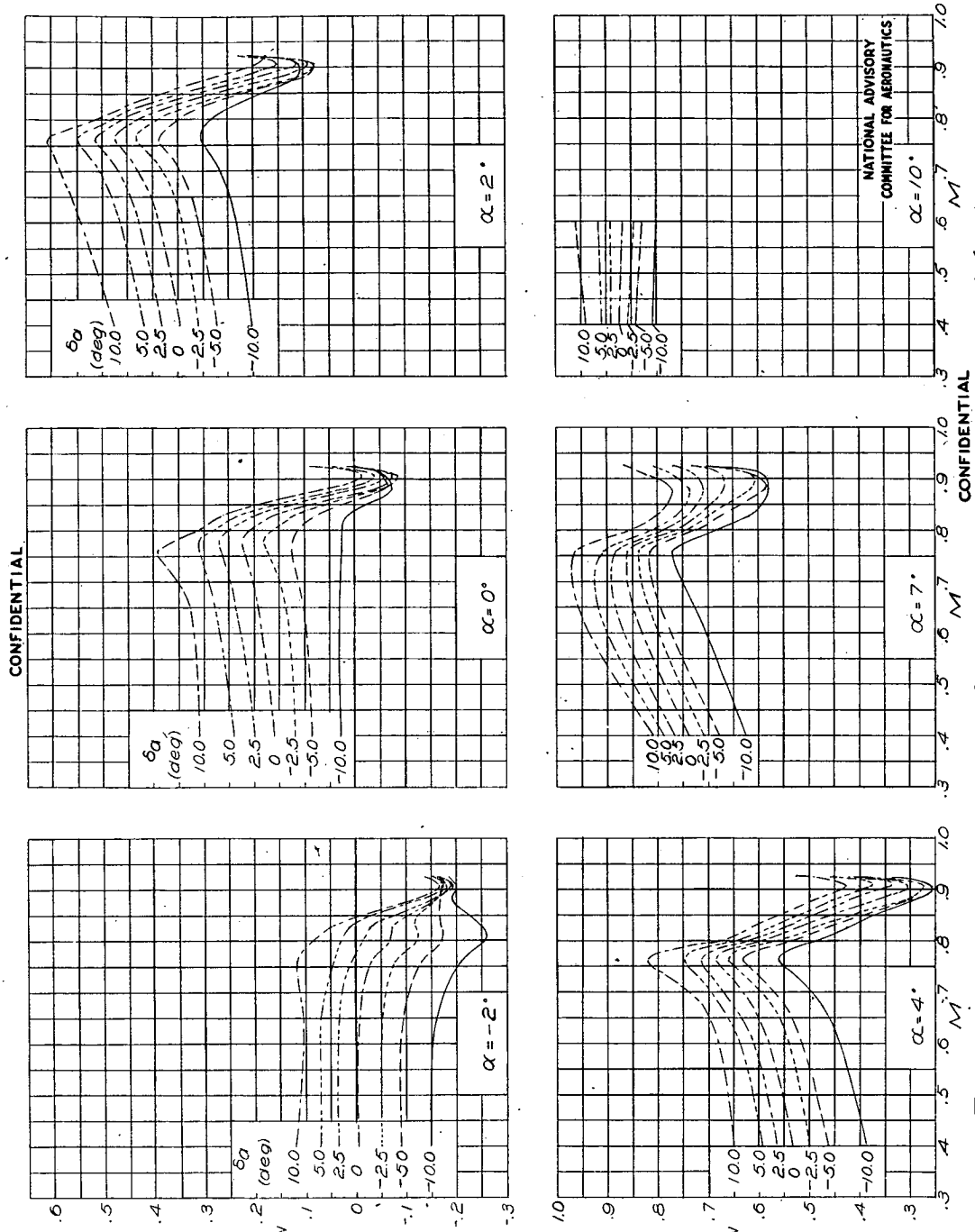

Figure 16.- Wing normal-force coefficient against Mach number at various aileron deflections and angles of attack.

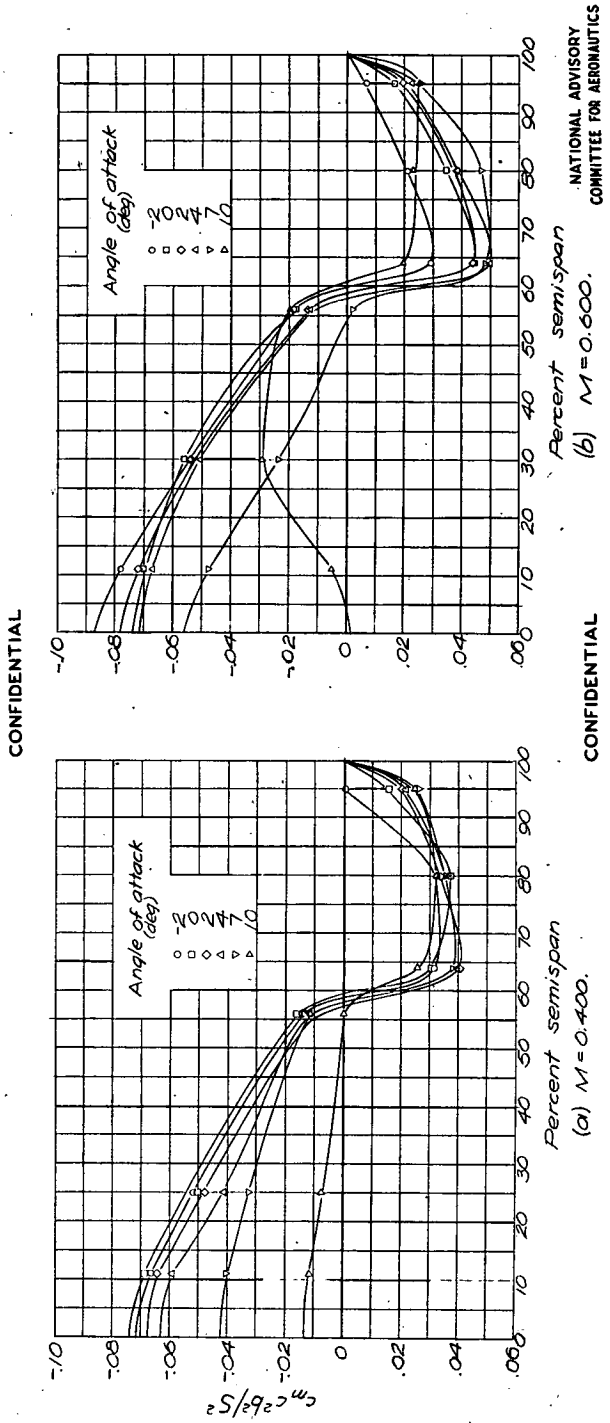

Figure 17.- Spanwise variation in section moment factor. $d_a = -10.0°$.

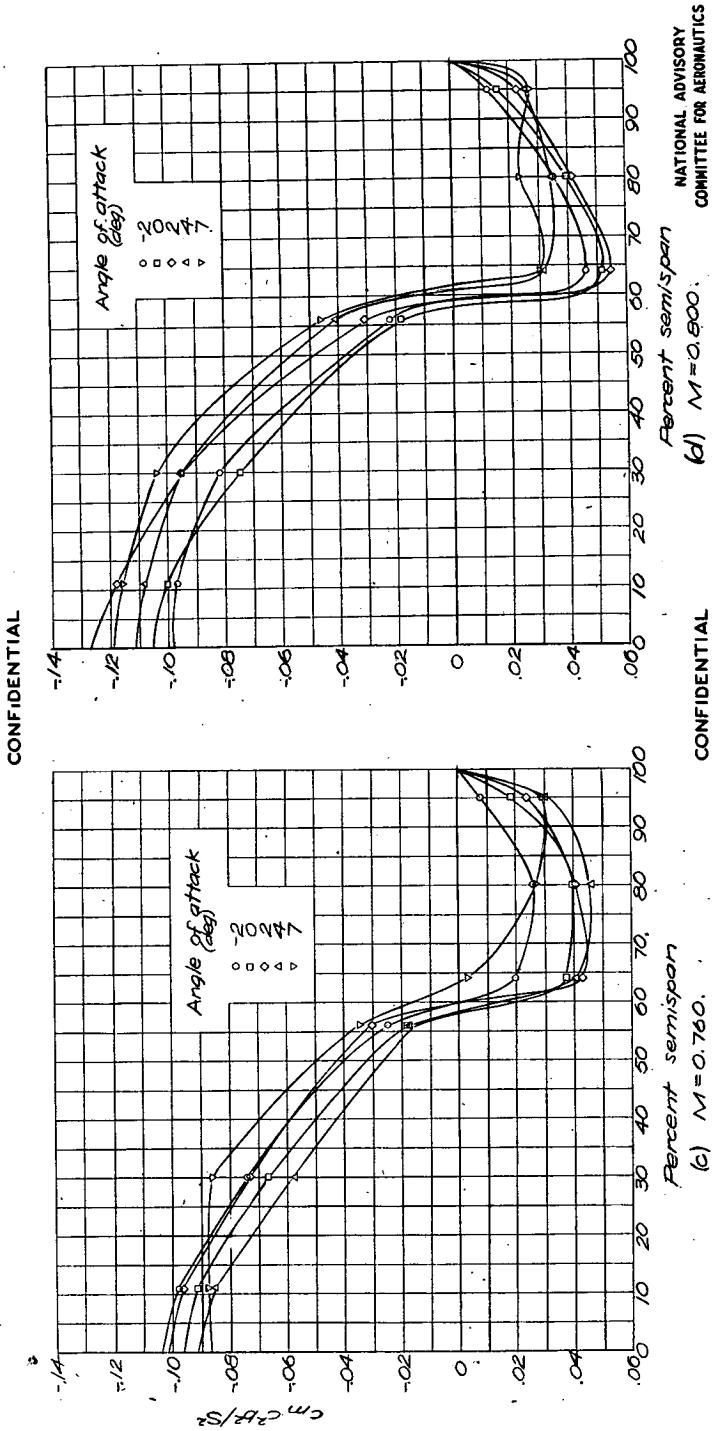

Figure 17.- Continued. $\delta_a = -10.0°$.

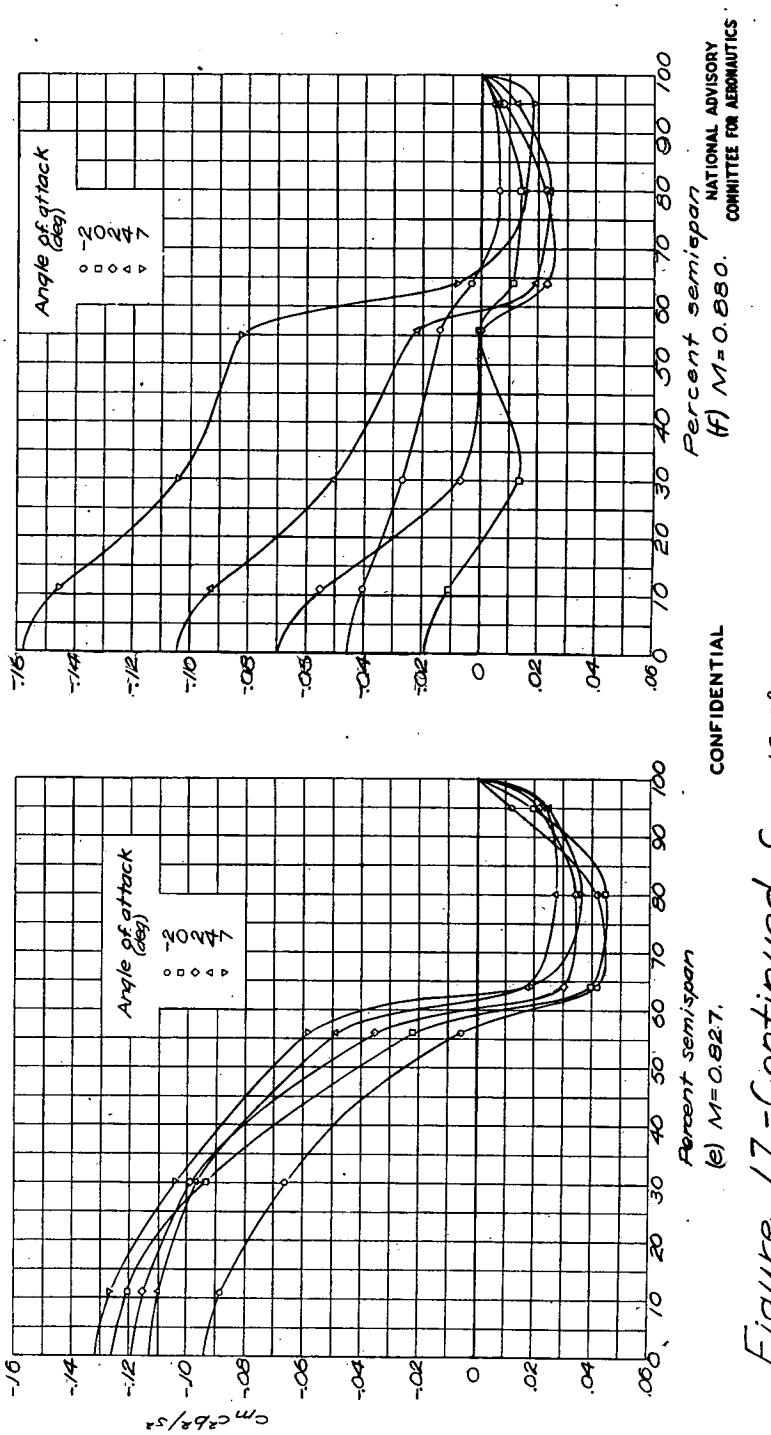

Figure 17.- Continued. $\delta_a = -10.0°$.

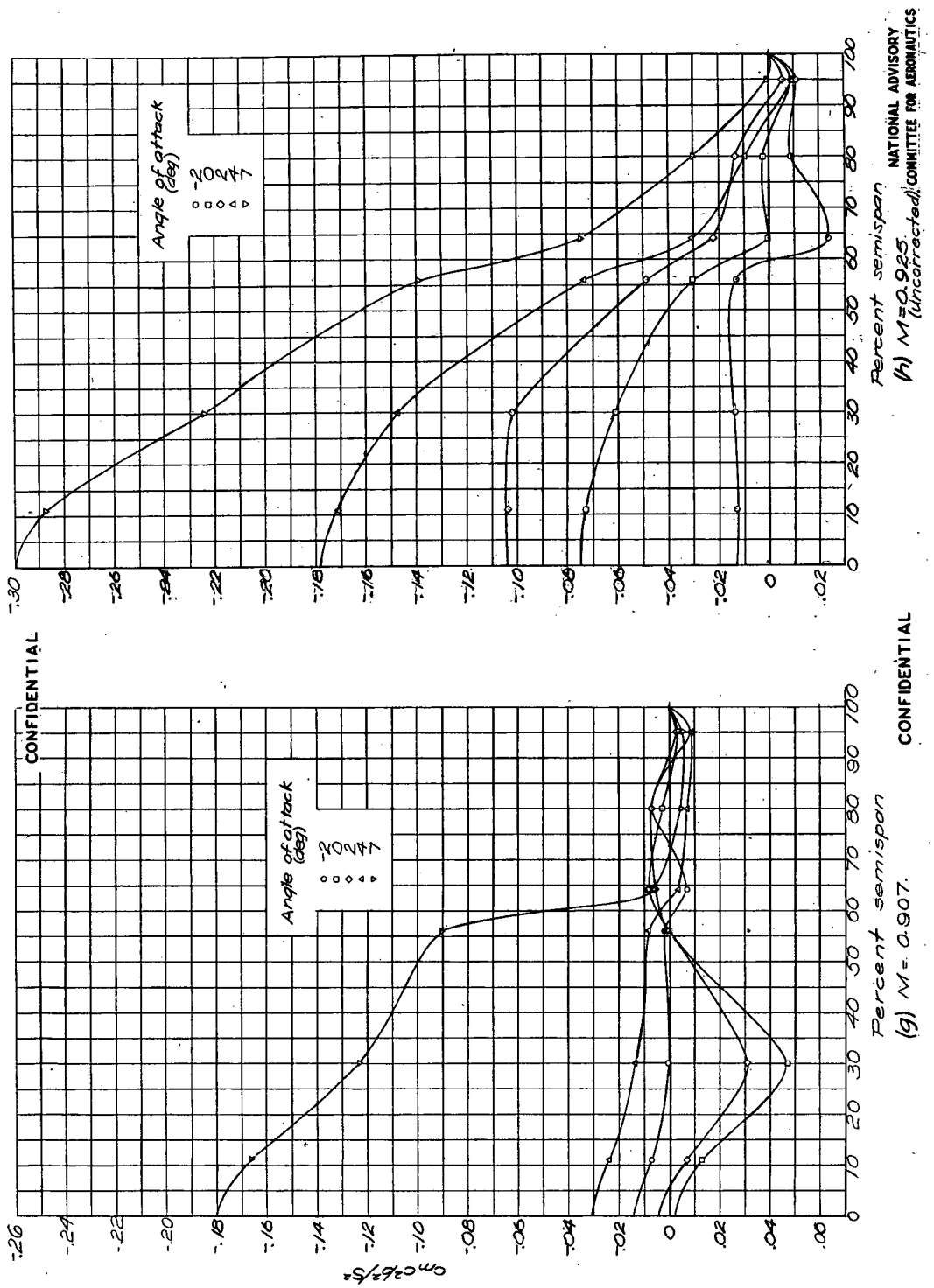

Figure 17.- Concluded. $\delta_a = -10.0°$

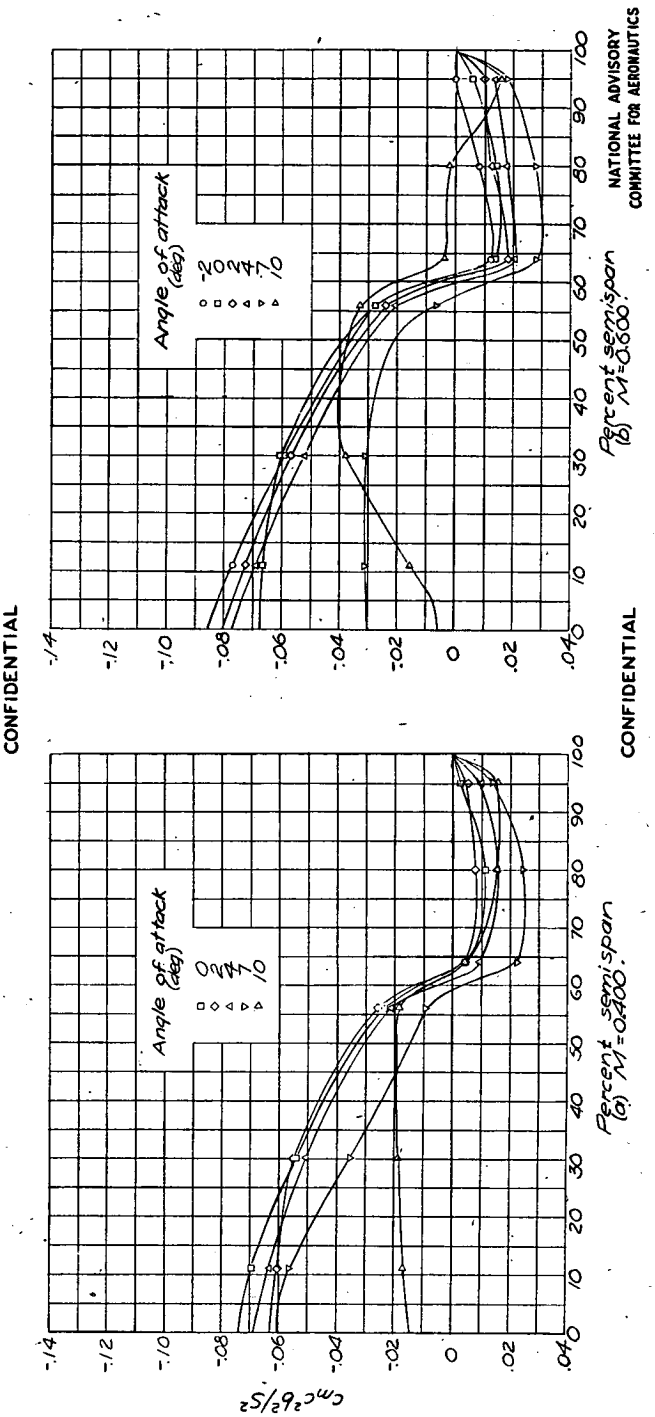

Figure 18.- Spanwise variation in section moment factor. $d_0 = -5.7$.

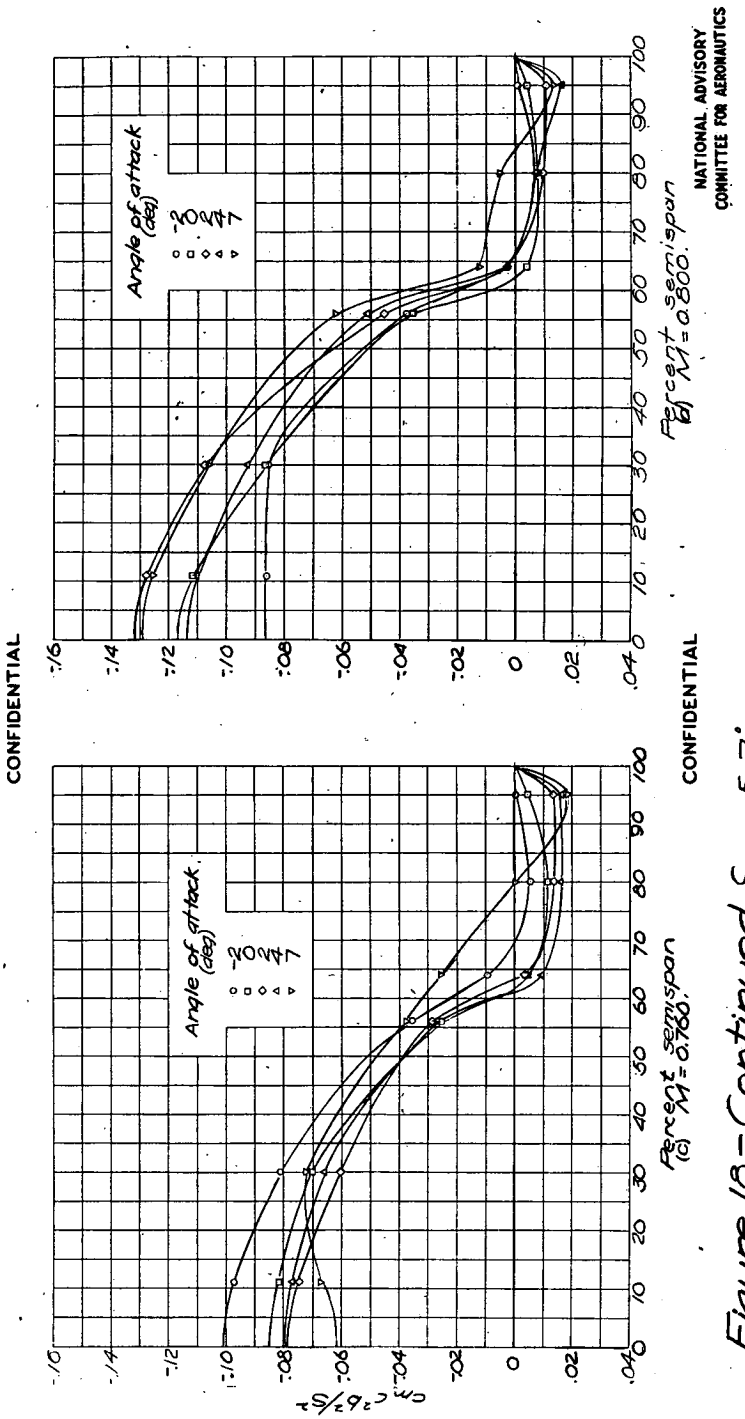

Figure 18.- Continued. $\delta_0 = -5.7°$

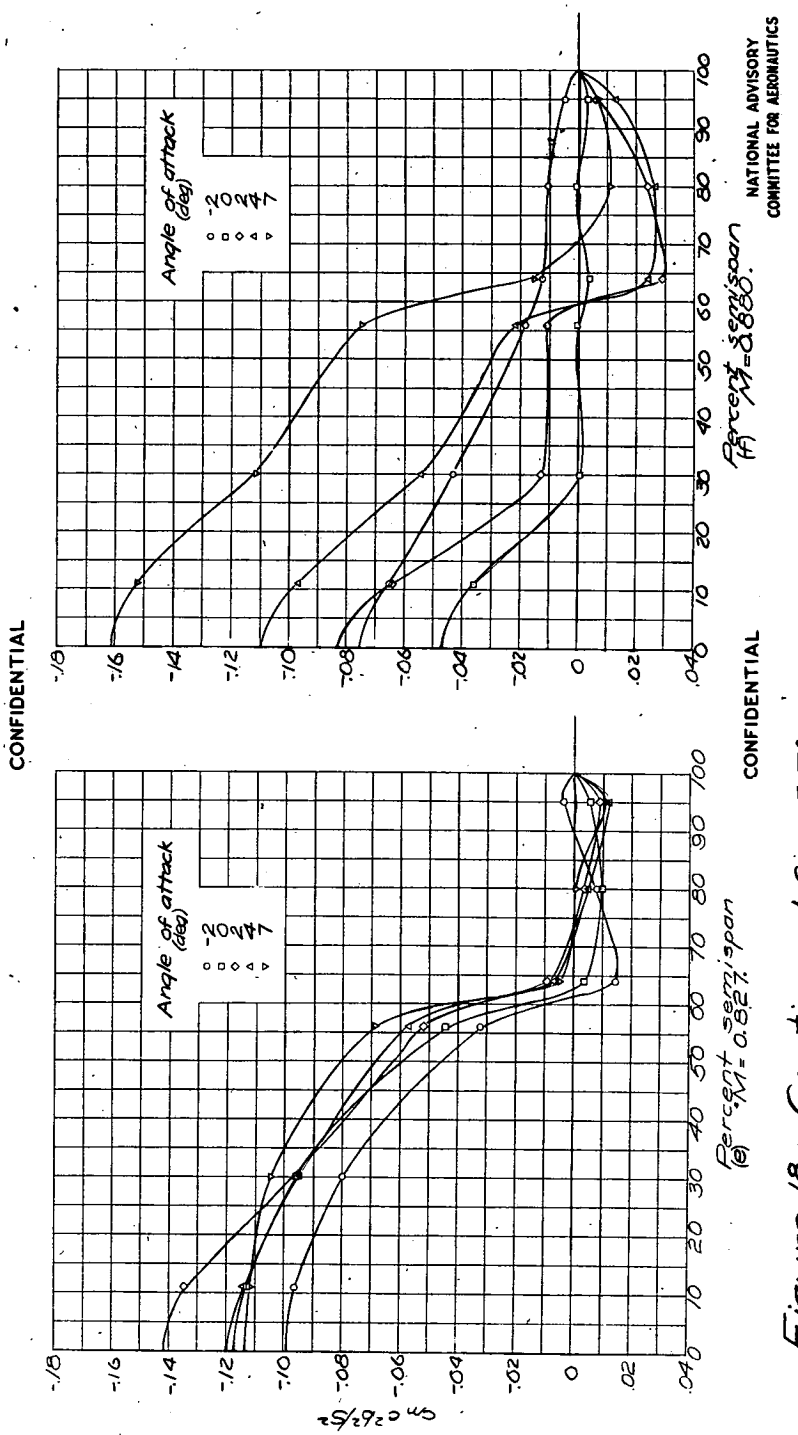

Figure 18.- Continued. $\delta_b = -5.7°$.

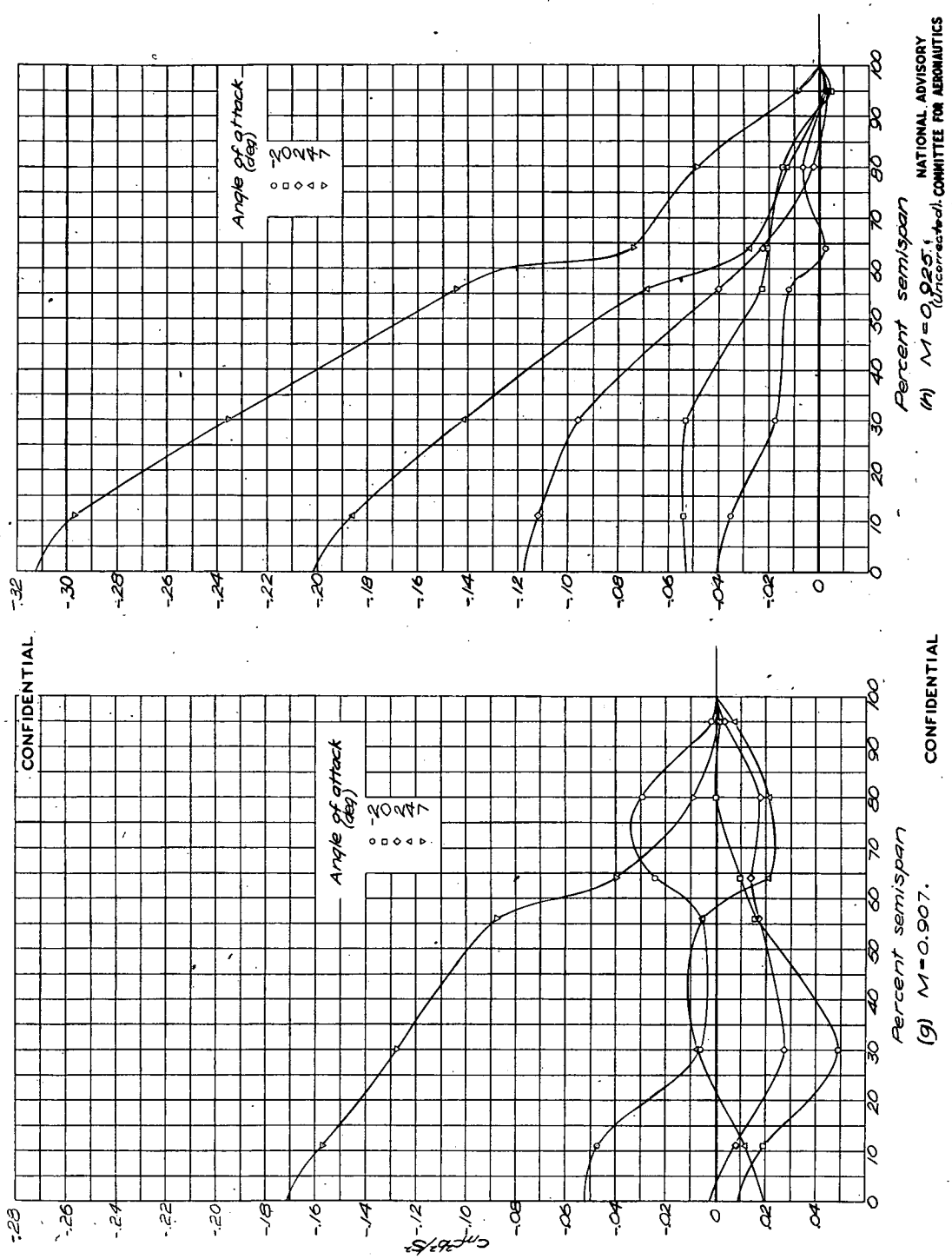

Figure 18.- Concluded. $\delta_a = -5.7°$

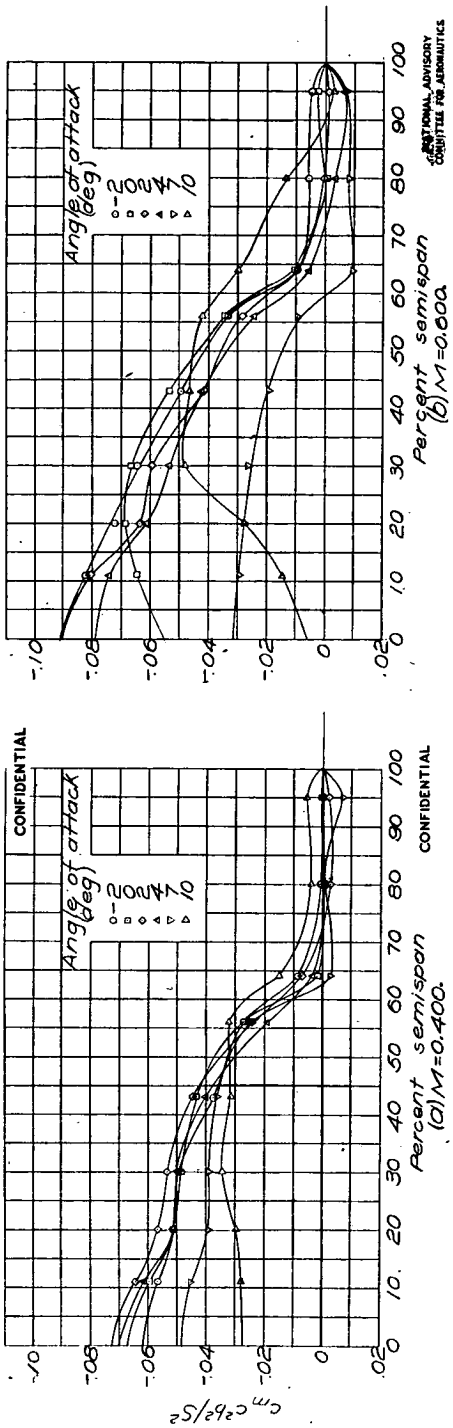

Figure 19.- Spanwise variation in section moment factor.
$\delta_a = -3.2°$.

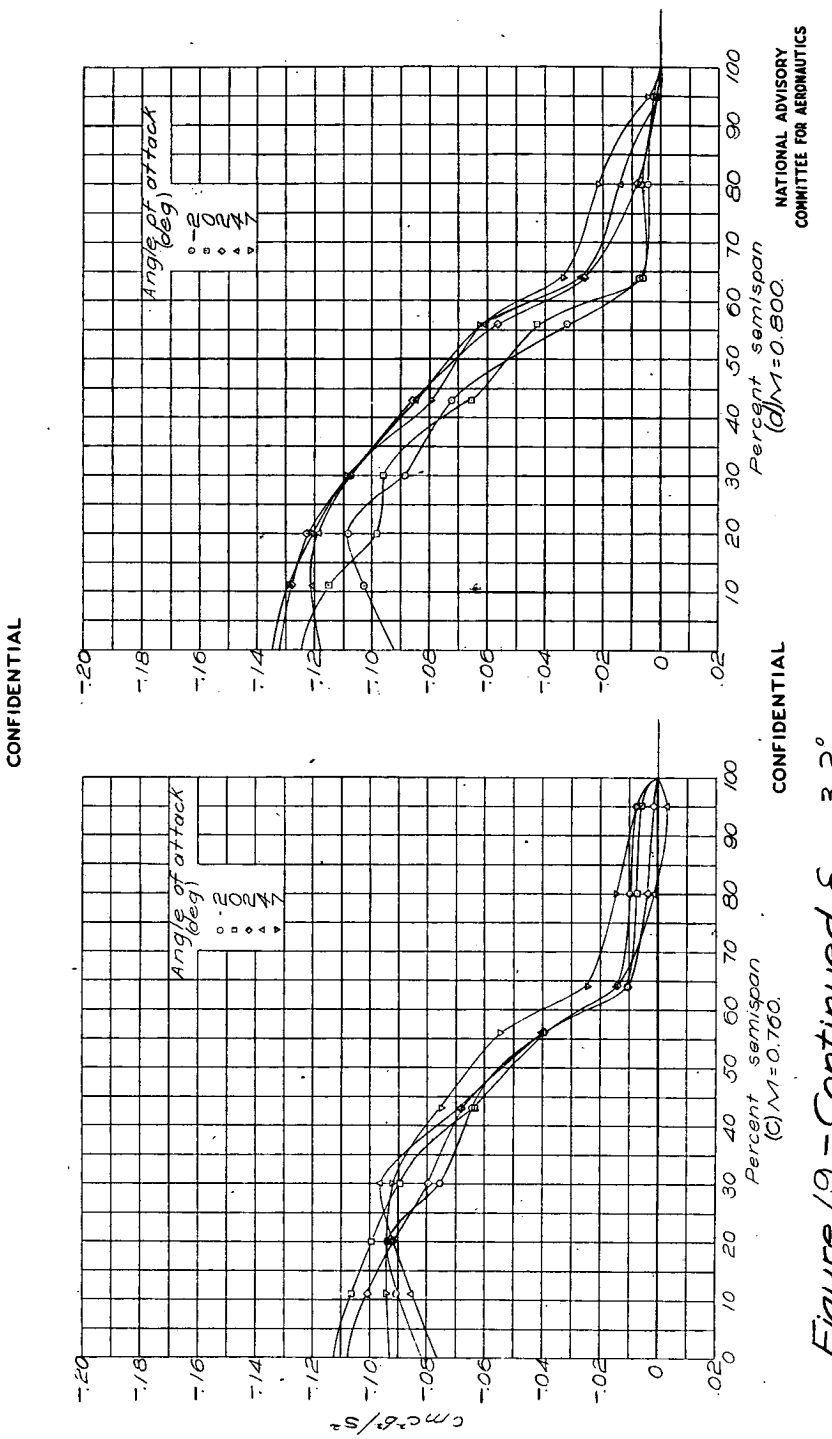

Figure 19.- Continued. $\delta_a = -3.2°$.

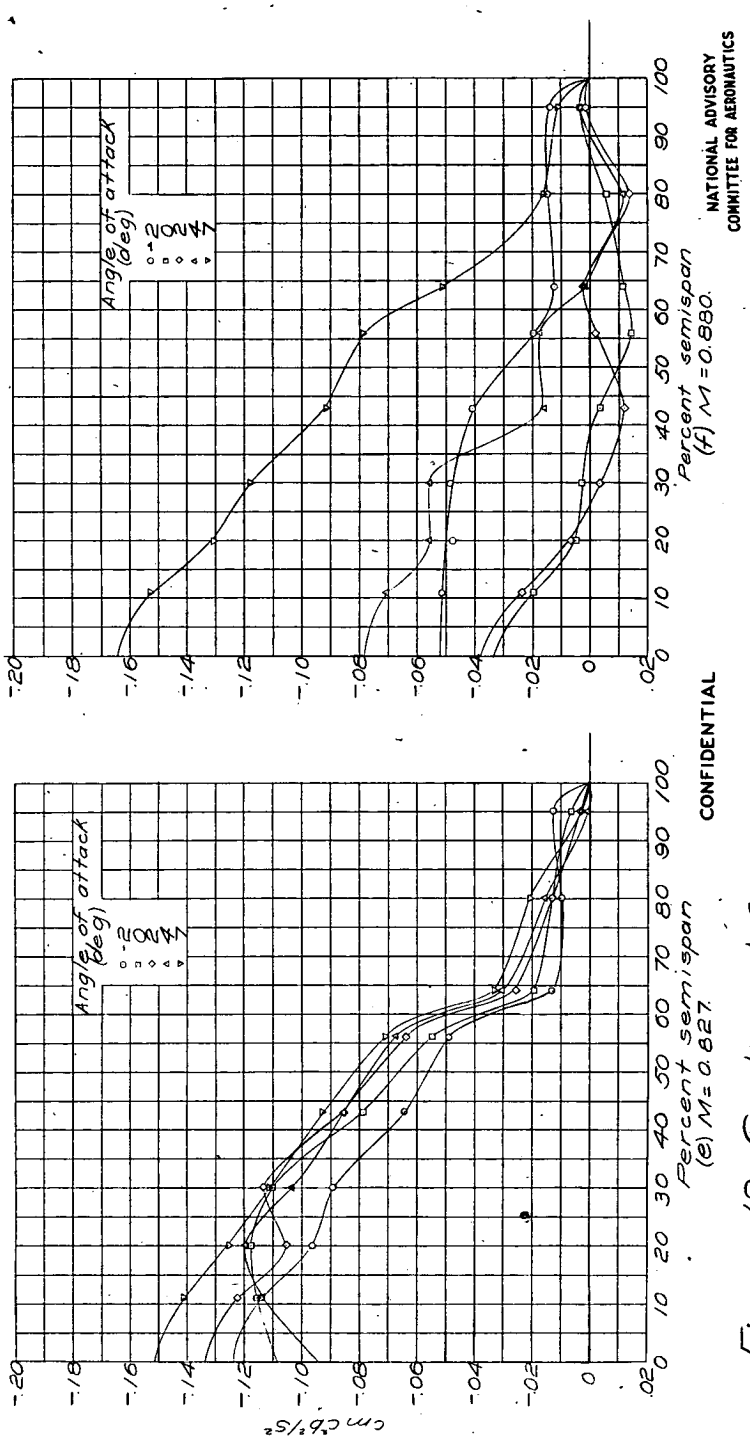

Figure 19.- Continued. $\delta_a = -3.2°$

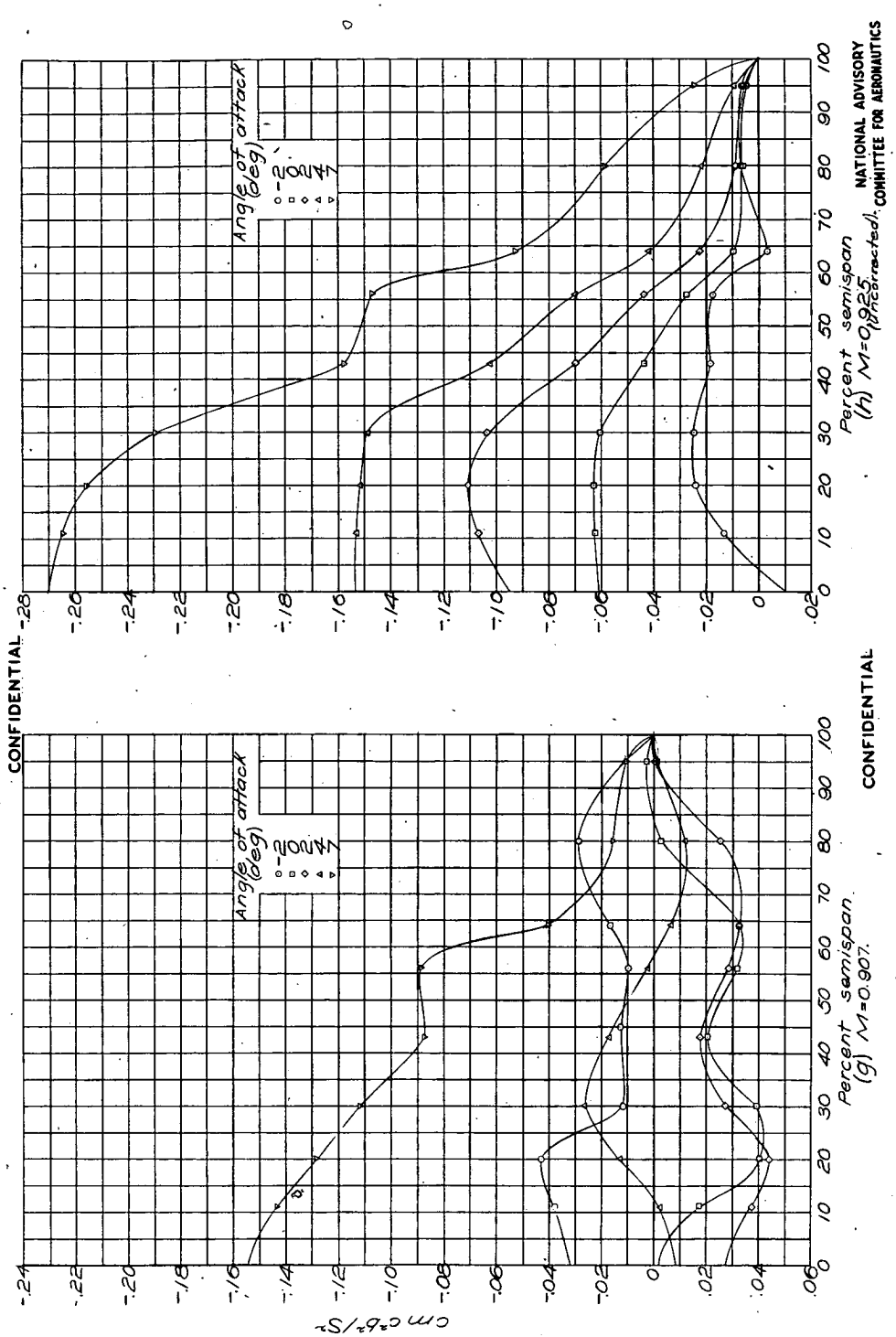

Figure 19.- Concluded. $\delta_a = -3.2°$.

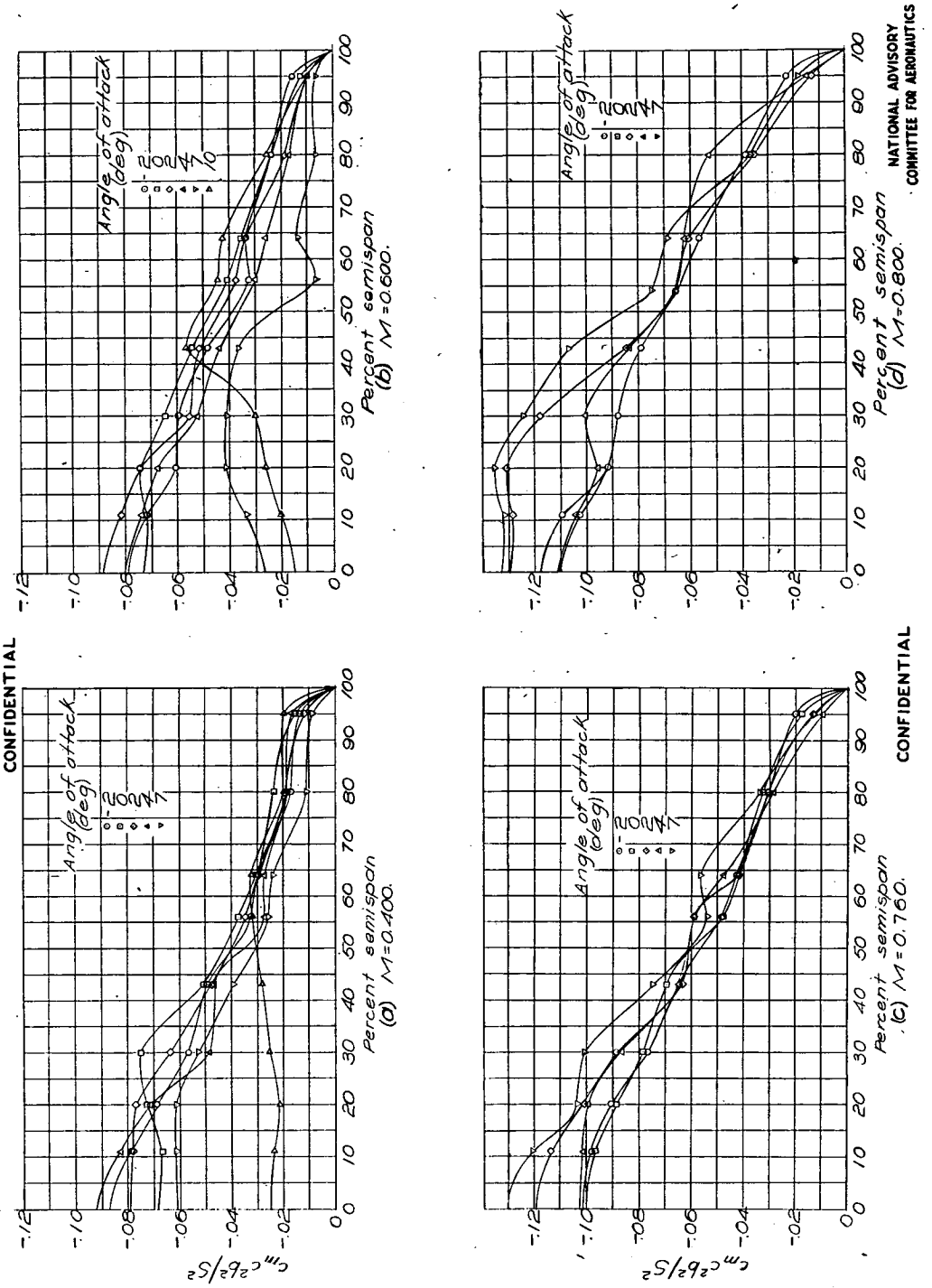

Figure 20.- Spanwise variation in section moment factor. $\delta_a = 0.5°$.

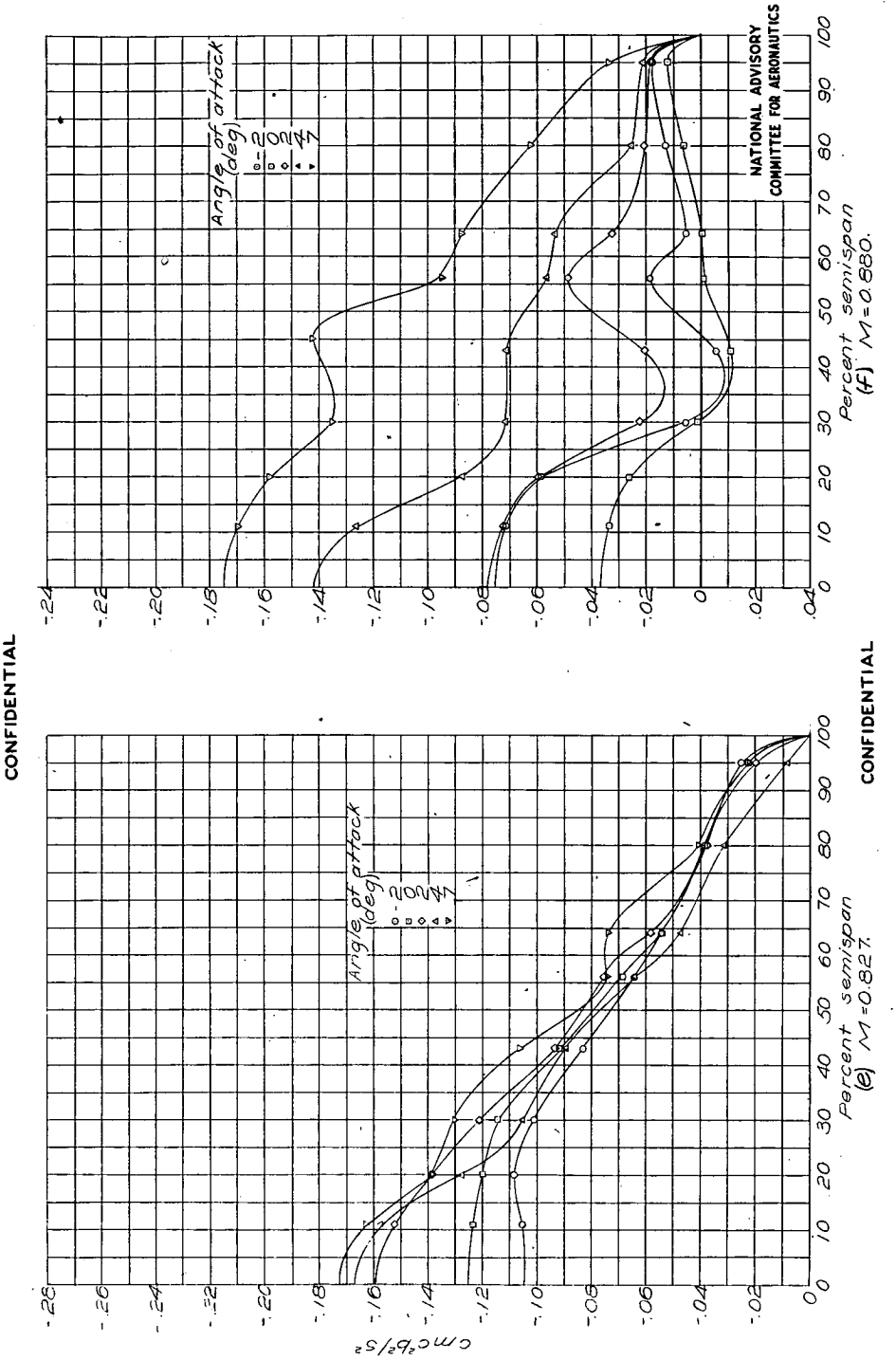

Figure 20.- Continued. $\delta_a = 0.5°$.

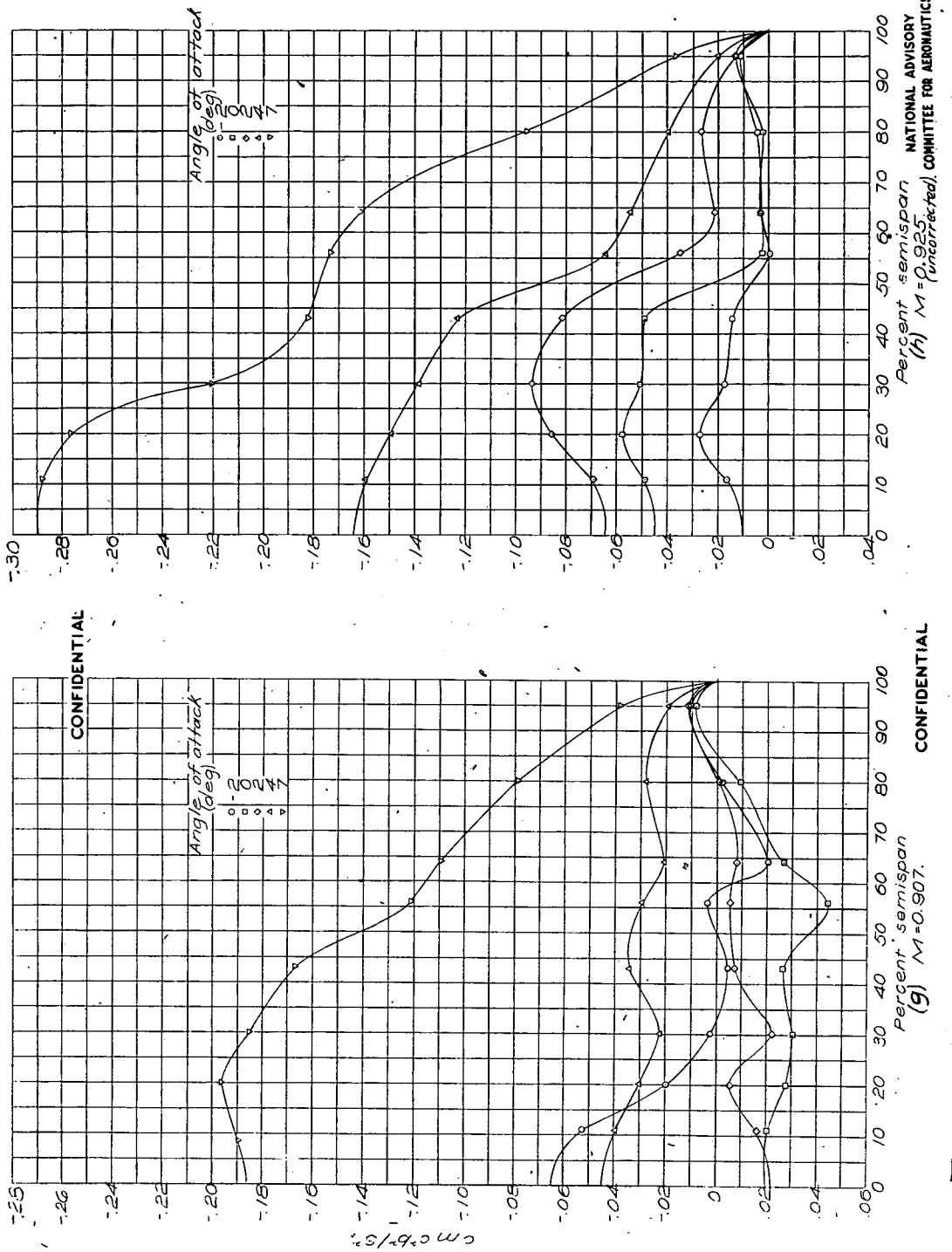

Figure 20.- Concluded. $\delta_a = 0.5°$.

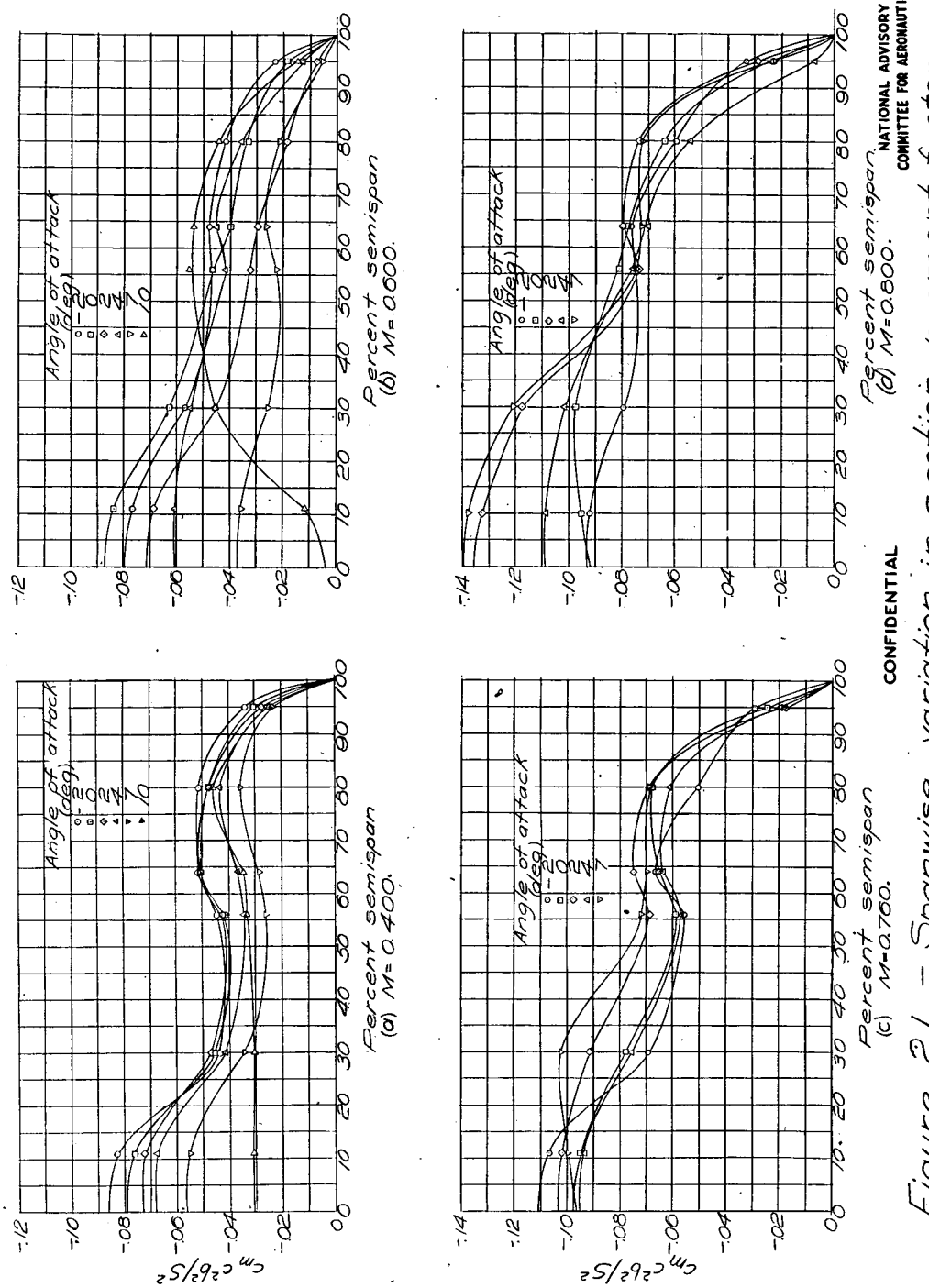

Figure 21. - Spanwise variation in section moment factor. $\alpha_a = 2.9°$.

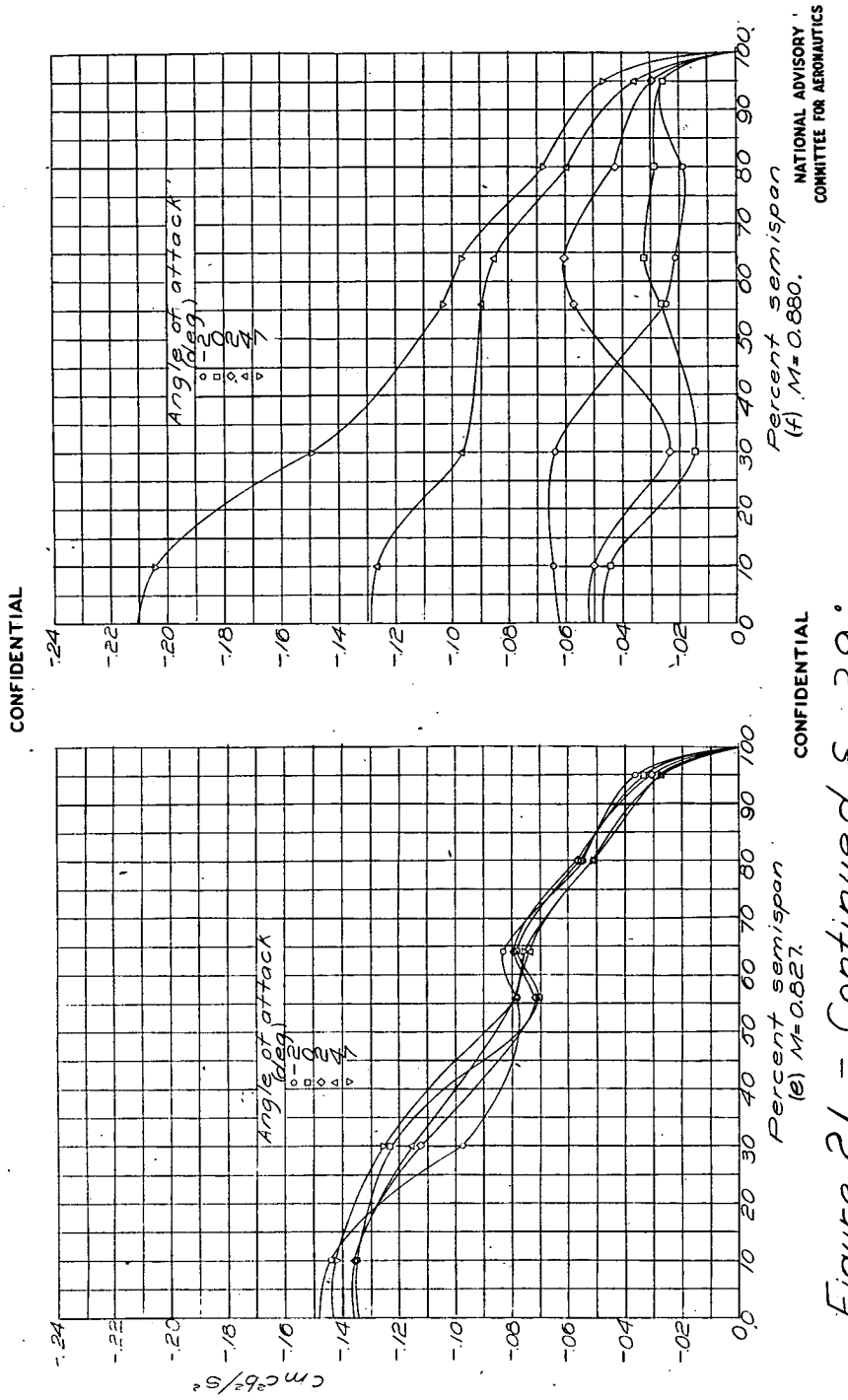

Figure 21.- Continued. $\delta_a = 2.9°$.

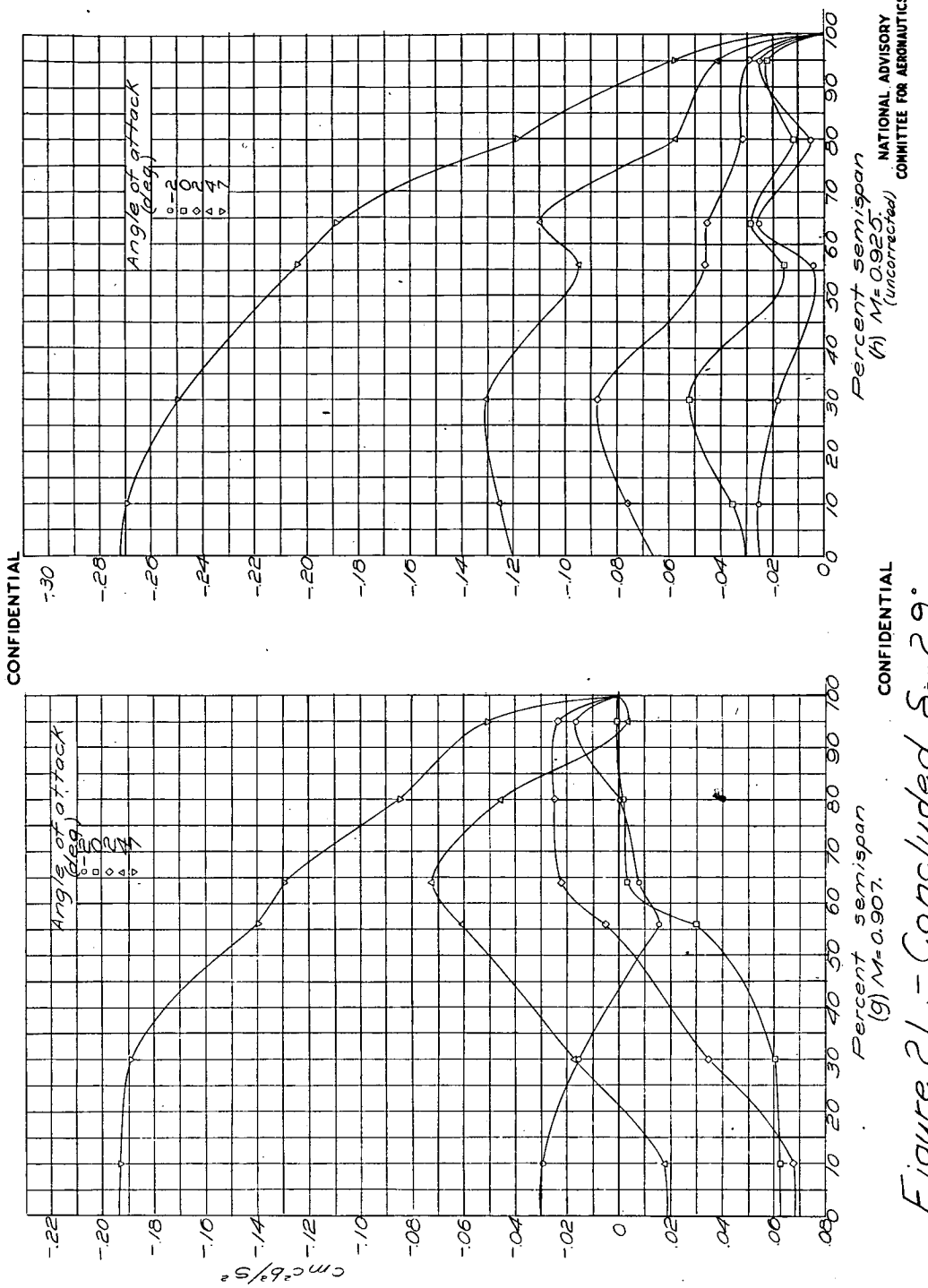

Figure 21. - Concluded. $\delta_a = 2.9°$.

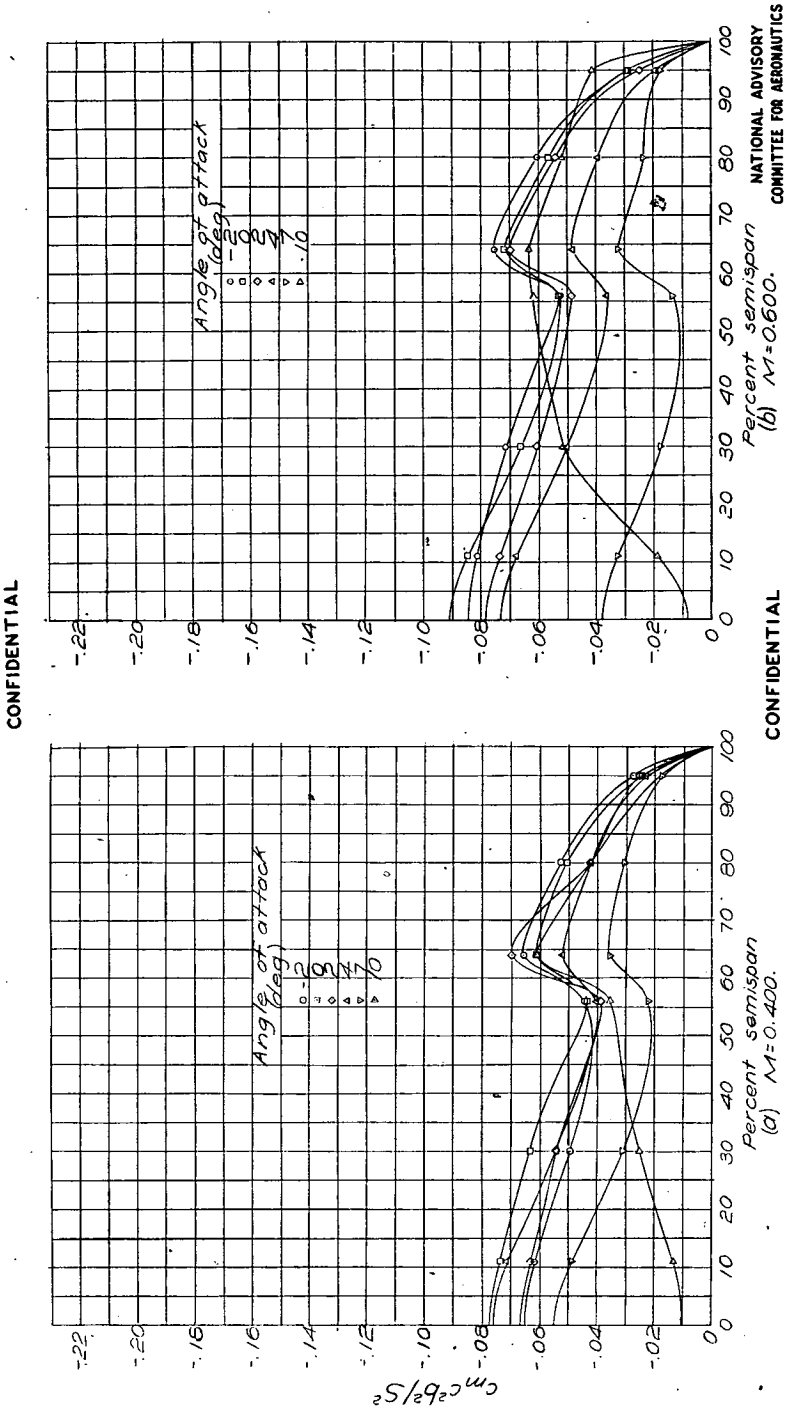

Figure 22.- Spanwise variation in section moment factor. $\delta_a = 5.8°$.

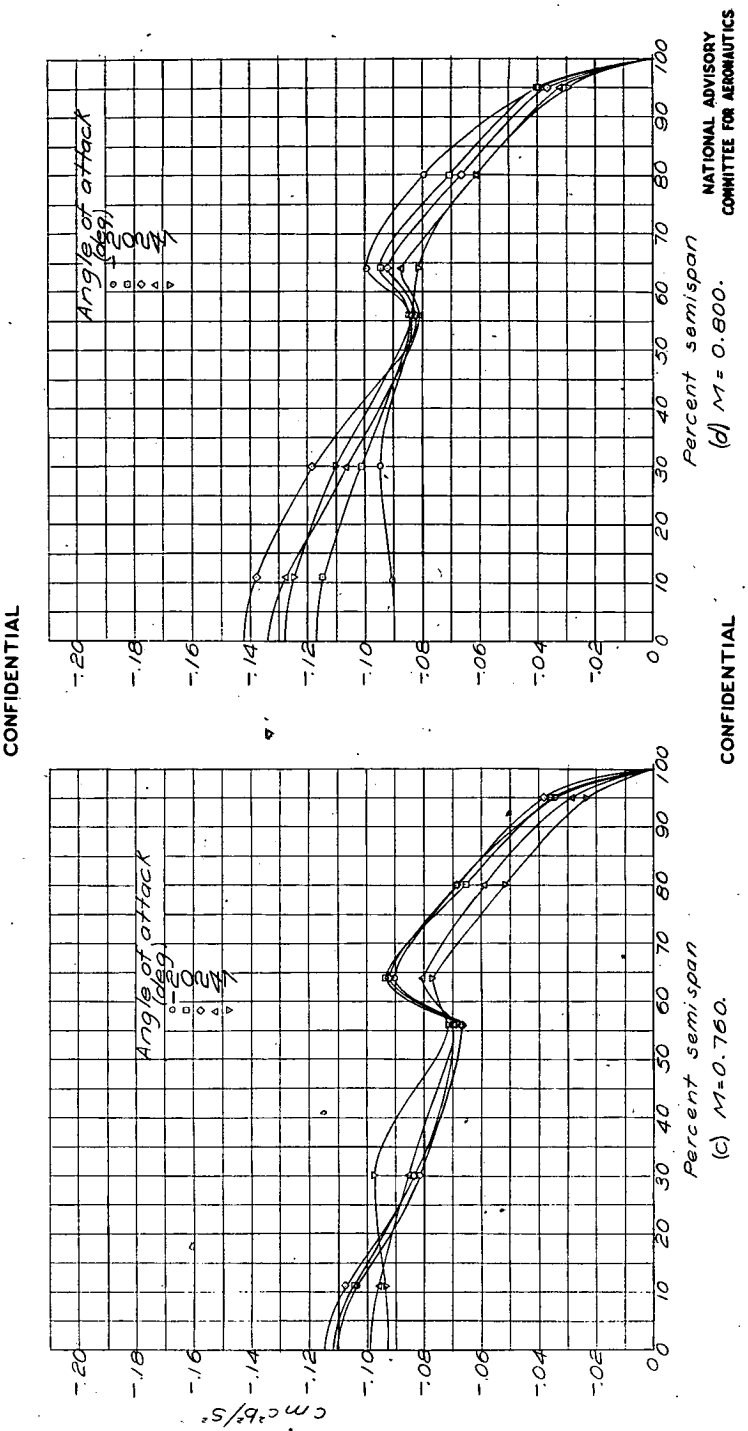

Figure 22.-Continued. $\delta_a = 5.8°$.

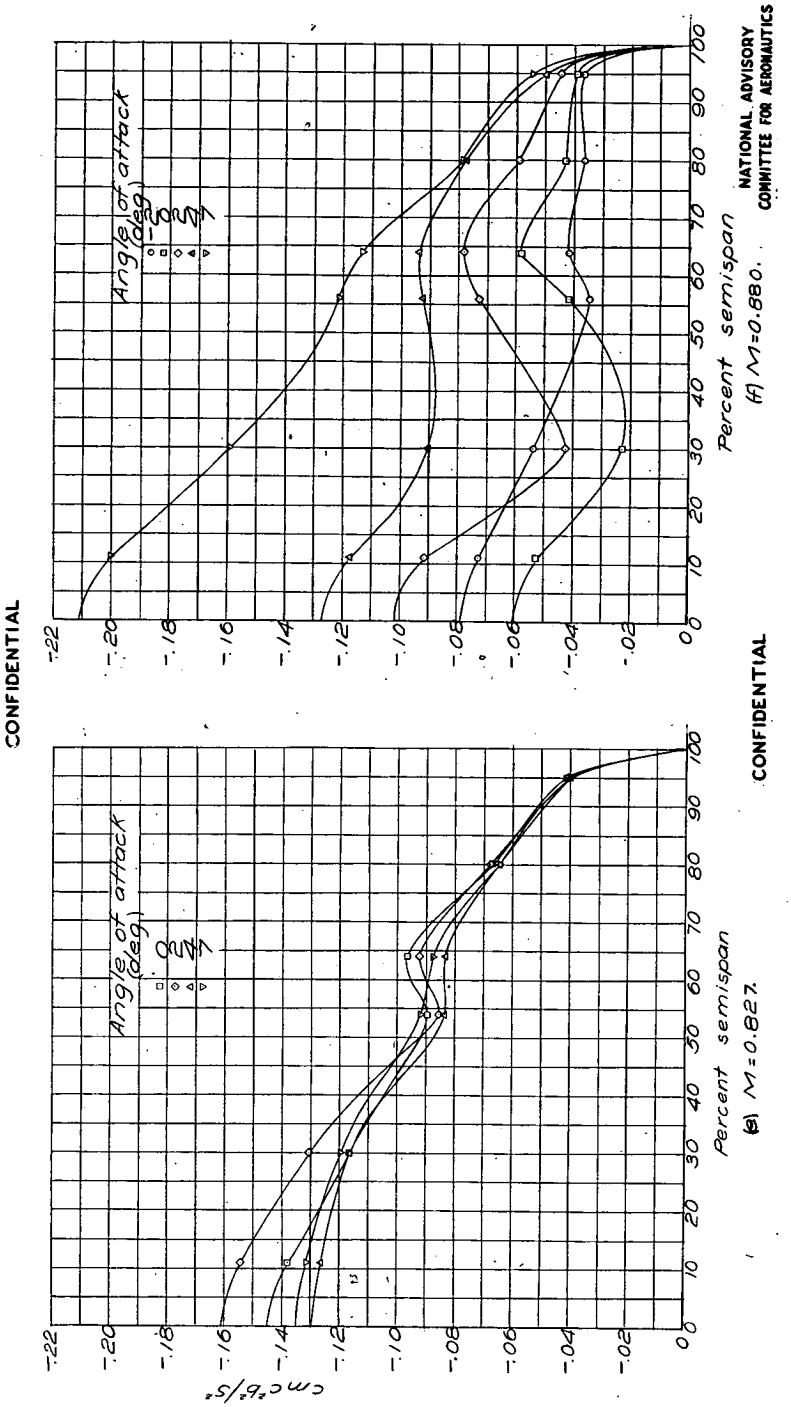

Figure 22.- Continued. $\delta_o = 5.8°$

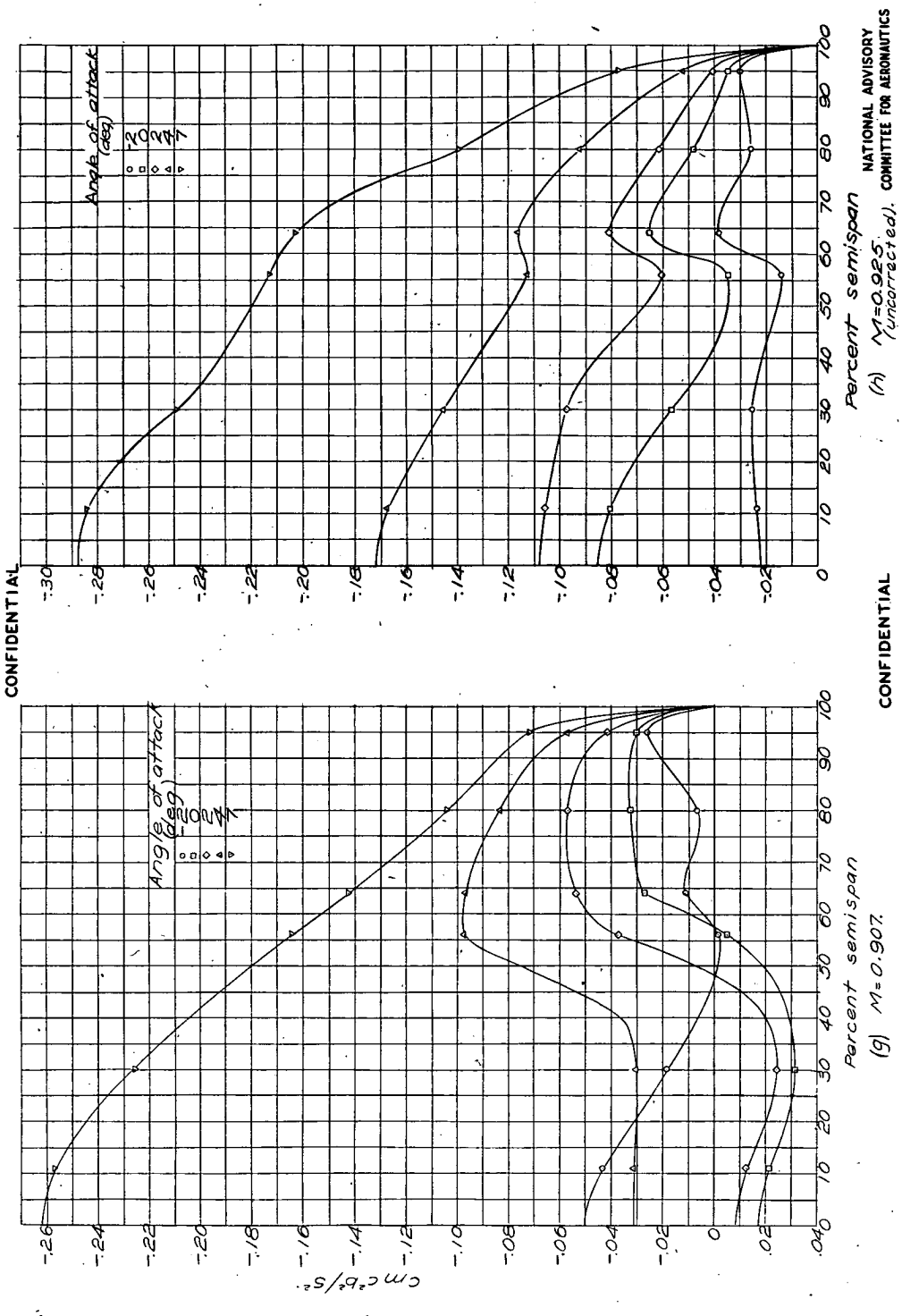

Figure 22.- Concluded. $\delta_a = 5.8°$

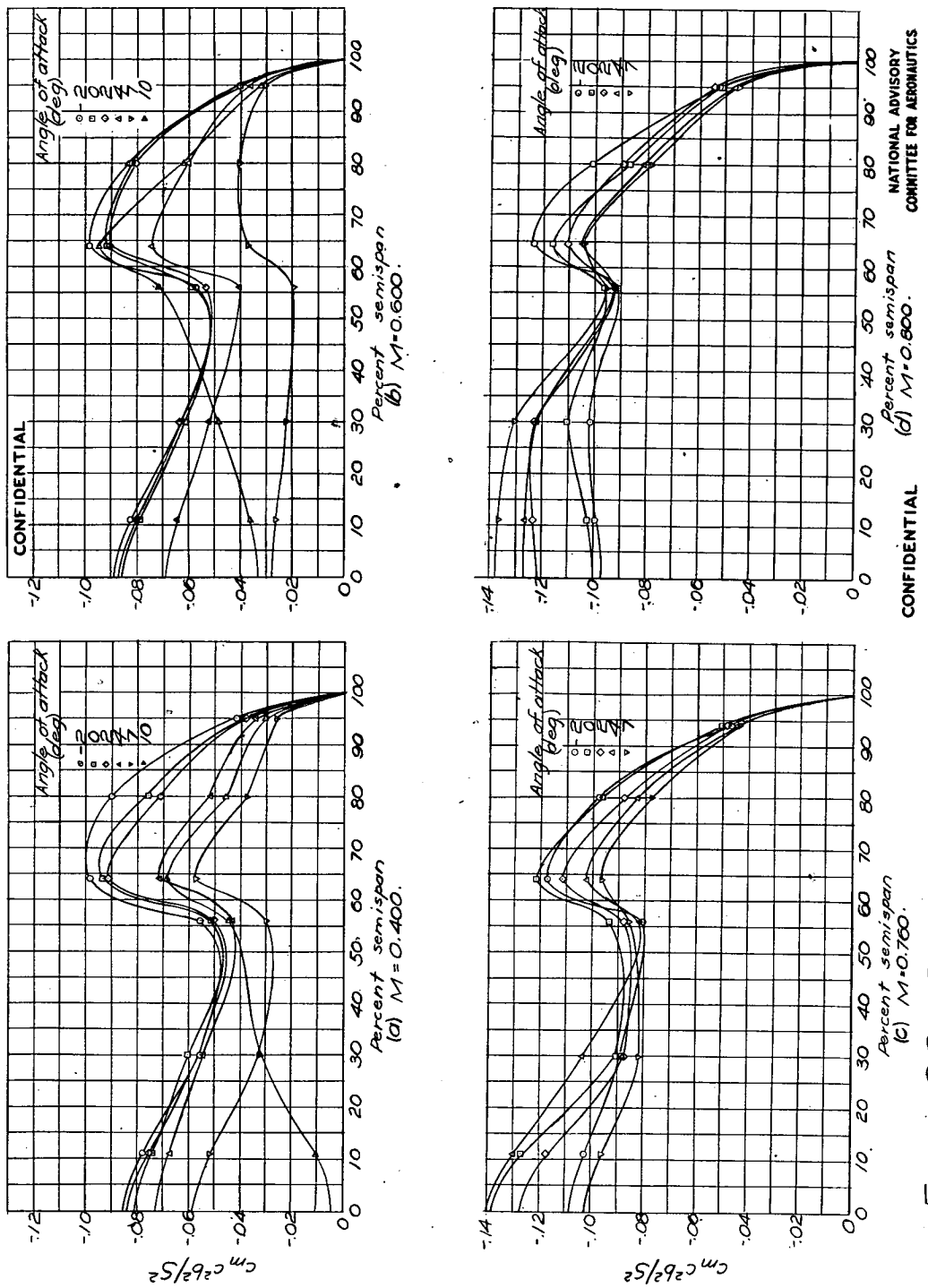

Figure 23.- Spanwise variation in section moment factor. $\delta_a = 9.6°$.

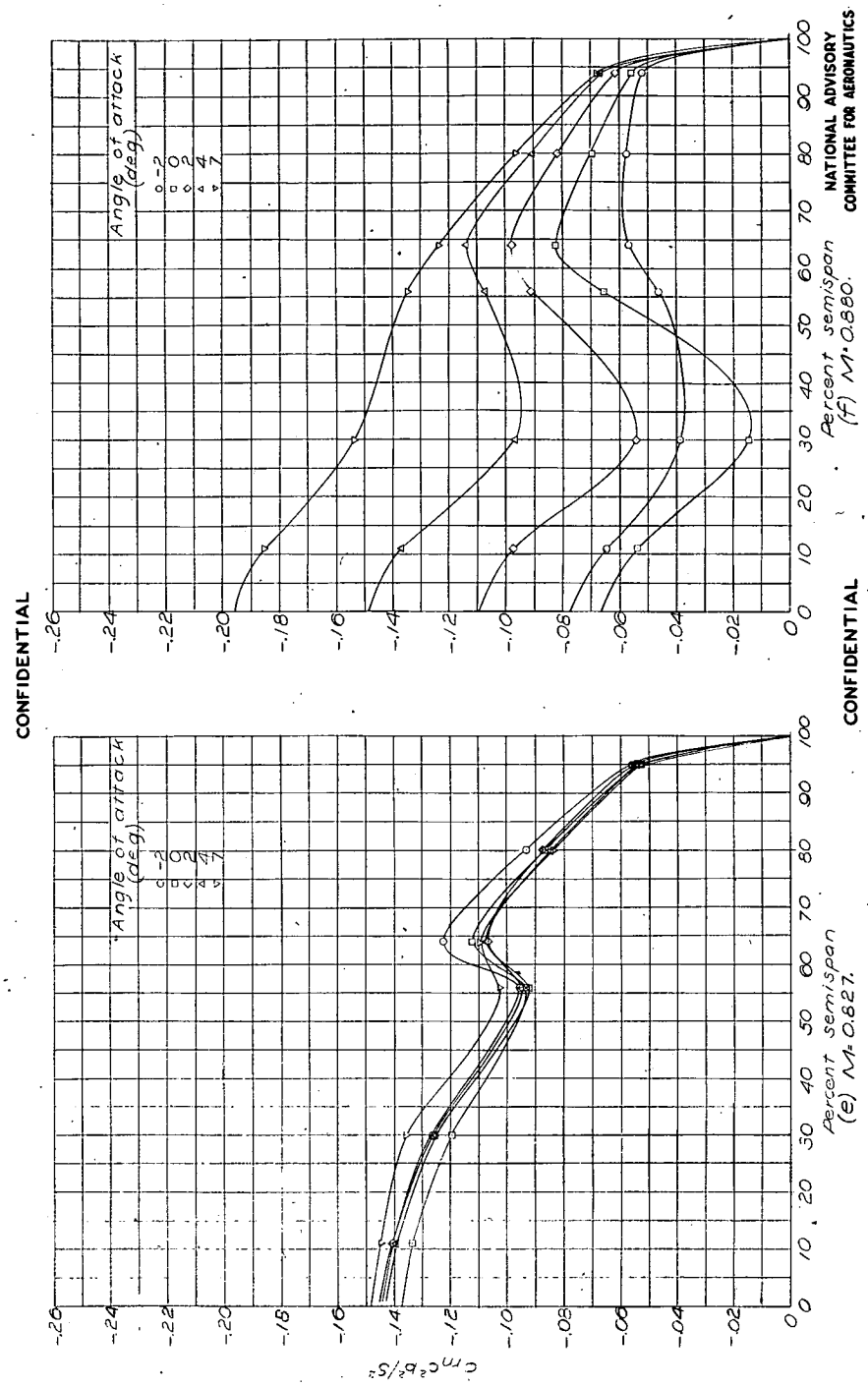

Figure 23.- Continued. $\delta_a = 9.6°$.

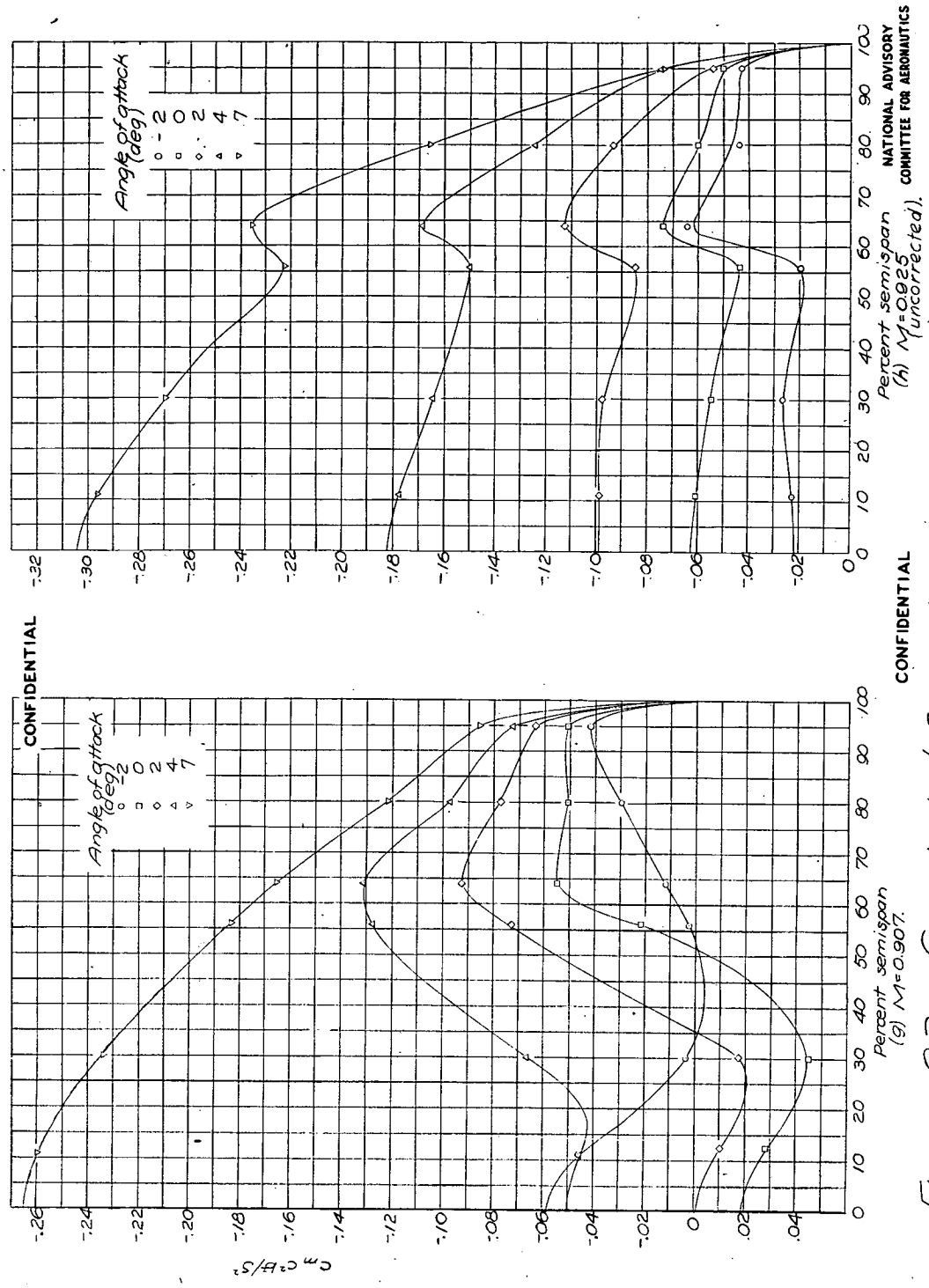

Figure 23.- Concluded. $\delta_a = 9.6°$.

CONFIDENTIAL

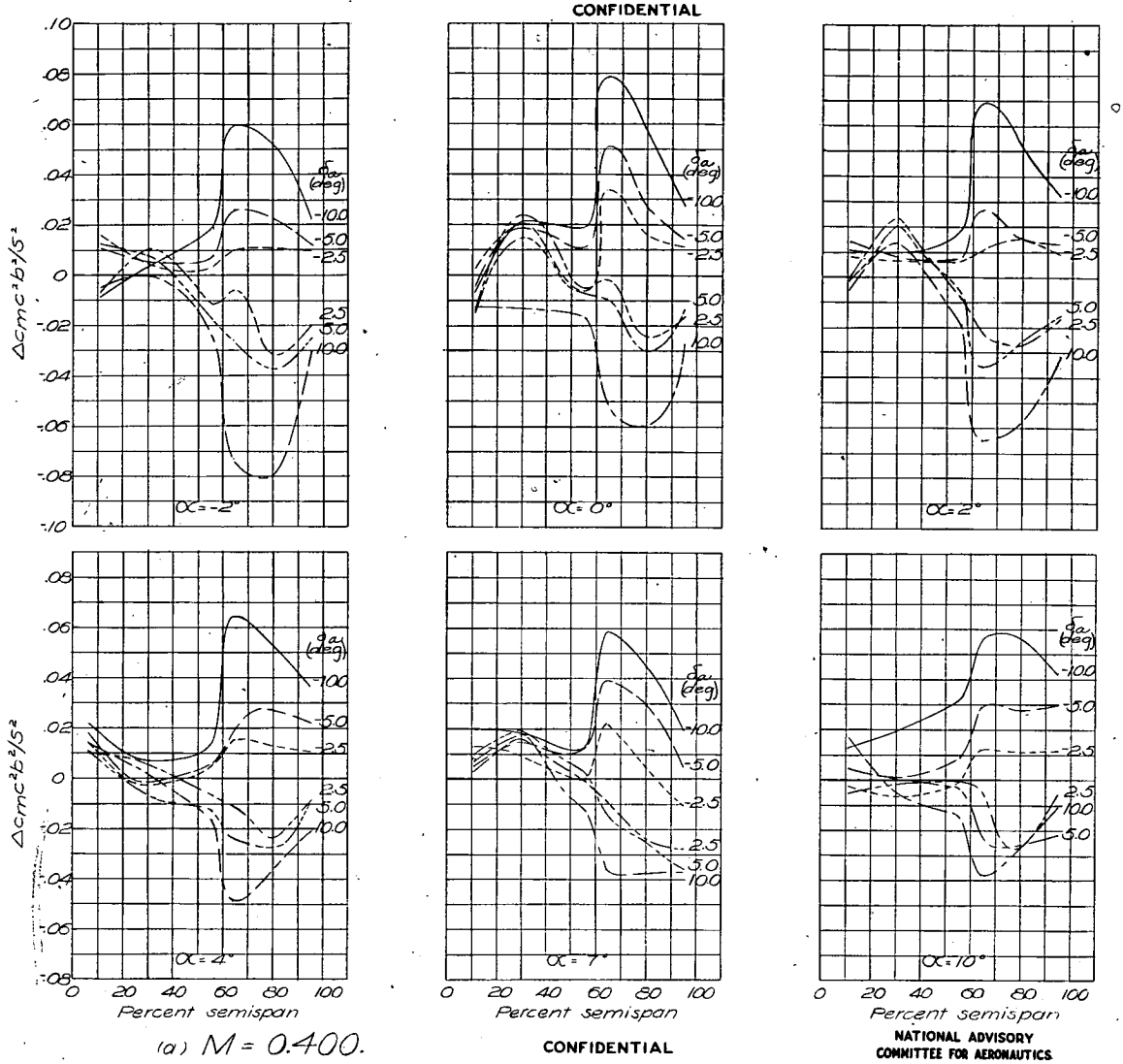

(a) $M = 0.400$.

CONFIDENTIAL

NATIONAL ADVISORY COMMITTEE FOR AERONAUTICS

Figure 24.- Spanwise variations in section moment factor due to aileron deflection.

CONFIDENTIAL

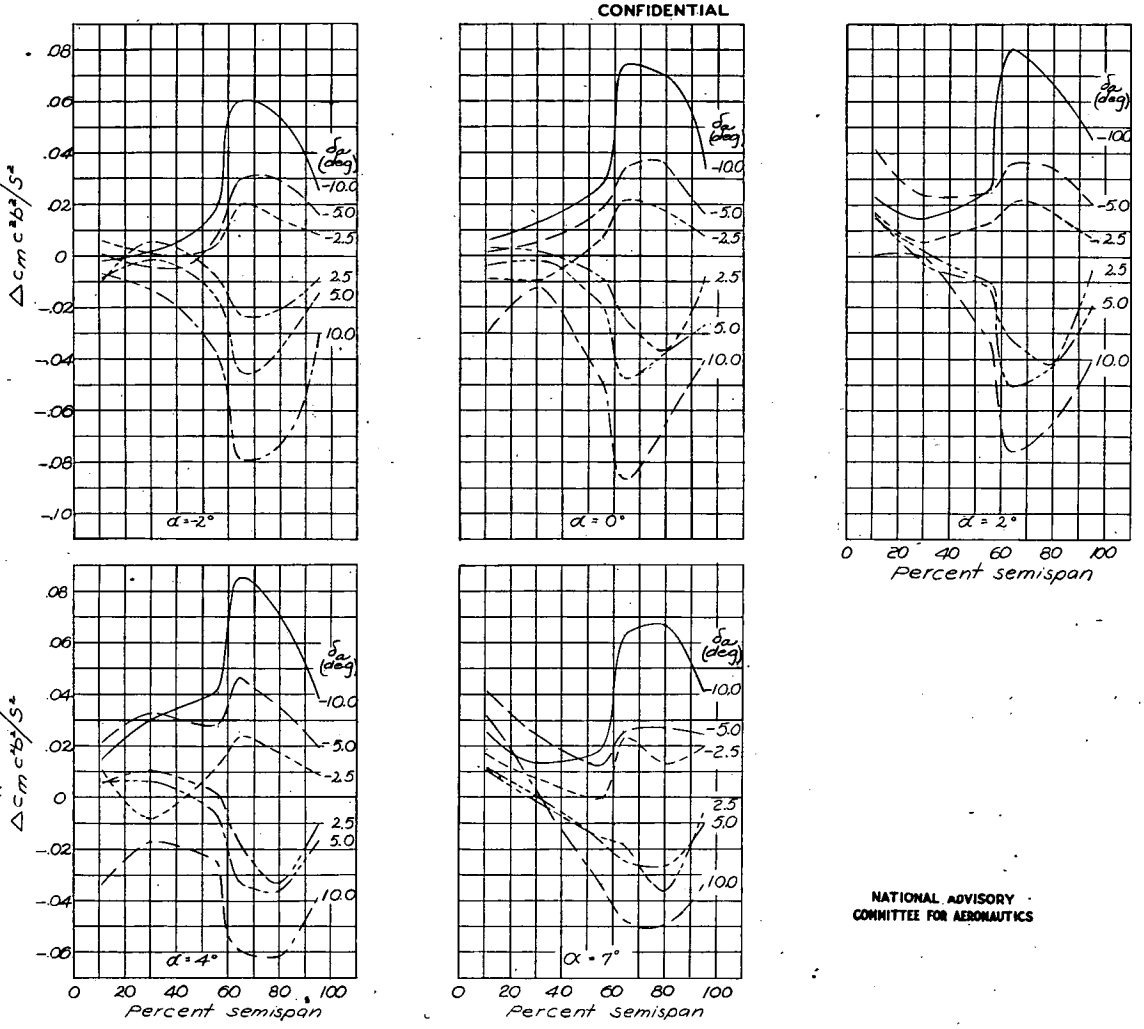

(b) $M = 0.760$.

Figure 24.- Continued.

CONFIDENTIAL

NATIONAL ADVISORY COMMITTEE FOR AERONAUTICS

CONFIDENTIAL

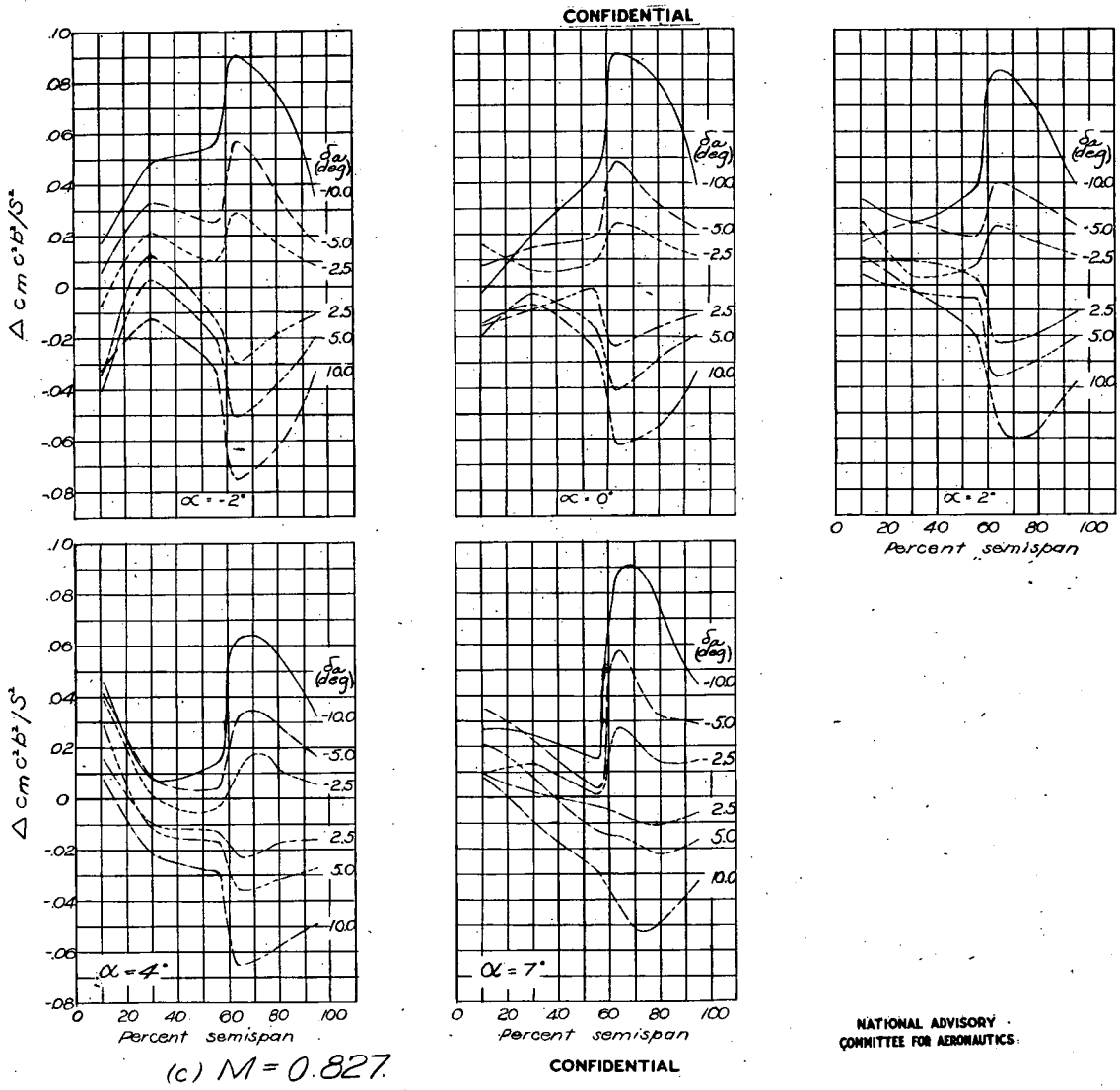

NATIONAL ADVISORY COMMITTEE FOR AERONAUTICS

CONFIDENTIAL

(c) $M = 0.827$

Figure 24.- Continued.

CONFIDENTIAL

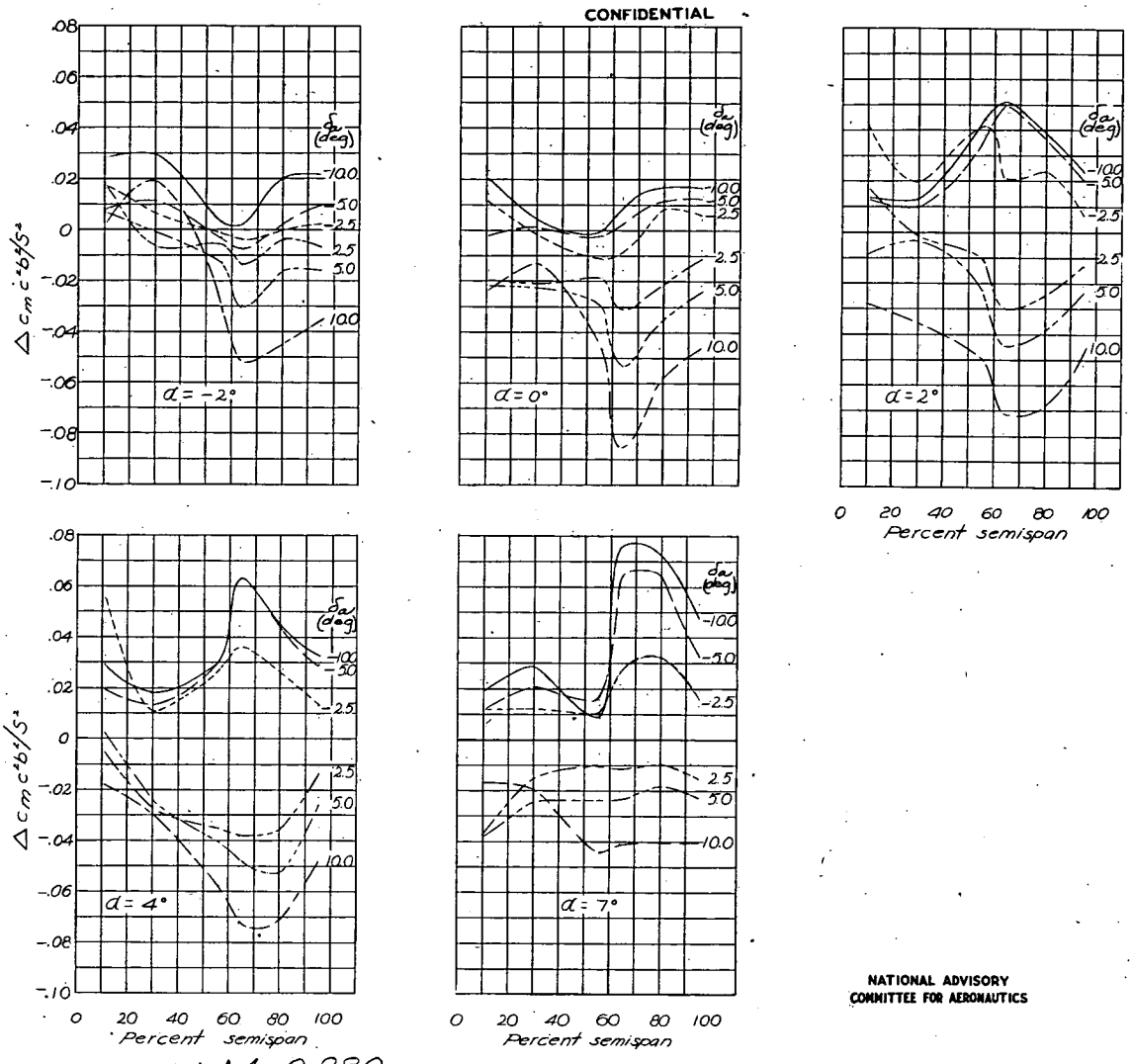

(d) $M = 0.880$.

Figure 24.- Concluded.

NATIONAL ADVISORY
COMMITTEE FOR AERONAUTICS

CONFIDENTIAL

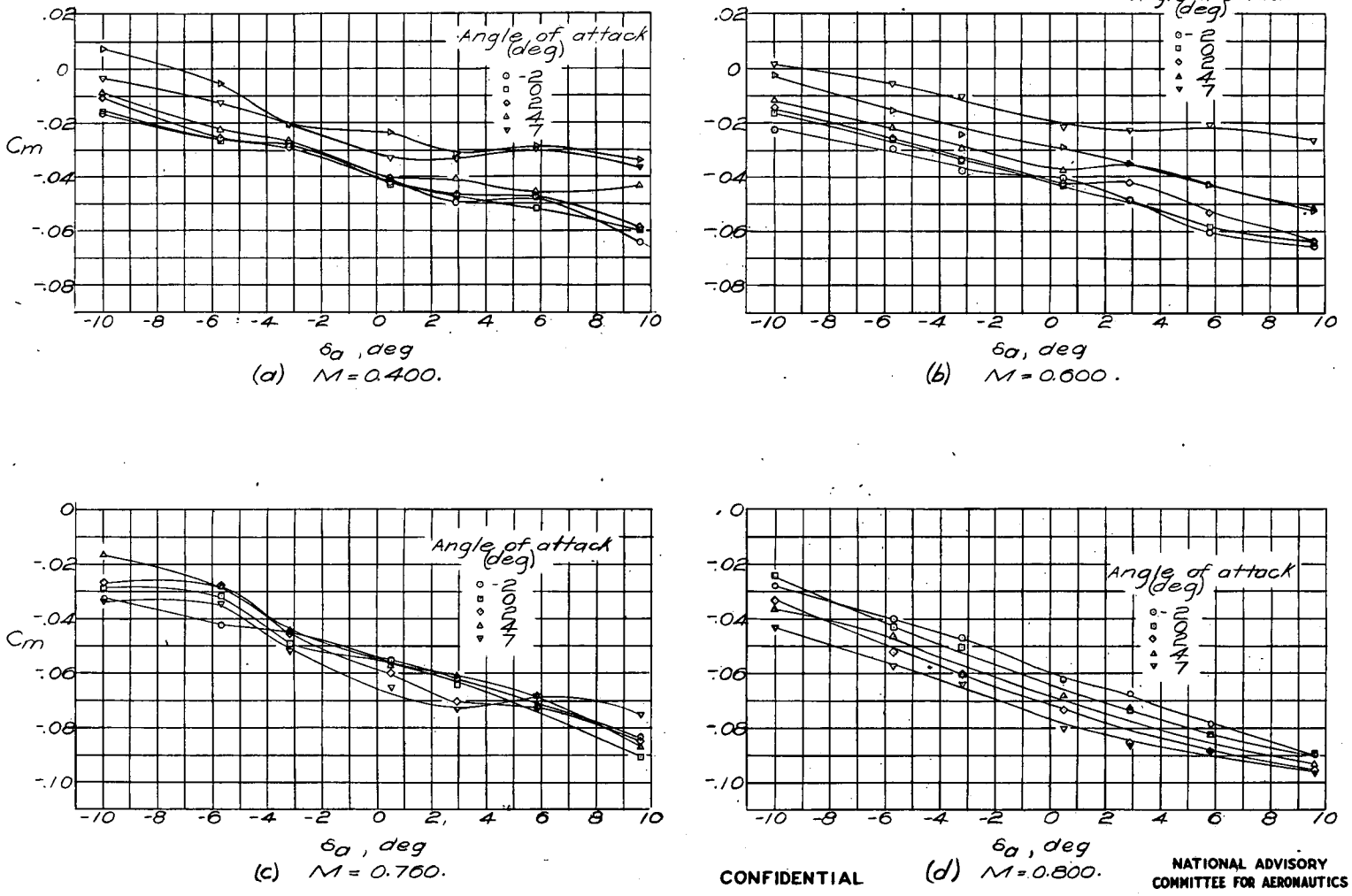

Figure 25.- Wing pitching-moment coefficient against aileron deflection at various Mach numbers and angles of attack.

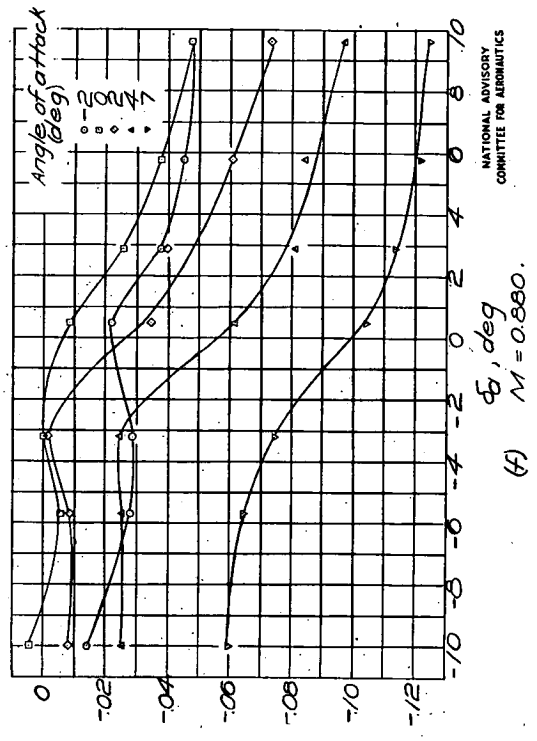

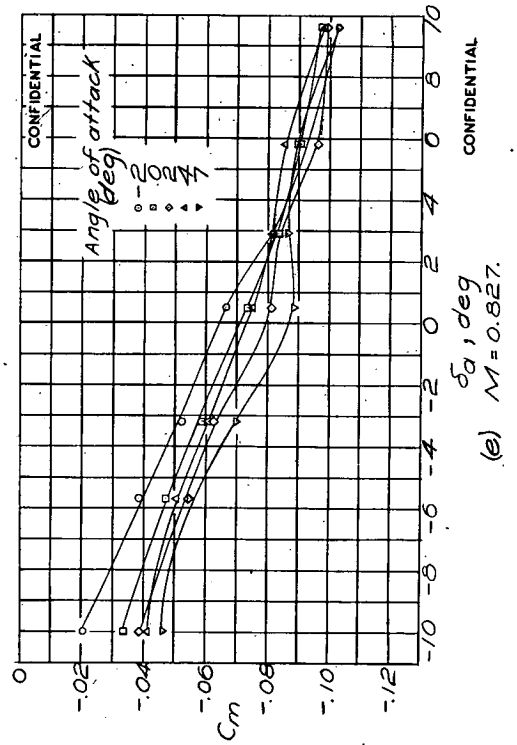

Figure 25.- Continued.

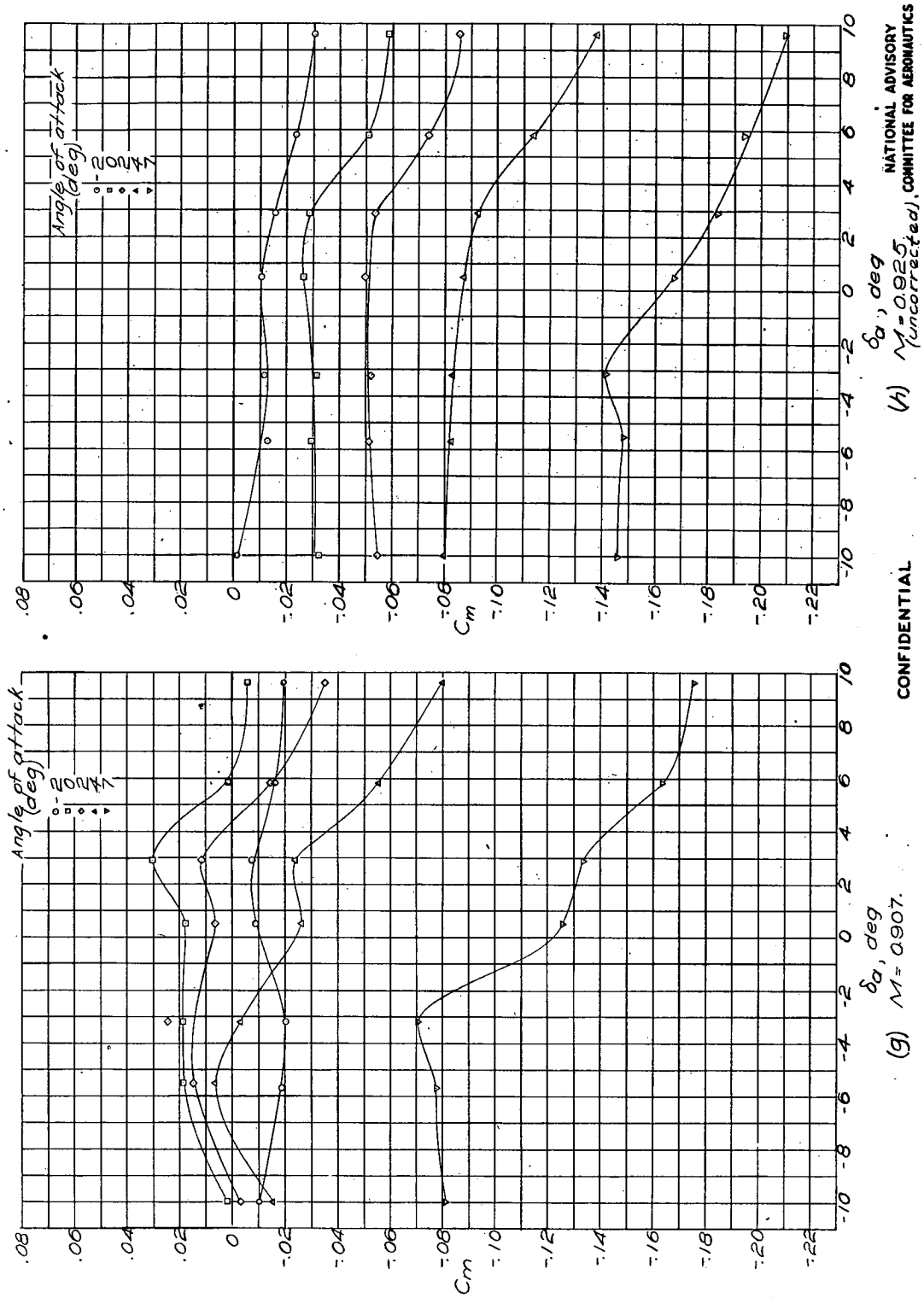

Figure 25.-Concluded.

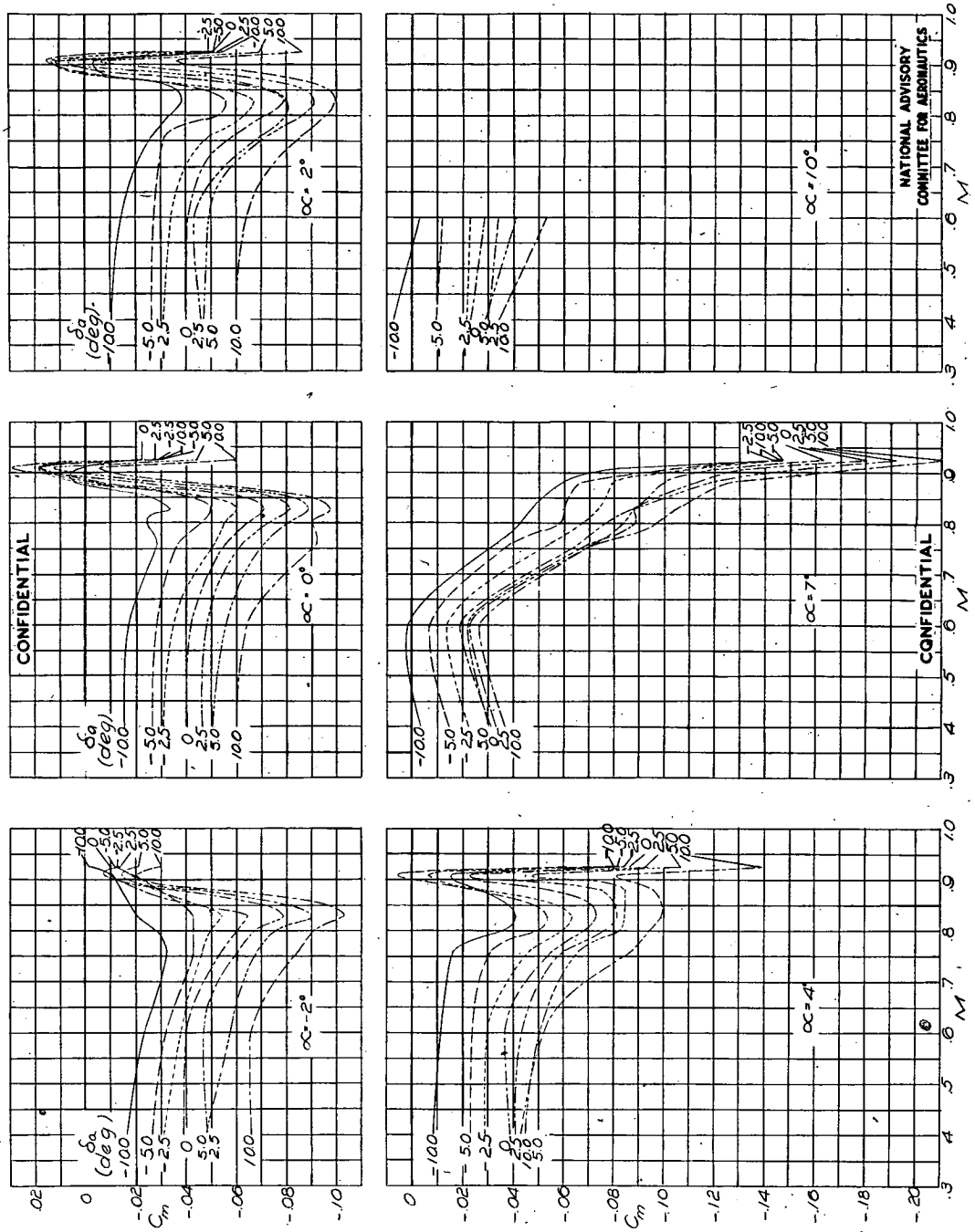

Figure 26.- Wing pitching-moment coefficient against Mach number at various aileron deflections and angles of attack.

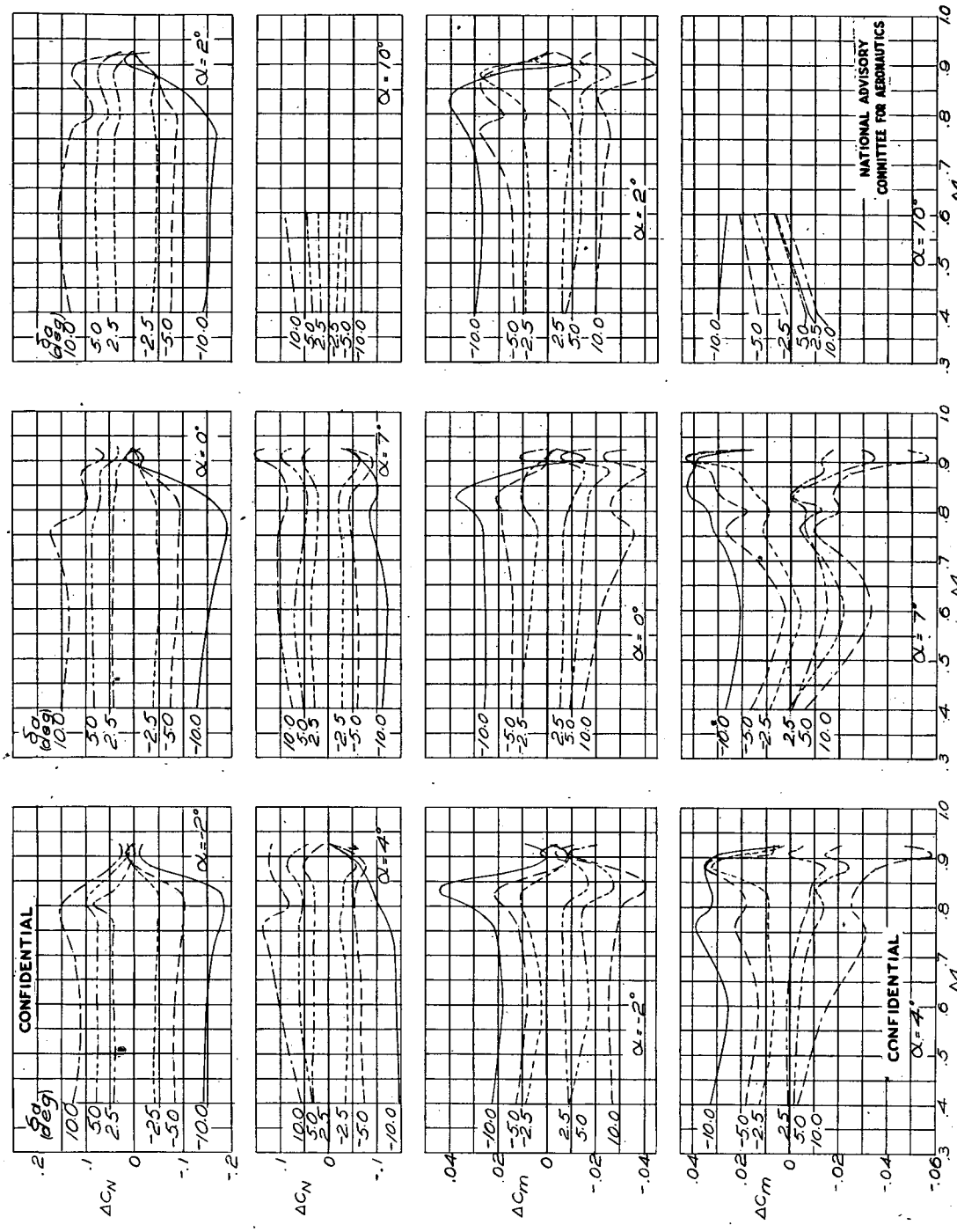

Figure 27.- Wing normal-force coefficient and pitching-moment coefficient due to aileron deflection against Mach number.

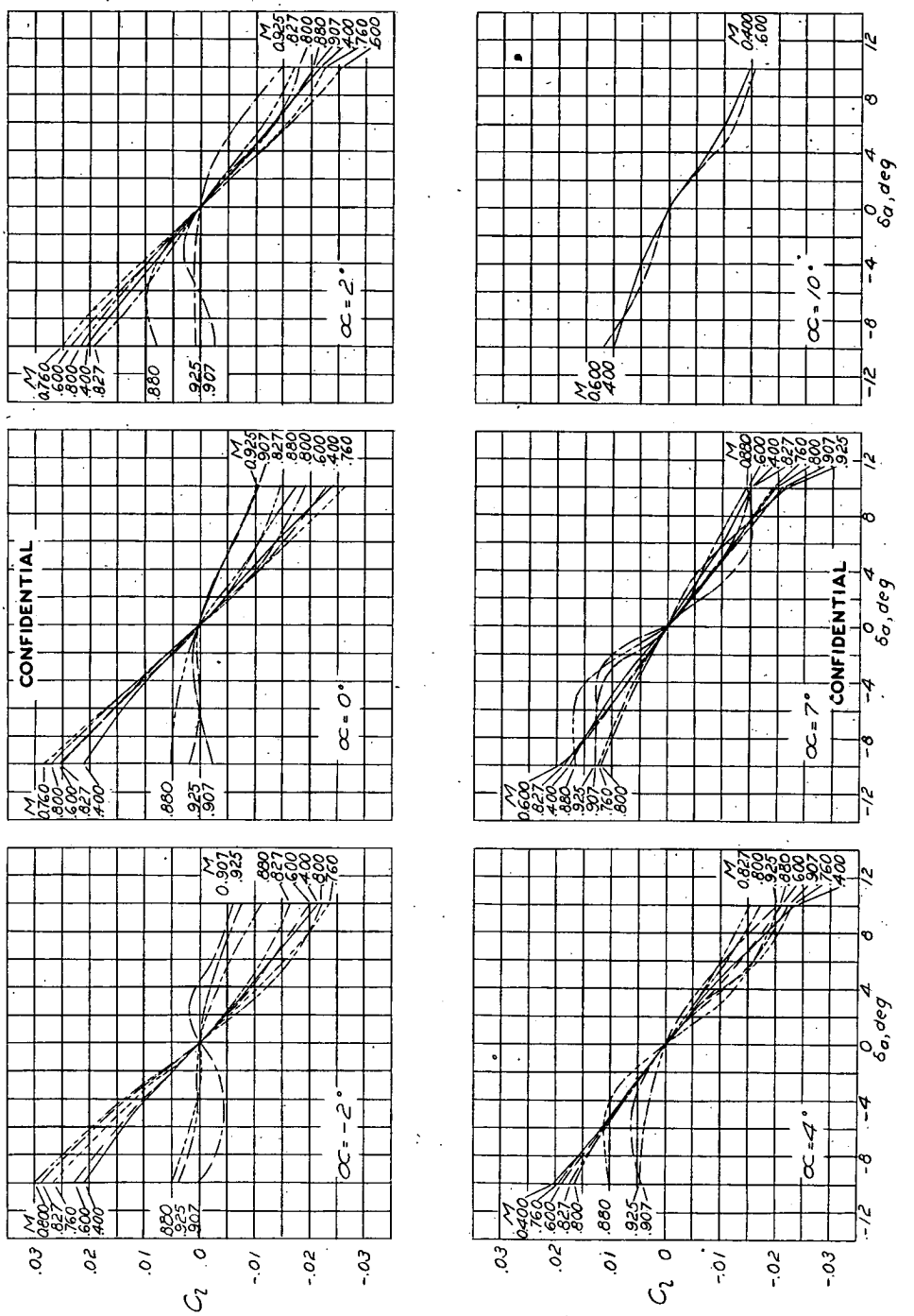

Figure 28.- Aileron rolling-moment coefficient against aileron deflection at various Mach numbers and angles of attack. Sealed aileron.

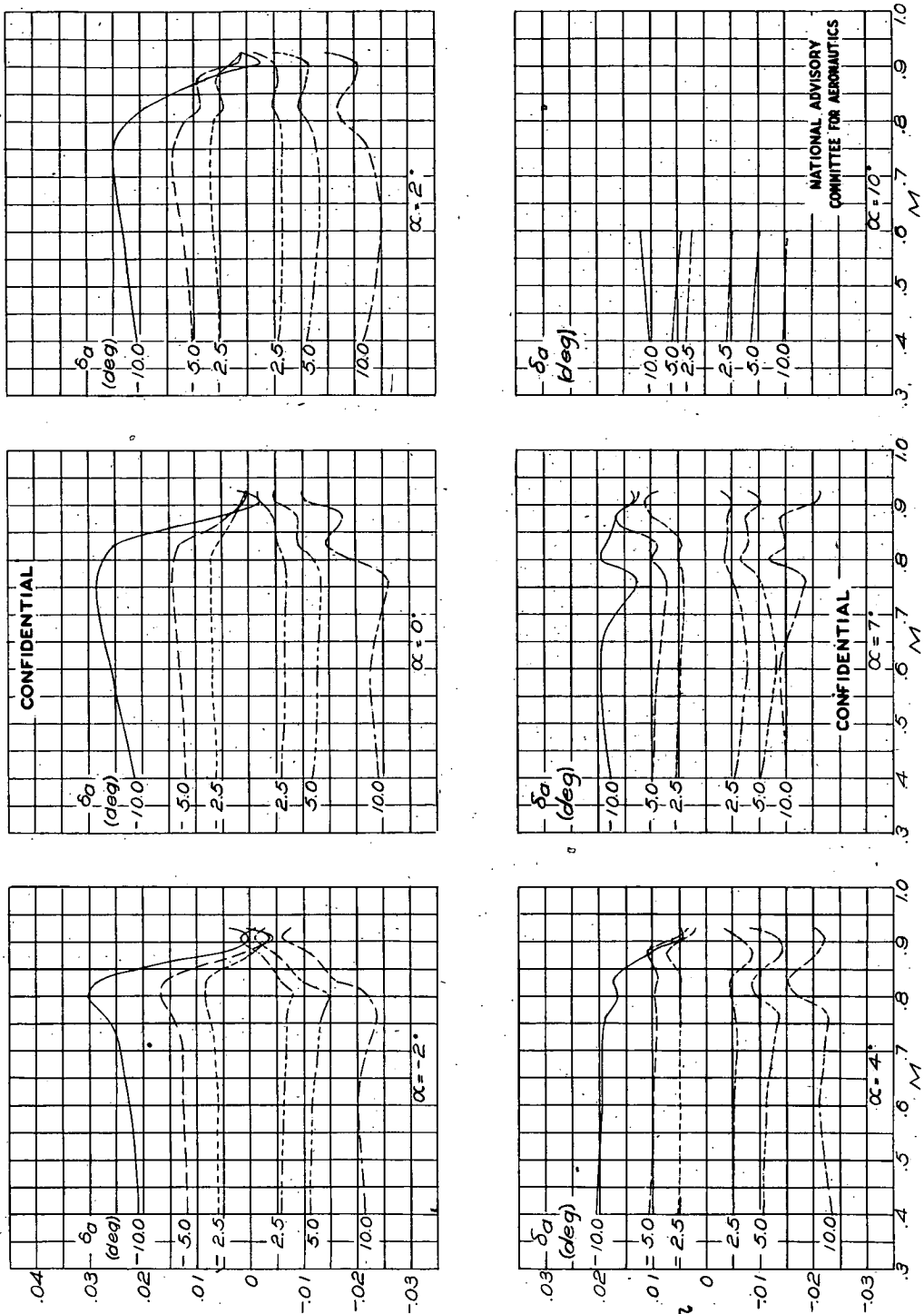

Figure 29 - Aileron rolling-moment coefficient against Mach number at various aileron deflections and angles of attack. Sealed aileron.

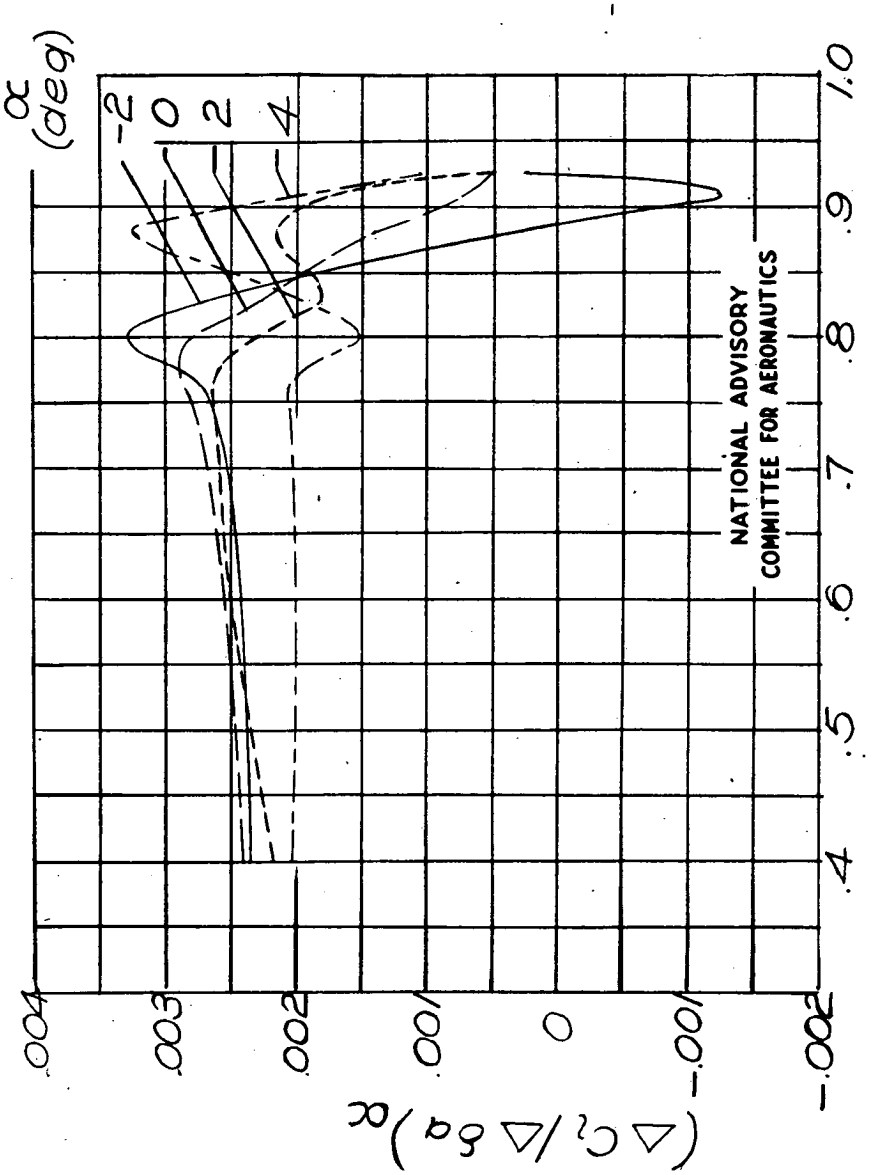

CONFIDENTIAL

CONFIDENTIAL

Figure 30.- Effect of compressibility on rolling-moment coefficient per unit aileron deflection at various angles of attack. Sealed aileron.

Mach number, M

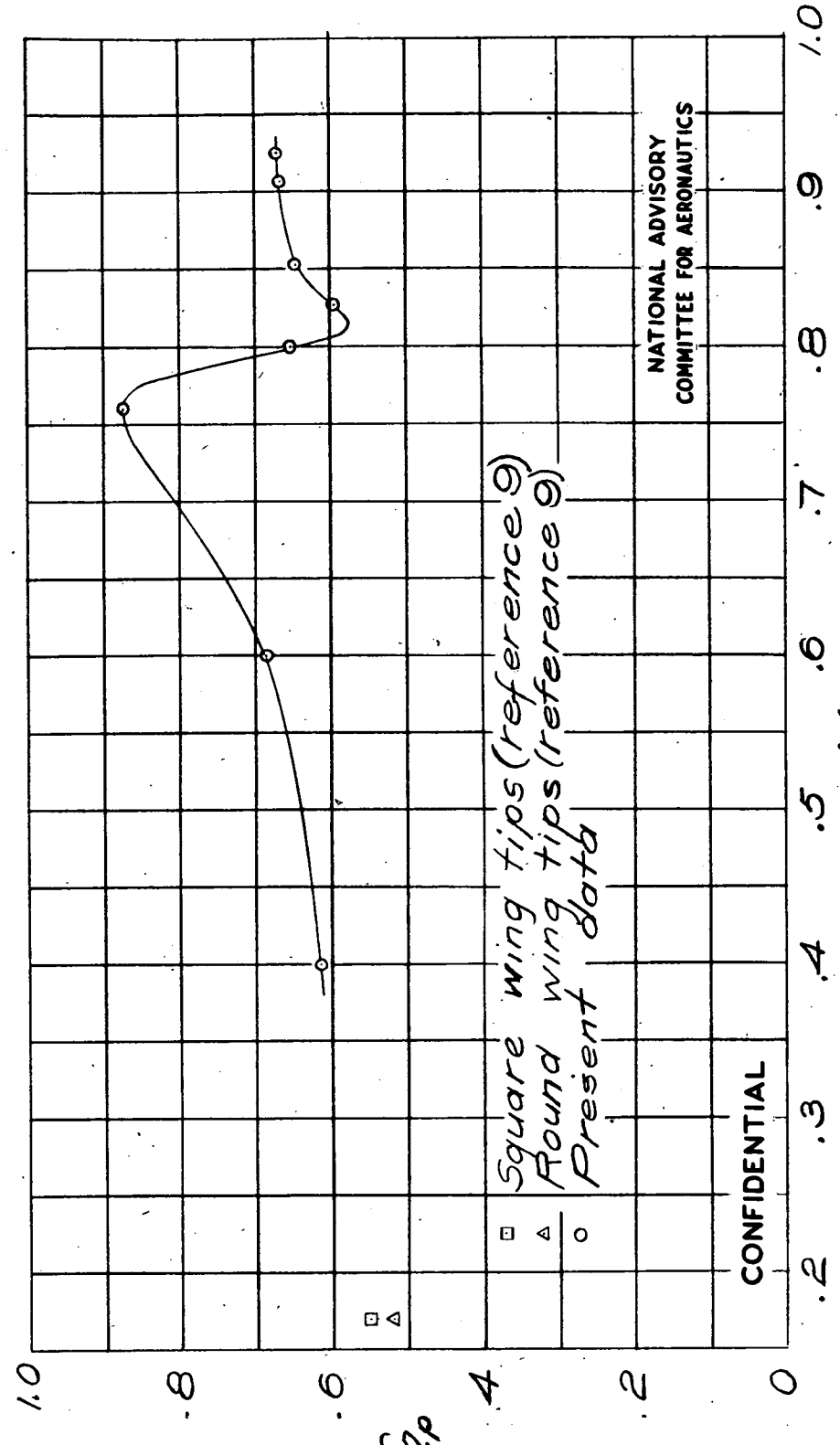

Figure 31.- Effect of compressibility on damping-moment coefficient for $\delta_a = 0°$.

CONFIDENTIAL

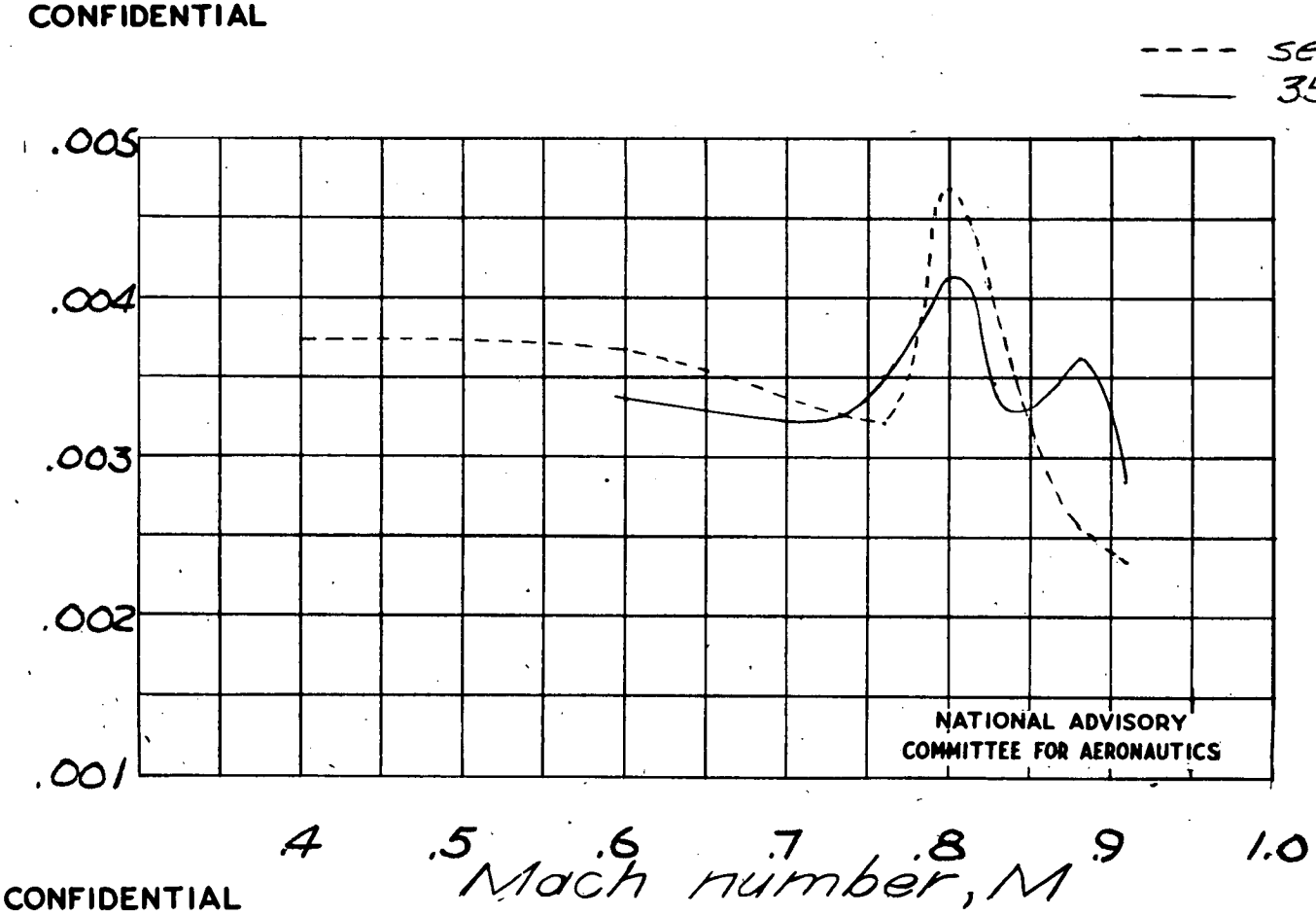

Figure 32.- Effect of compressibility on calculated rate of roll per unit aileron deflection for a rigid wing at two altitudes. Sealed aileron.

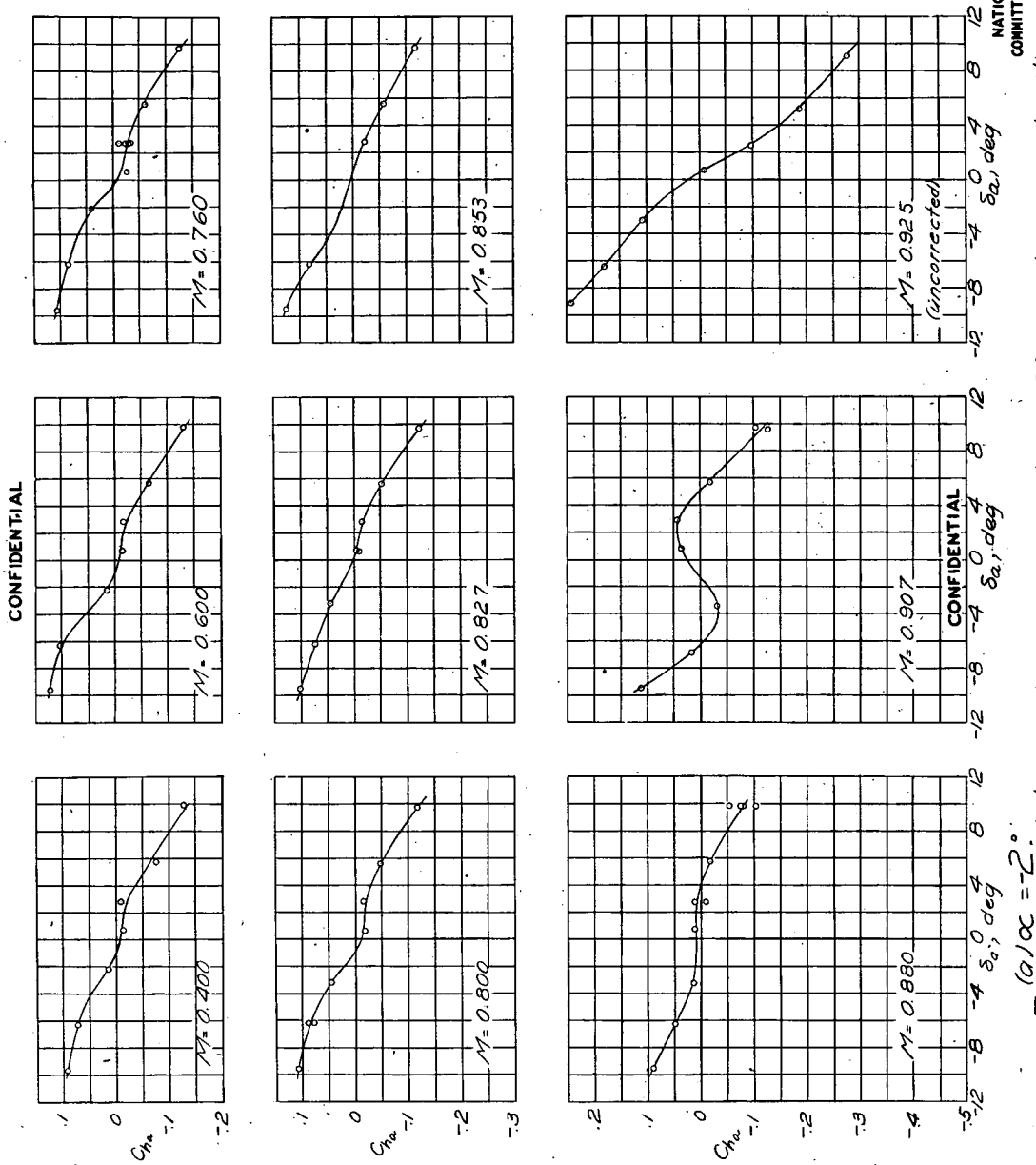

(a) $\alpha = -2°$.

Figure 33.- Aileron hinge-moment coefficient against aileron deflection at various Mach numbers. Unsealed aileron.

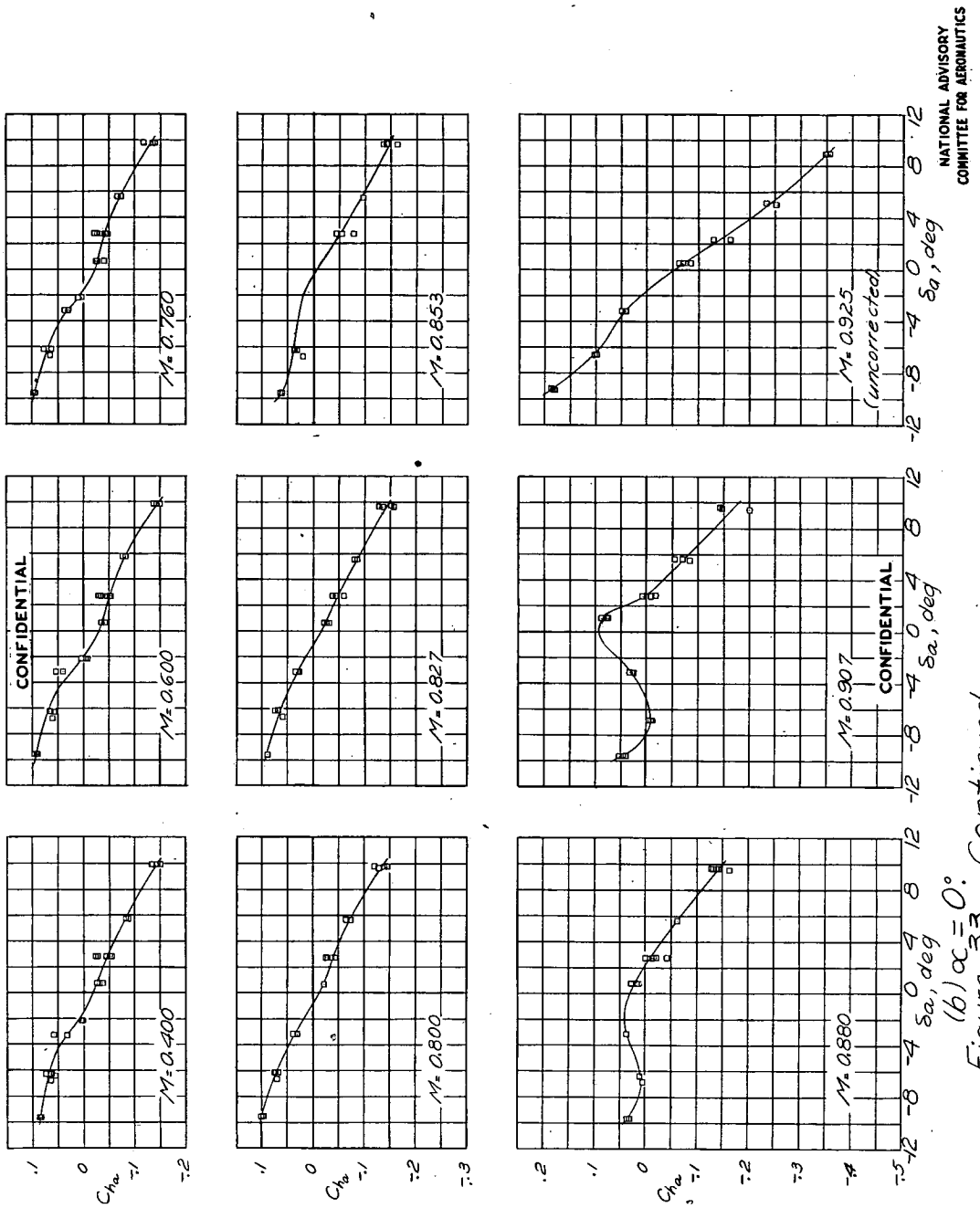

(b) $\alpha = 0°$.

Figure 33.- Continued.

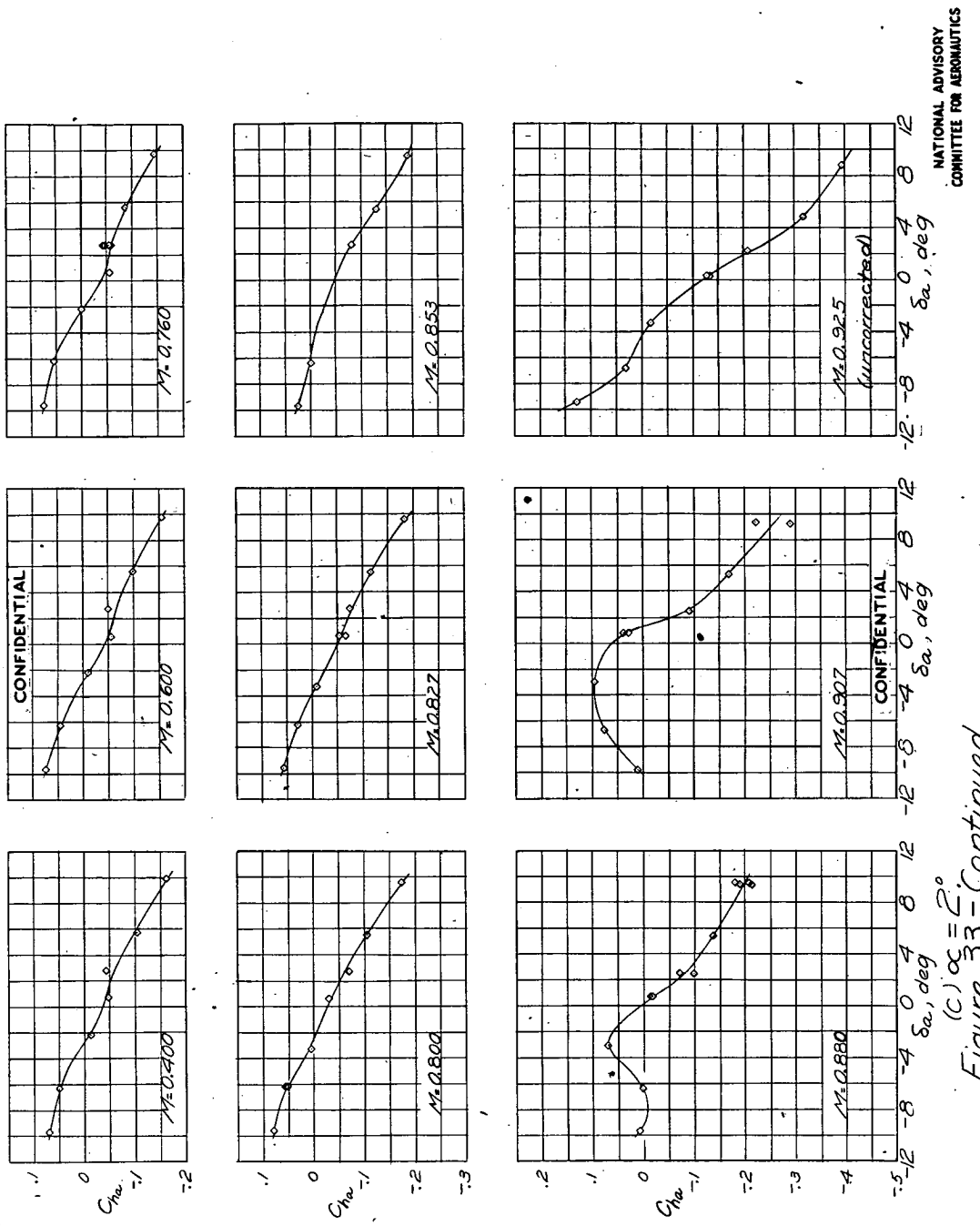

(c) $\alpha = 2°$

Figure 33.- Continued.

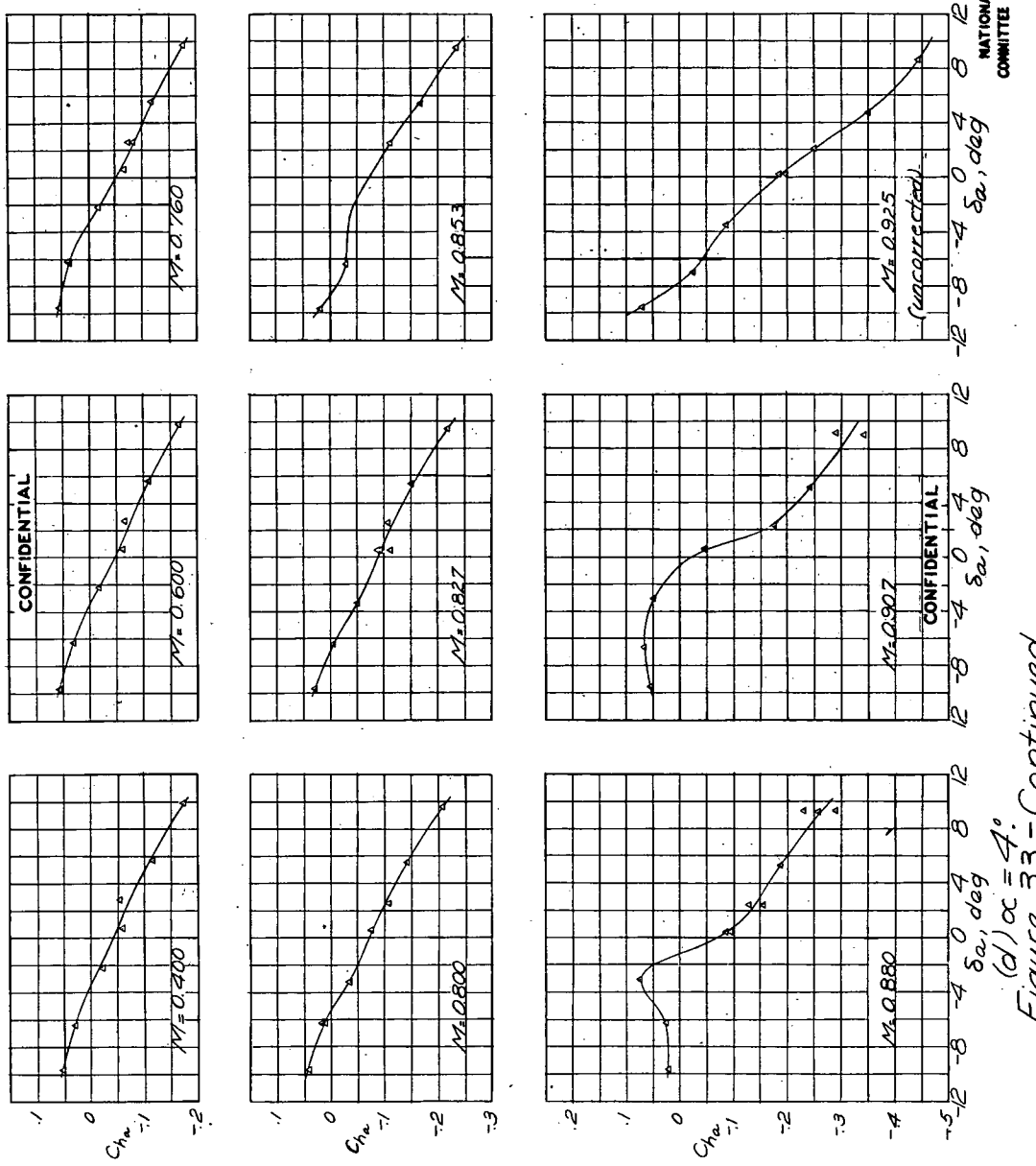

(d) $\alpha = 4°$

Figure 33.- Continued.

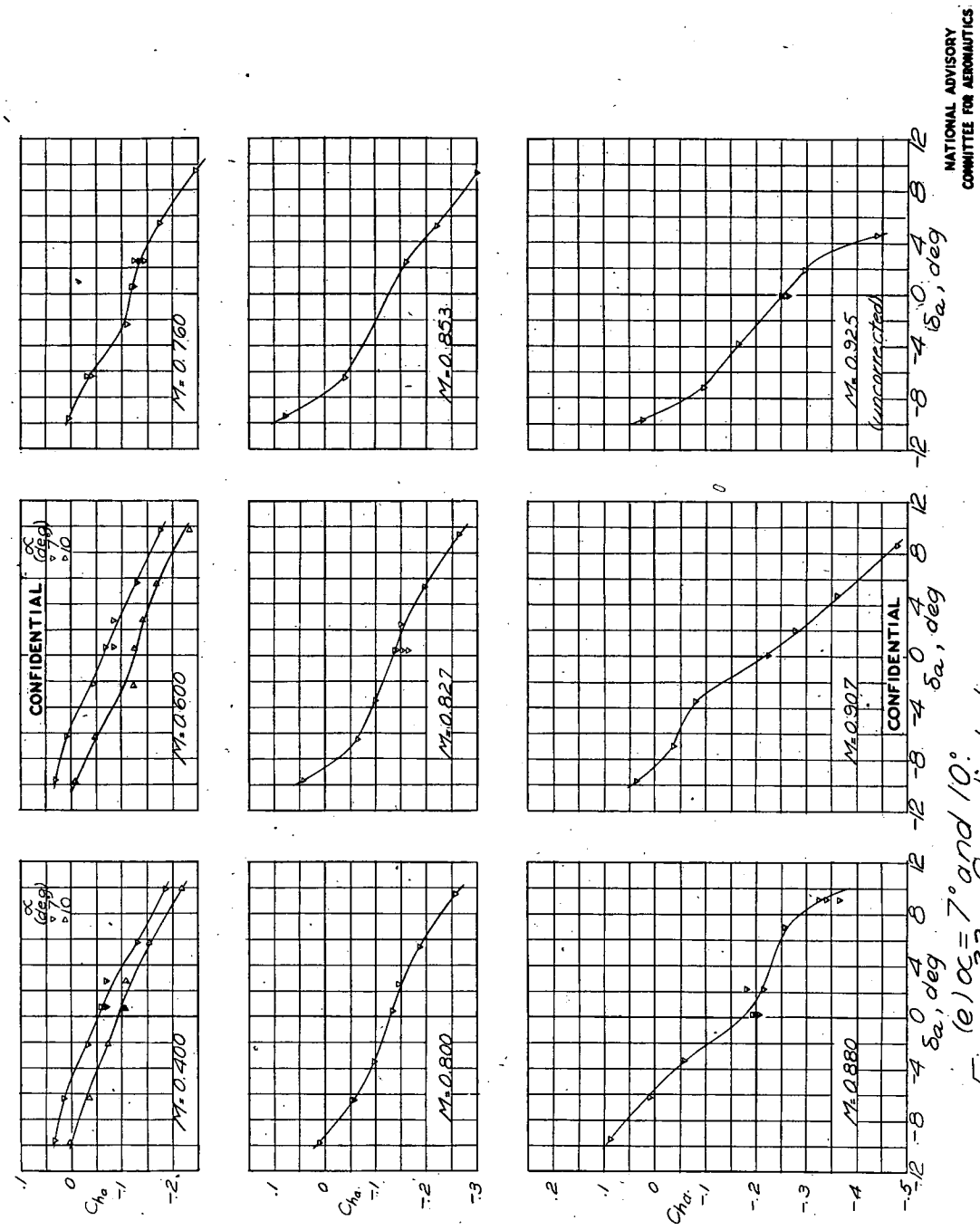

Figure 33.- Concluded.
(e) $\alpha_c = 7°$ and 10°.

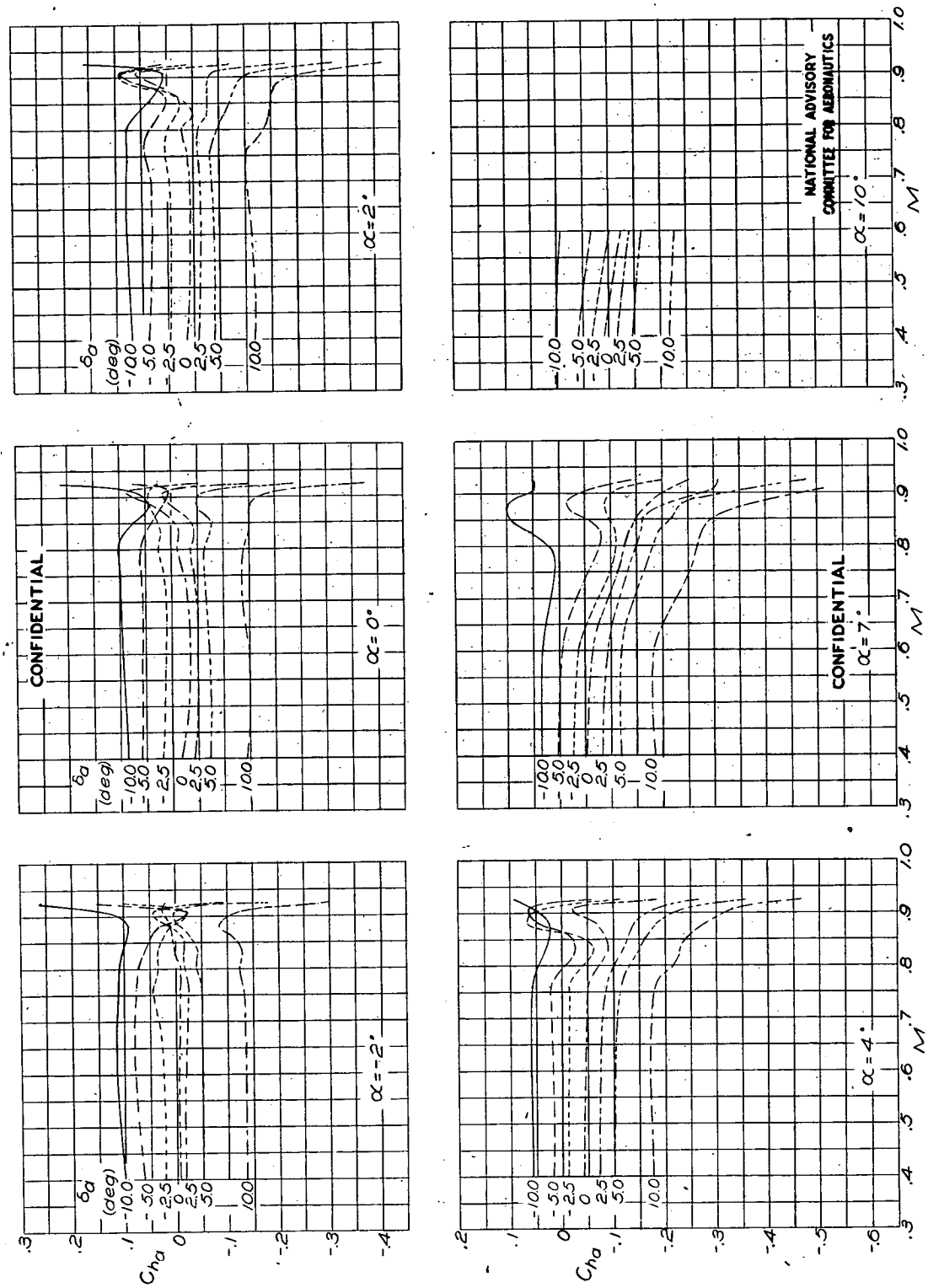

Figure 34.- Aileron hinge-moment coefficient against Mach number at various aileron deflections and angles of attack. Unsealed aileron

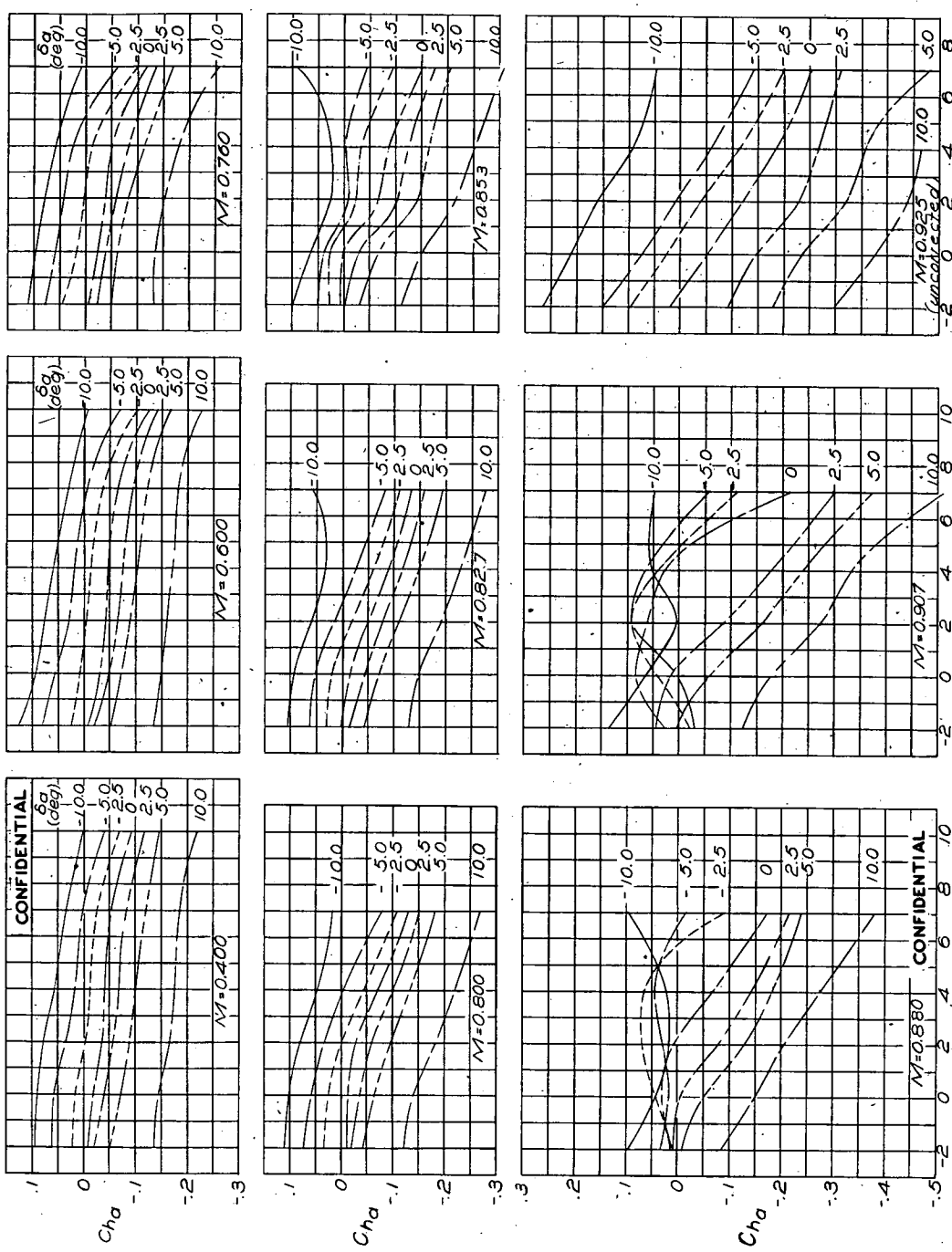

Figure 35.- Aileron hinge-moment coefficient against angle of attack at various aileron deflections and Mach numbers. Unsealed aileron.

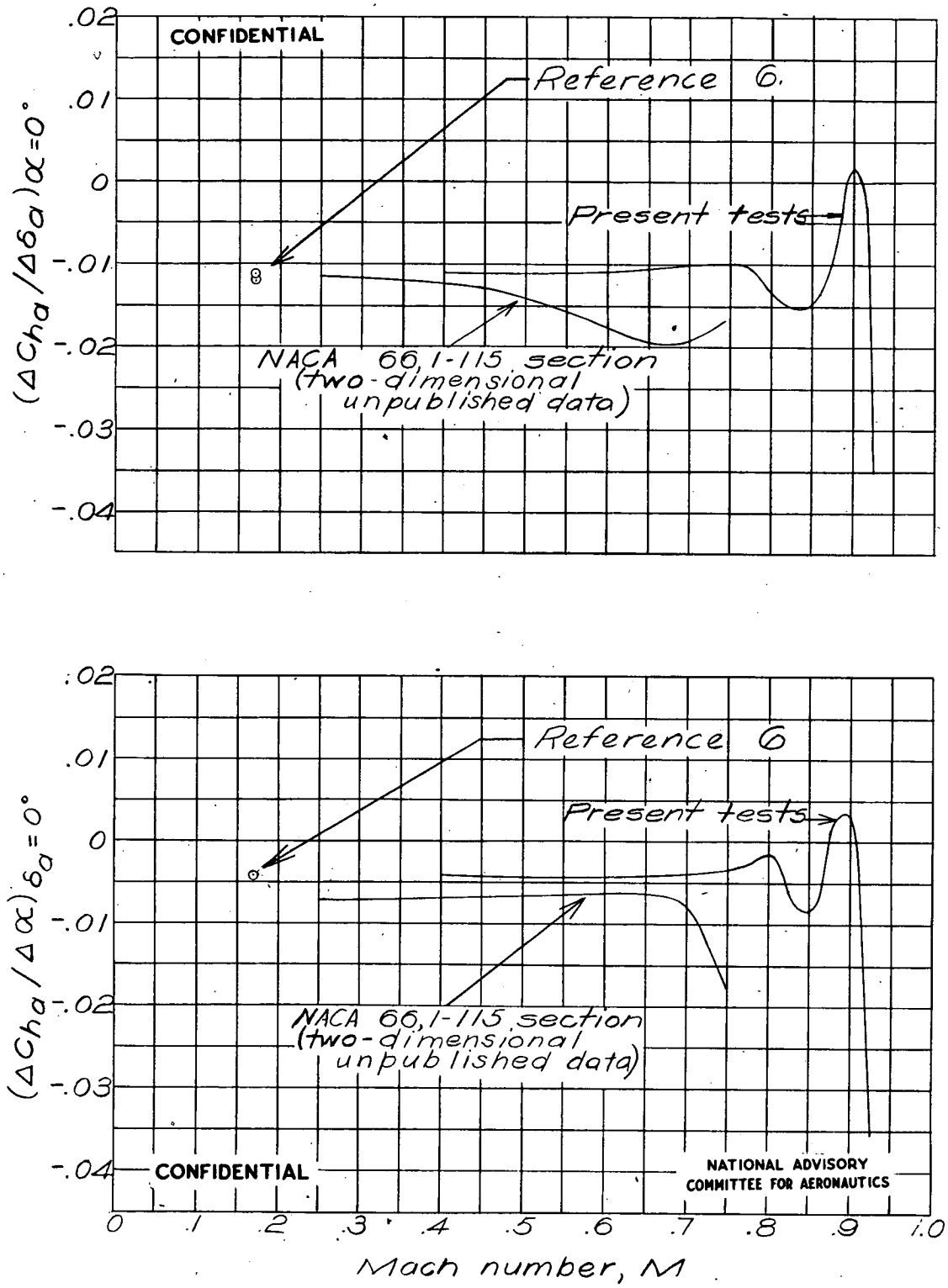

Figure 36.- Effect of Mach number on $(\Delta C_{h_a}/\Delta\delta_a)_{\alpha=0°}$ and $(\Delta C_{h_a}/\Delta\alpha)_{\delta_a=0°}$. Unsealed aileron.

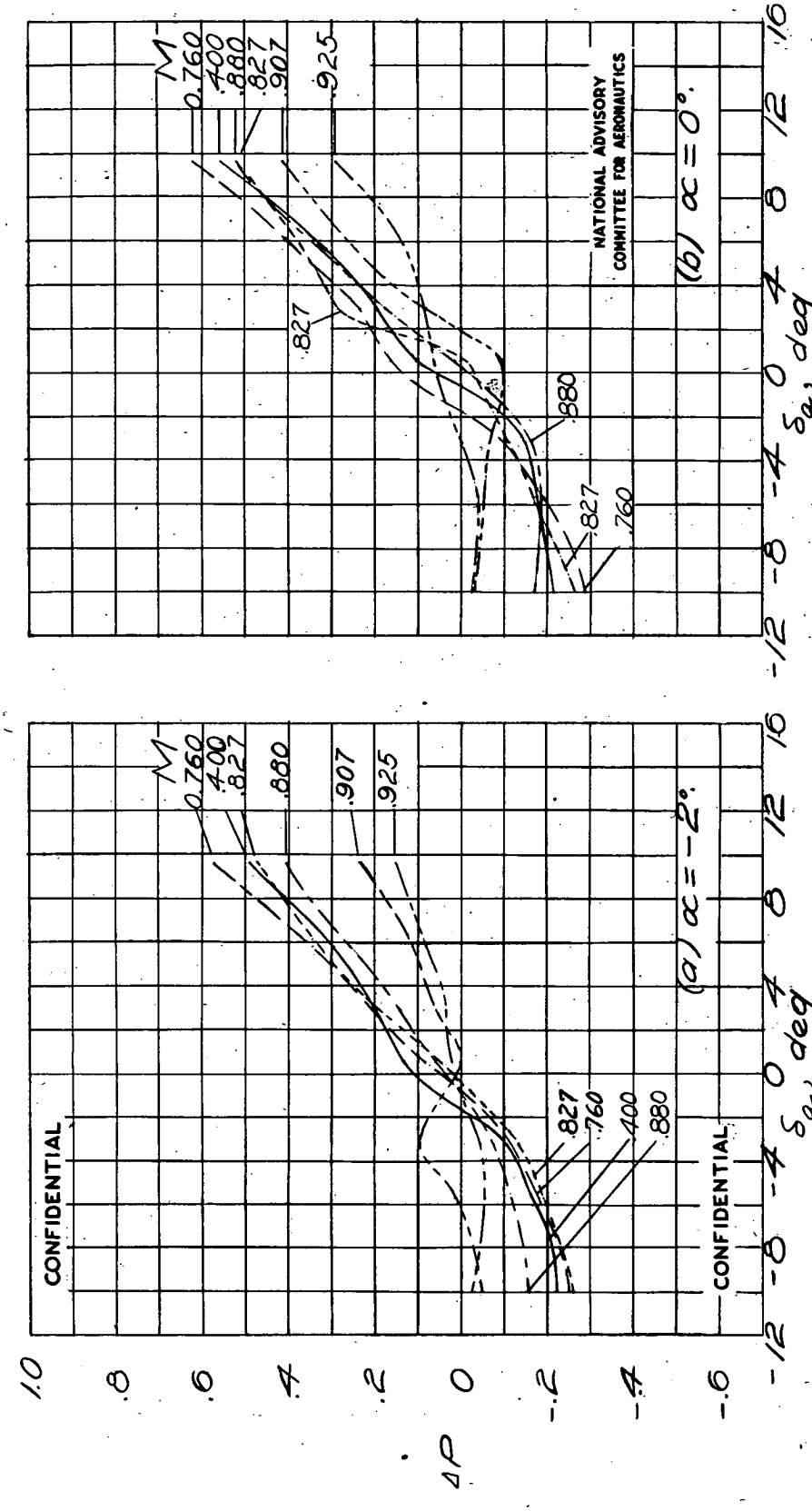

Figure 37.- Resultant pressure coefficient across aileron seal against aileron deflection at various Mach numbers.

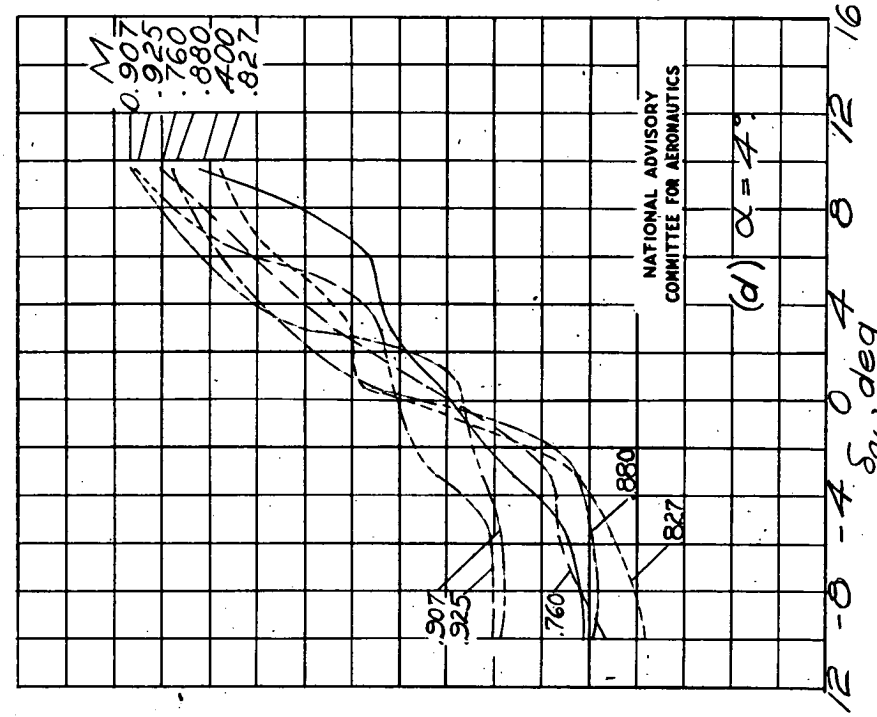

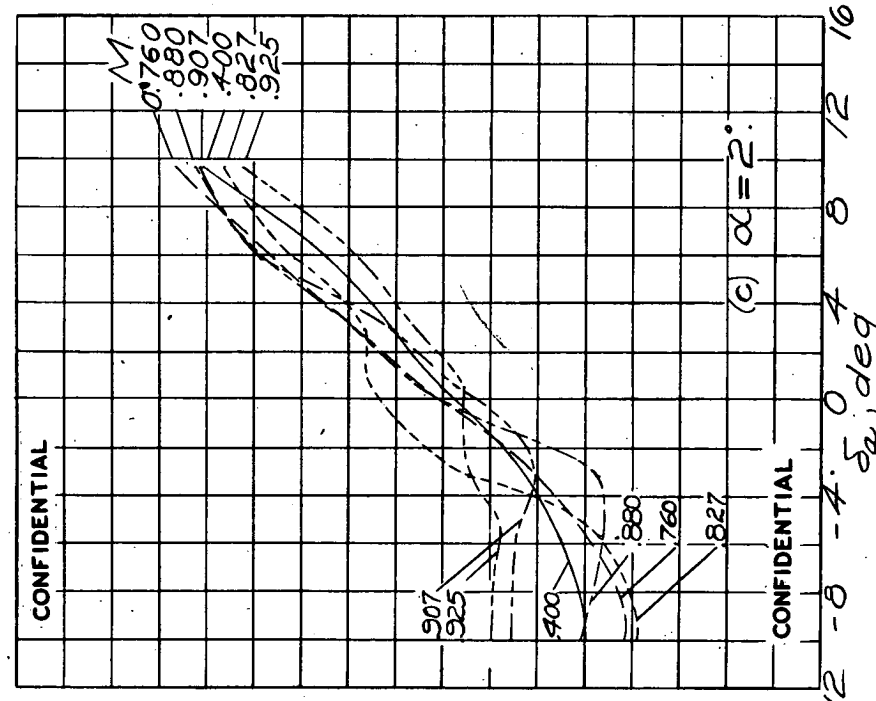

Figure 37. - Continued.

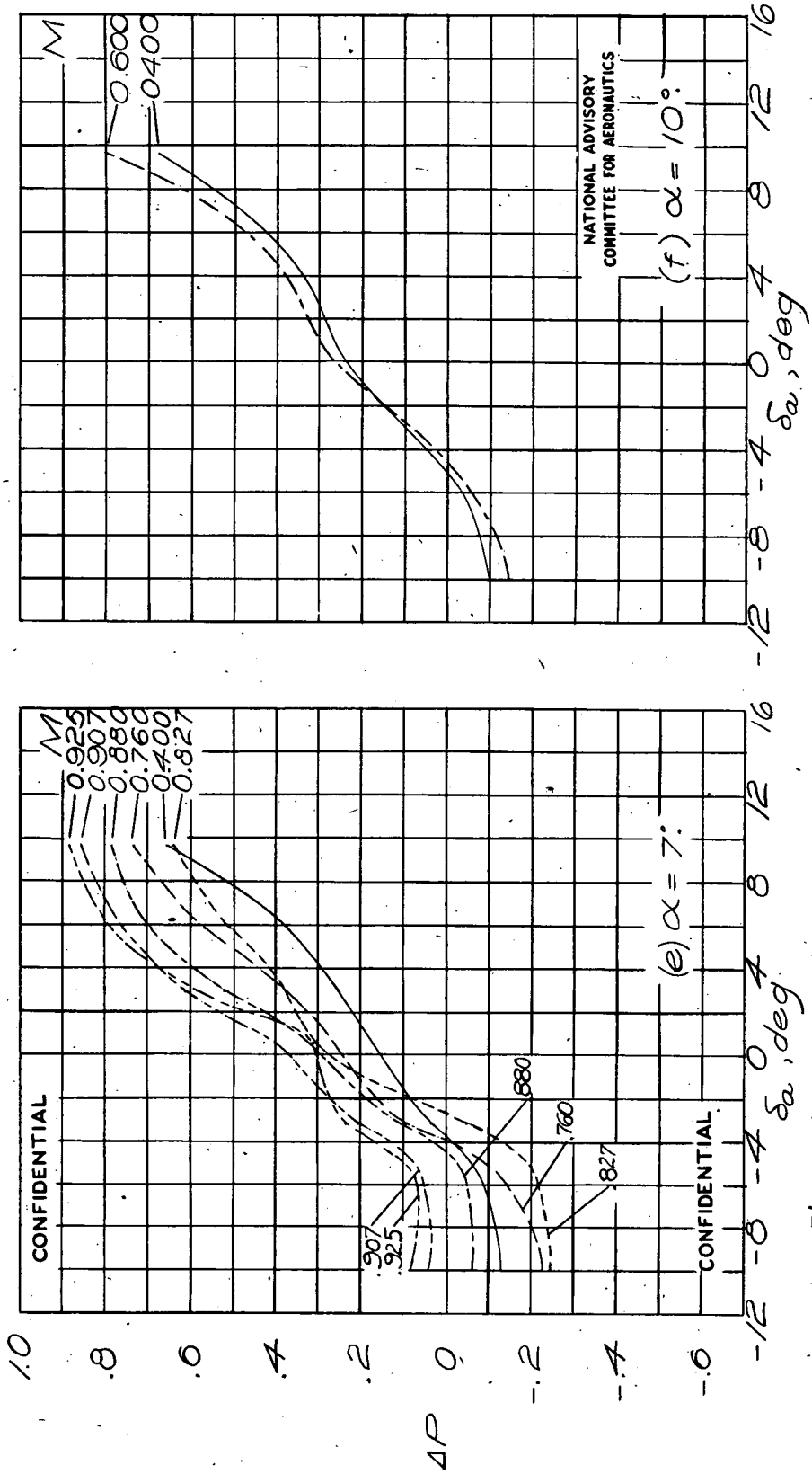

Figure 37. — Concluded.